Computational Design of Electrocatalysts for Oxygen Reduction Reaction

Sinha, Sukanya

Publication date:
2023

Document Version
Publisher's PDF, also known as Version of record

DTU Energy
Department of Energy Conversion and Storage

Computational Design of Electrocatalysts for Oxygen Reduction Reaction

Sukanya Sinha

PhD Thesis, November 2023

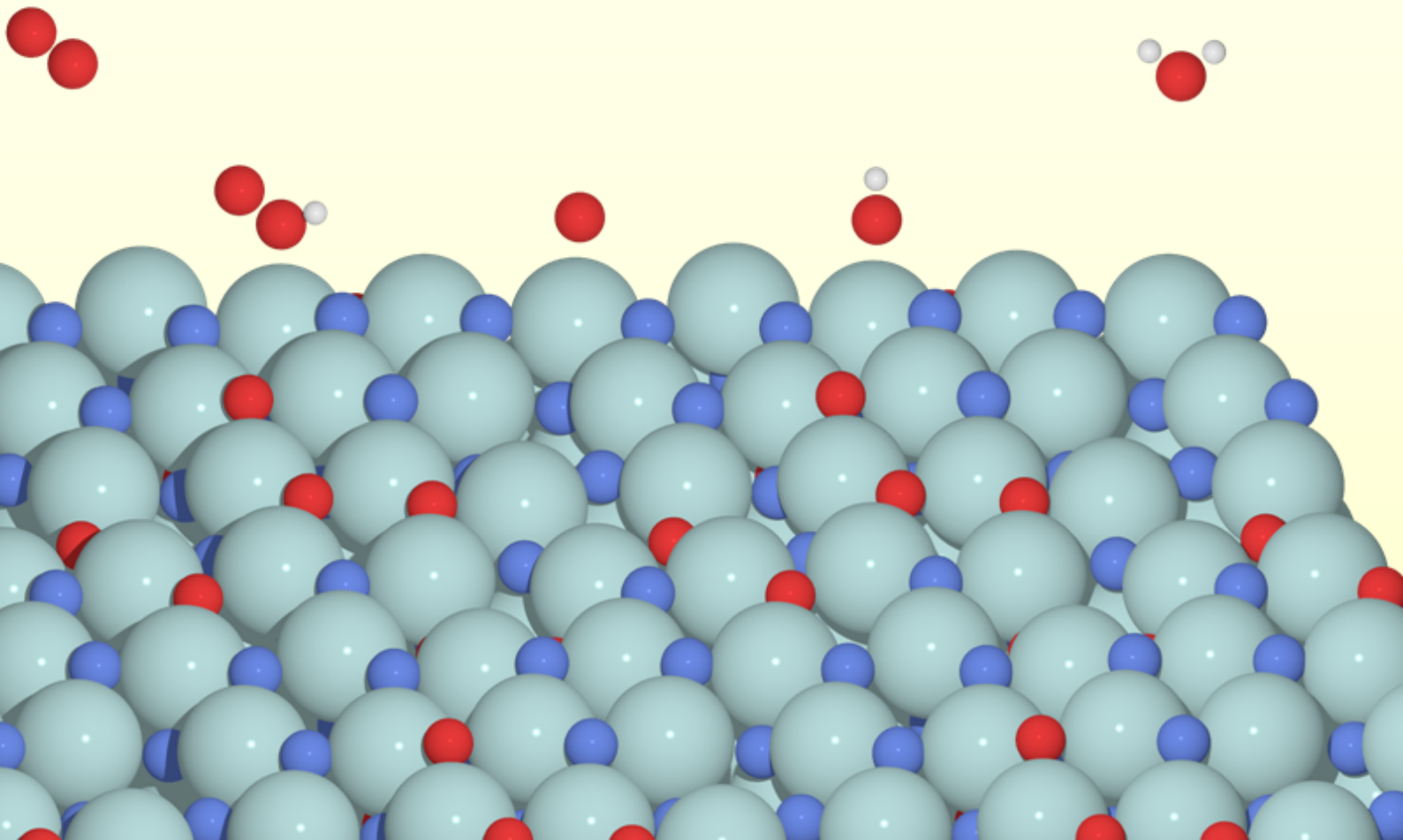

SUKANYA SINHA

Computational Design of Electrocatalysts for Oxygen Reduction Reaction

PhD Thesis
November 2023

Department of Energy Conversion and Storage
Technical University of Denmark

Computational Design of Electrocatalysts for Oxygen Reduction Reaction

Author:
Sukanya Sinha
suksi@dtu.dk

Supervisor: Assoc. Prof. Heine Anton Hansen
Section for Atomic Scale Materials Modelling (ASM)
Department of Energy Conversion and Storage
Technical University of Denmark
E-mail: heih@dtu.dk

Co-supervisor: Prof. Tejs Vegge
Section for Autonomous Materials Discovery (AMD)
Department of Energy Conversion and Storage
Technical University of Denmark
E-mail: teve@dtu.dk

DTU Energy
Department of Energy Conversion and Storage
Technical University of Denmark
Anker Engelunds Vej
Building 301
2800 Kongens Lyngby
Denmark
info@energy.dtu.dk
www.energy.dtu.dk

-720

Preface

This thesis is submitted in candidacy for a Doctor of Philosophy (PhD) degree from the Technical University of Denmark (DTU). The work has been carried out between November 2020 and November 2023 at the Section for Atomic Scale Materials Modelling (ASM) at the Department of Energy Conversion and Storage. The studies have been supervised by Associate Professor Heine Anton Hansen and Professor Tejs Vegge. Part of the work was carried out during a three month external stay at SUNCAT Center for Interface Science and Catalysis, SLAC National Accelerator Laboratory hosted by Dr. Kirsten T. Winther. The PhD project was funded by by the Villum Foundation through the research center V-Sustain (grant number 9455).

Sukanya Sinha
Kongens Lyngby, November 2023

Acknowledgements

I would like to express my sincere gratitude to a lot of people who have played a crucial role in the completion of my Ph.D. thesis.
First and foremost, I extend my deepest appreciation to my supervisor team. My main supervisor Heine Anton Hansen and co-supervisor Tejs Vegge for their invaluable guidance, unwavering support and mentorship throughout the entire research process. Their expertise and insightful feedback have significantly enriched the quality of this work.
Many thanks to Kirsten Winther for making my external stay at SLAC an incredible learning opportunity. Furthermore, I will also like to thank the members of the SUNCAT group for a warm welcome and making my stay in California memorable. In particular, I would like to thank Neha Bothra for her insightful comments into my work.
I am extremely grateful to all of my current and former colleagues at the ASM and AMD sections for fostering a wonderful social and work environment. Special thanks to Steen Lysgaard for helping me with all the technical and scientific issues that I encountered throughout my PhD and also for being a very friendly office mate along with Pernille Pedersen for proofreading this thesis thoroughly, introducing me to the best flea markets in Copenhagen and for being a great friend. I would also like to thank Xiaotong Zhang, Smobin Vincient and Yogeshwaran Krishnan for proof reading my thesis, Changzi Ai and Tippaporn Patniboom for helping me whenever I was unable to implement a new calculation or analysis technique. Special thanks to William Hansen for translating the abstract into Danish. Also thank you Juan Maria García Lastra for being a wonderful manager. I always had the confidence that if I needed any help with a work problem I could always come to you for advice.
I would also like to thank all of my friends aka the first floor lunch group, my badminton mates and the Friday Hygge team for creating a great environment where we could talk about anything and have a lot of fun.
Last but not the least, I would like to thank my family and friends back in India for always believing in me. Thank you Ma for being my support all the time.

Abstract

The ever increasing fossil fuel consumption has been linked to anthropogenic global warming, which might result in a 4°C increase in the global mean temperature during the 21st century under certain “business as usual” fossil-rich scenarios. Apart from carbon dioxide emission, fossil fuel combustion is also responsible for the emission of many other toxic air pollutants. The synergistic effect between climatic change and air pollution can magnify health hazards. Thus, technologies for more environmentally friendly energy conversion are therefore actively being pursued. One such technology is the polymer electrolyte membrane fuel cell (PEMFC).

In PEMFCs, a fuel such as methanol or hydrogen is oxidized at the anode and oxygen is reduced to water at the cathode. Possible applications of PEMFC ranges from stationary to mobile and portable applications, in e.g. auxiliary power units (APU) and fuel cell electric vehicles (FCEV). However, the widespread use of hydrogen fuel cells continue to face several challenges, the most significant of which is the high cost of the platinum-based catalyst used in the electrodes, which contributes to almost 55% of the total cost. Ideally, to decrease the overall cost of PEMFCs, development of new and cost-efficient catalyst candidates for both cathode and anode is highly desirable but the slow oxygen reduction reaction (ORR) at the cathode requires much more platinum than the much faster hydrogen oxidation reaction at the anode. The sluggish kinetics of the ORR at the PEMFC cathode can lead to nearly 30% efficiency decrease of the PEMFCs. Thus, in particular, the development of cost-efficient, non-precious metal catalysts for the ORR with a high catalytic efficiency has received much attention.

Some of the possible alternatives can be catalysts based on transition metals in nitrogen doped graphitic cathodes, oxides and oxynitrides of transition metals e.g. tantalum, zirconium oxide based catalysts with multiwalled carbon nanotubes (MWCNTs) support and niobium-titanium complex oxides among others.

In this thesis, zirconium based catalysts were systematically studied to understand the possibility of achieving enhanced ORR activity using a non platinum group metal (non-PGM) transition metal catalyst using Density Functional Theory (DFT).

In the first study, DFT was used to explore the viability of zirconium oxynitride as an ORR catalyst. The catalyst surface was studied systematically to explore the presence of active catalytic sites along with computation of adsorption energies of various intermediates. For ORR the adsorption energies of different intermediates, irrespective of the catalyst material, are related by the so-called standard scaling relations. We explored the possibility of deviation from the standard scaling relations for ORR taking place over zirconium oxynitride catalyst which can give rise to enhanced electrocatlysis.

In the second study, we explored electronic descriptors in order to predict adsorption energy of the ORR intermediates and consequently the ORR activity over zirconium based catalysts. During the course of our first study, we studied several electronic descriptors, however none of them could fully capture the complexity of the zirconium oxynitride catalyst surface. Integrated crystal orbital Hamiltonian population (ICOHP) had been previously successfully used as an electronic descriptor to understand trends in O* and OH adsorption on transition metal oxides. Hence, we investigated ICOHP as an electronic descriptor for a simplified model catalyst system, i.e anion substituted zirconia.

Resumé

Det stadigt stigende forbrug af fossile brændstoffer har ført til øgede niveauer af atmosfærisk kuldioxid. Forbrændingen af fossile brændstoffer er blevet forbundet med menneskeskabt global opvarmning, hvilket kan resultere i en stigning på $4^{\circ}C$ i den globale middeltemperatur i løbet af det 21. århundrede under visse "business as usual" fossilrige scenarier. Bortset fra emission af kuldioxid er forbrænding af fossilt brændstof også ansvarlig for emissionen af mange andre giftige og luftforurenende stoffer. Den synergistiske effekt imellem klimaændringer og luftforurening kan øge sundhedsrisici. Der arbejdes derfor aktivt med udvikling af teknologier til mere miljøvenlig energiomdannelse. Polymerelektrolytmembranbrændselscellen (PEMFC) er sådan en teknologi.
I PEMFC'er oxideres et brændstof som methanol eller brint ved anoden, og oxygen reduceres til vand ved katoden. Mulige anvendelser af PEMFC spænder fra stationære til mobile og bærbare anvendelser, i f.eks. auxiliary power units (APU) og brændselscelledrevne elektriske køretøjer (FCEV). Dog står den udbredte brug af brintbrændselsceller fortsat over for adskillige udfordringer, hvoraf den vigtigste er de høje omkostninger ved den platinbaserede katalysator, der anvendes i elektroderne, som bidrager til næsten 55% af de samlede omkostninger.
For at reducere de samlede omkostninger ved PEMFC'er bør katalysatorerne til begge elektroder ideelt udskiftes, men den langsomme oxygenreduktionsreaktion (ORR) ved katoden kræver meget mere platin end den meget hurtigere hydrogenoxidationsreaktion ved anoden. Den langsomme kinetik af ORR ved PEMFC-katoden kan føre til en næsten 30% effektivitetsreduktion af PEMFC'erne. Udviklingen af en billig og effektiv ikke-ædelmetalkatalysator til oxygenreduktionsreaktionen har således fået stor opmærksomhed. Nogle af de mulige alternativer kan være katalysatorer baseret på overgangsmetaller i nitrogen-doterede grafitiske katoder, oxider og oxynitrider af overgangsmetaller f.eks. tantal, zirconiumoxid baserede katalysatorer med flervæggede kulstofnanorør støtte (MWCNT'er) og niobium-titanium komplekse oxider blandt andet. I denne afhandling bliver zirkoniumbaserede katalysatorer systematisk undersøgt for at forstå muligheden for at opnå øget ORR-aktivitet ved hjælp af en overgangsmetalkatalysator uden platinmetaller ved brug af tæthedsfunktionalteori (DFT).
I det første studie bruger vi DFT til at udforske levedygtigheden af zirconiumoxynitrid som en ORR-katalysator. Katalysatoroverfladen blev undersøgt systematisk for at udforske tilstedeværelsen af aktive katalytiske steder sammen med beregning af adsorptionsenergier for forskellige mellemprodukter. For ORR er adsorptionsenergierne for forskellige mellemprodukter, uanset katalysatormaterialet, relateret til hinanden ved relationer kendt som standardskaleringsrelationer. Vi undersøgte muligheden for at afvige fra standardskaleringsrelationerne for ORR, der finder sted over zirconiumoxynitrid-katalysator, som kan give anledning til forbedret elektrokatalyse.
I det andet studie udforsker vi elektroniske deskriptorer for at forudsige adsorptionsenergi af ORR-mellemprodukterne og følgelig ORR-aktiviteten over zirconiumbaserede katalysatorer. I løbet af vores første studie studerede vi adskillige deskriptorer, men ingen af dem kunne fange kompleksiteten af zirconiumoxynitrid-katalysatoroverfladen. ICOHP var tidligere med succes blevet brugt som en elektronisk deskriptor til at forstå tendenser i O*- og OH-adsorption på overgangsmetaloxider. Derfor undersøgte vi integreret krystalorbital Hamiltonian-population (ICOHP) som en elektronisk deskriptor for et forenklet modelkatalysatorsystem, dvs. anionsubstitueret zirconia.

List of Publications

Publications included in this thesis

- **Paper I**

  Bending the ORR Scaling Relations on Zirconium Oxynitride for Enhanced Oxygen Electrocatalysis
  Sukanya Sinha, Tejs Vegge, Heine A. Hansen,
  ChemCatChem(2023), 14, e202300349

- **Paper II**

  Understanding the electronic and structural effects in ORR intermediate binding on anion-substituted zirconia surfaces
  Sukanya Sinha, Tejs Vegge, Kirsten T. Winther, Heine A. Hansen,
  Submitted

Contents

List of Figures

1 Introduction

A key global challenge at present is the green transition from fossil fuels to more environmentally friendly energy conversion technologies. Currently, the leading contenders for alternatives to fossil fuel available commercially are hydroelectric power, nuclear energy along with wind and solar power [1]. While hydroelectric power is renewable and reliable, to harness the said power source, building dams is required for its implementation. This causes major environmental impact like deforestation, loss of habitat for different species, which can ultimately lead to their extinction. Inspite of its potential to generate large amount of electricity, nuclear power comes with its concern for safety and radioactive waste disposal [2]. When it comes to clean energy sources, the renewable energy sources are excellent contenders as they have a smaller impact on the environment [3]. However, the intermittent nature of the renewable sources have been a detrimental factor in their wide spread usage.

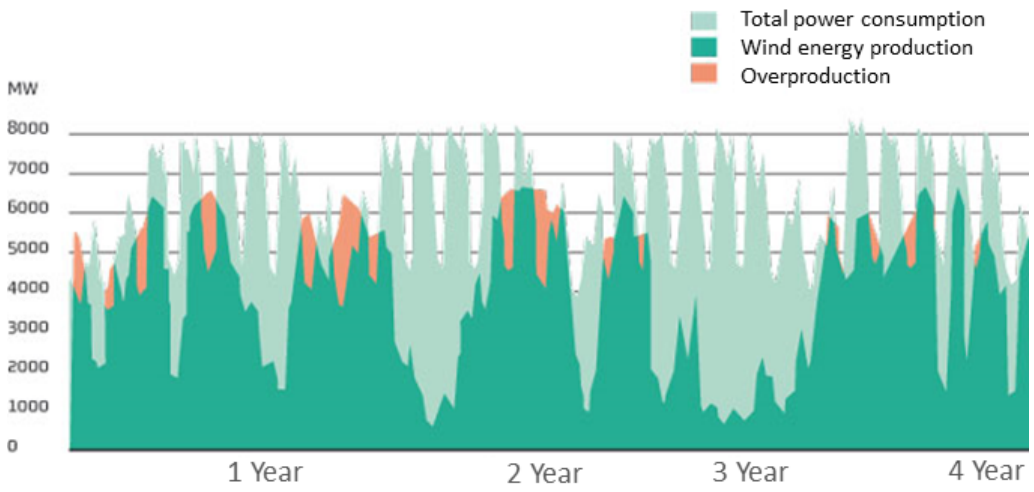

Figure 1.1: Plot of electricity consumption in light green and the wind power production in dark green. The x-axis is in weeks, covering a total of about a month. The orange areas represent overproduction, meaning that wind power alone produced more electricity than that was consumed at that time. Reproduced from reference [4].

One of the strategies of overcoming this bottleneck depends on reliable energy storage technologies, for example through the use of batteries. However such batteries might be massive as well as expensive and has a wide range of environmental impact, ranging from resource depletion of metallic and non-metallic raw material like lead, cadmium, graphite among others, generation of hazardous waste and emissions during manufacturing process transportation, disposal and recycling to human and animal health hazard from potential exposure to heavy metals used in batteries [5]. An alternative is to use excess electricity produced by renewable energy source to produce a fuel which can then be used in the transport sector which accounts for a sizeable segment of energy consumption [6].

1.1 Application in Transport Sector

A major challenge in green transition from fossil fuels to renewable energy sources lies in the transport sector. In terms of applications in the transport sector, liquid fossil fuels are particularly convenient with high gravimetric and volumetric energy density. It is difficult to achieve this using renewable sources of energy. We can observe from the figure 1.2 that liquid fuels, produced primarily from petroleum, have extremely high energy density both in terms of weight and volume. While it is possible to produce hydrocarbons from renewable energy sources using electrochemistry [7], the technology is not yet mature and would require a great deal of research efforts into the same [8, 9, 10, 11, 12].

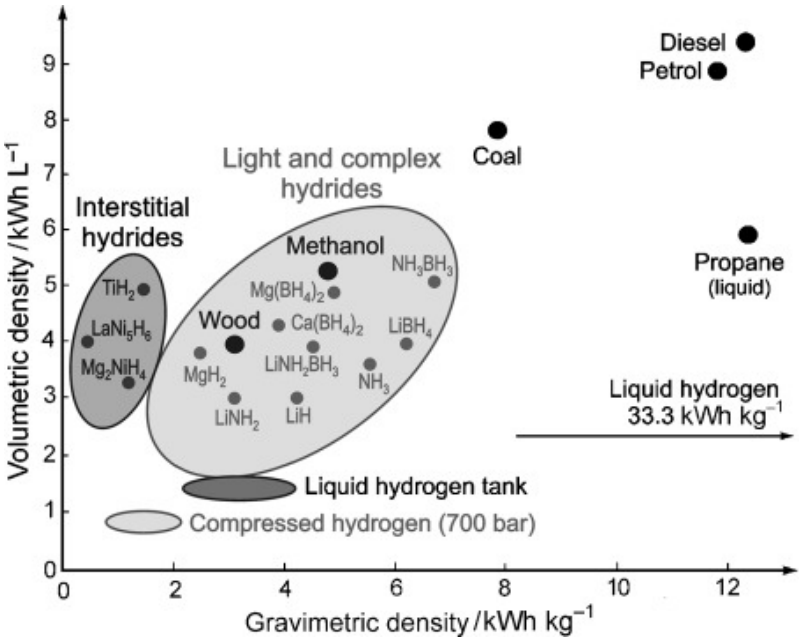

Figure 1.2: Plot of gravimetric vs volumetric energy density for various energy storage materials. The most desirable ones are in the top right corner. Reproduced from reference [13].

Another material with high gravimetric energy density is hydrogen which can be produced from water, through electrolysis, and then converted back to water producing electricity in a hydrogen fuel cell [14].

1.2 Fuel Cell Technology

Fuel cells are devices that can utilize fuels like hydrogen or methane, through electrochemical reaction, to produce electrical energy. Conventional power generation methods produce heat and mechanical work during intermediate steps, which is avoided in fuel cells. Since the fuel cells are not constrained by thermodynamic limitations like Carnot efficiency, theoretically they can be more efficient than heat engines. If hydrogen is used as a fuel in an internal combustion engine (ICE), the efficiency is in the range of 10 to 20% [15]. On the other hand, for hydrogen fuel cell, the ideal thermodynamic efficiency is about 83% at 25°C [16]. There are several different types of fuel cell technologies available, however in the present thesis the focus is on Polymer Electrolyte Membrane Fuel Cells (PEMFCs), illustrated in fig 1.3. PEMFCs allow environmentally friendly conversion of energy using hydrogen as a fuel to produce electricity. The quick start time and low operating temperatures, less than 100°C, low weight, compactness, and suitability for

discontinuous operation makes them particularly attractive option in terms of applications in transport sector [17, 18, 19, 20, 21, 22]. Storage of hydrogen in vehicles, in either compressed, liquefied or solid-solution state, is an obstacle. However this discussion is beyond the scope of this thesis.

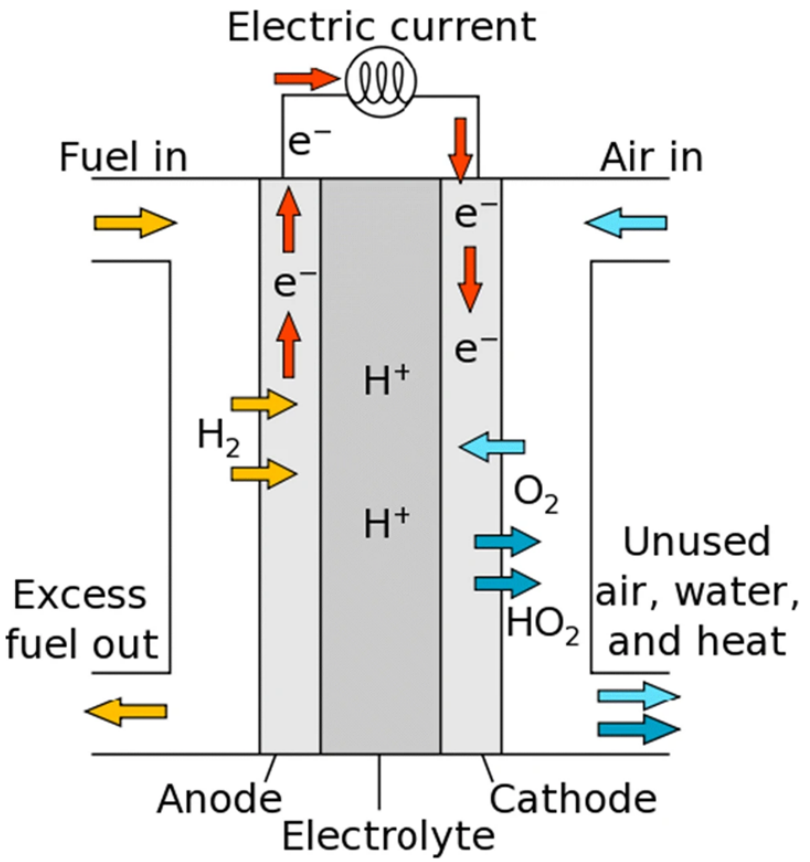

Figure 1.3: Schematic of a polymer electrolyte membrane fuel cell. Reproduced from reference [14].

There are various challenges that continue to limit the widespread use of hydrogen fuel cells, the most significant one being the high cost of the platinum-based catalyst used at the electrodes which contributes to almost 55% of the total cost [23]. Ideally to reduce the cost, catalyst at both the electrodes should be replaced. However the sluggish kinetics of Oxygen Reaction Reaction (ORR) at the cathode requires more catalyst than the fast Hydrogen Oxidation Reaction (HOR) at the anode. The sluggish kinetics of ORR can lead to nearly 30% decrease in the overall efficiency of PEMFCs [24]. The quest for cost-effective and efficient non-precious metal catalysts for the oxygen reduction reaction (ORR) has garnered significant interest [25, 26, 27, 28]. Potential alternatives include catalysts utilizing transition metals within nitrogen-doped graphitic cathodes [25], as well as oxides and oxynitrides of transition metals like tantalum [29, 30]. Additionally, catalysts based on zirconium oxide supported by multiwalled carbon nanotubes (MWCNTs) [31] and complex oxides of niobium and titanium have also been explored [32], among various other options.

1.3 The Oxygen Reduction Reaction (ORR)

Depending upon the solvent and catalyst used, ORR can proceed through either two electron or four electron pathway. The significance of reduction pathways varies depending on their specific applications. In the context of fuel cell processes, the four electron direct pathway is the particularly preferred since it maximizes the efficiency of the conversion of fuel (typically hydrogen) and oxygen into electricity and water. This pathway allows for a complete reduction of oxygen to water and minimizes the production of harmful byproducts or intermediates. Conversely, in industrial settings, the two electron reduction pathway finds utilization in the production of hydrogen peroxide [33].
The four electron pathway can involve either the associative or dissociative mechanism. The associative mechanism involves three distinct intermediates: *OOH, *O, and *OH. In contrast, the dissociative pathway only involves *O and *OH intermediates [34].
One is the 'associative mechanism' which can be described as follows:

$$* + O_2 + H^+ + e^- \longrightarrow *OOH \tag{1.1}$$

$$*OOH + H^+ + e^- \longrightarrow *O + H_2O \tag{1.2}$$

$$*O + H^+ + e^- \longrightarrow *OH \tag{1.3}$$

$$*OH + H^+ + e^- \longrightarrow * + H_2O \tag{1.4}$$

The other mechanism is called the 'dissociative mechanism' where the initial step is oxygen dissociation.

$$* + O_2 \longrightarrow *O \tag{1.5}$$

$$*O + H^+ + e^- \; *OH \tag{1.6}$$

$$*OH + H^+ + e^- \longrightarrow * + H_2O \tag{1.7}$$

where * denotes the active sites on the catalyst surface [35].

1.4 Non-PGM catalysts for ORR

The significant overpotential observed in ORR, coupled with other challenges such as the cost of catalyst materials and their instability during operation, has a profound consequence: at present, proton exchange membrane fuel cell (PEMFC) technology is prohibitively expensive to rival internal combustion engines in the automotive market. The most effective ORR electrocatalysts presently rely on rare and costly platinum. Consequently, the catalyst alone accounts for approximately 55% of the total cost associated with the PEMFCs [23].
A commonly discussed strategy involves enhancing the efficiency of platinum-based catalysts while simultaneously reducing the amount of platinum metal used. This dual objective can be realized, for instance, through the process of alloying platinum with other transition metals that are more affordable. Numerous comprehensive review articles describe this topic in detail [23, 36, 37, 38].
Scaling relations are the correlations present between the adsorptions energies of ORR intermediates over catalyst surfaces. Such correlations are, in several cases, unique to an intermediate pair and independent of the catalyst material itself. Hence scaling relations for ORR are also called standard scaling relations. A future-oriented approach is to discover a catalyst that does not adhere to the ORR scaling relations. Several strategies have been suggested to accomplish this, typically involving the introduction of a third dimension (like use of bi-functional catalysts or promoters, exposing interfacial sites or

electrolyte engineering among other. Refer to figure 1.4). Nonetheless, we are still awaiting experimental confirmation of this concept.

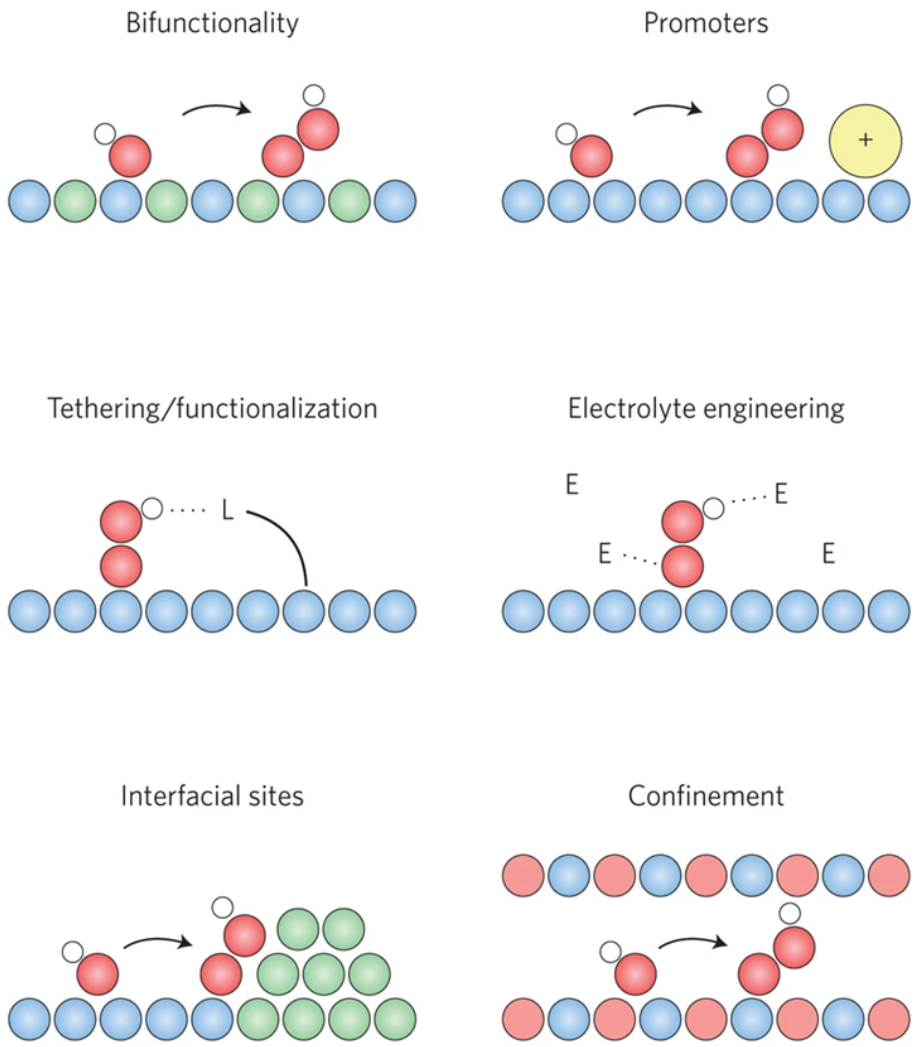

Figure 1.4: Approaches suggested to bypass the unfavorable scaling relations. Reproduced from reference [39].

Another frequently discussed strategy involves enhancing the performance of platinum-based catalysts while simultaneously reducing the platinum metal content. This can be accomplished by alloying platinum with other transition metals that are more cost-effective [23, 36, 37, 40].
At last, ORR catalysts have the potential to be composed entirely of non platinum group metals or in simple words non-PGM metals like tantalum, titanium, zirconium, iron, cobalt and others [29, 30, 31, 32]. Similar to platinum-based materials, the primary constraint on the performance of non-precious ORR catalysts is the presence of scaling relations. It is important to note that both groups of catalysts share the same highest theoretical activity but the inherently lower cost of materials makes non-precious substances especially intriguing as ORR catalysts. In this thesis, is investigated as a cost-efficient and effective alternative for the expensive platinum based ORR catalysts

1.5 Atomic Scale Modelling for ORR

Understanding the atomic-scale material properties is utmost significant in the discovery process of novel materials, also for catalytic processes, such as ORR. Computational methods like density functional theory (DFT) serve as potent instruments for comprehending the atomic-level mechanisms within electrochemical systems allowing us to gain insights and make predictions about material properties within areas that are challenging to access through experiments.
The application of DFT in the area of ORR catalysis is diverse and quite extensive:

- Studying the reaction mechanism and associated energy barriers. DFT can be used to investigate the adsorption and desorption of oxygen species on the catalyst surface and the associated energy barriers and provide insights into the rate-limiting steps [34, 35].
- Calculation of the adsorption energies of key reaction intermediates i.e OH*, OOH* and O* on catalyst surface can be done using DFT. These adsorption energies are crucial for understanding the thermodynamics of the ORR process [41].
- Studying the reaction mechanism and associated energy barriers of reactions taking place on catalyst surface for high throughput screening of various catalyst materials and their surfaces in order to determine the most promising ones [42].
- DFT can be used to determine the most active sites on a catalyst surface and gain understanding into the atomic configurations responsible for efficient ORR catalysis. This information can guide the design of improved catalysts [43].
- Understanding stability of catalyst materials under ORR conditions which in turn helps predicting their long-term durability and performance in practical applications can be assessed [44].
- Studing the kinetics of ORR, including reaction rates and activation energies to provide a comprehensive understanding of ORR [35].

Overall DFT plays a pivotal role in advancing the understanding of ORR catalysis and in the design and development of more efficient and sustainable catalyst materials for applications, such as fuel cells. Hence, atomic scale modelling techniques have unparalleled importance in development of the next generation of efficient, cost effective ORR catalysts.

1.5.1 Thesis Outline

This thesis consists of five chapters. The remaining four chapters are outlined below.

Chapter 2 introduces the computational techniques utilized in this thesis.

Chapter 3 is based on Paper 1 and presents a computational study of deviation of scaling relations for ORR taking place on zirconium oxynitride catalyst surface from standard ORR scaling relations.

Chapter 4 is based on Paper 2 and presents a computational study of ORR taking place on anion-substituted zirconia catalyst surface with integrated crystal orbital Hamiltonian population (ICOHP) as an electronic descriptor for prediction of O* and OH adsorption energies.

Chapter 5 summarizes the key findings and discusses possible routes of further study.

2 Theoretical Framework

This chapter gives a brief introduction on the basic theoretical framework used in the thesis including electronic structure problem and density functional theory.

2.1 Schrödinger Equation

From fundamental understanding of the atom, it is known that the nuclei and the electrons interact with each other via electrostatic forces of attraction. A fundamental property of any system is its energy which is determined by the atomic positions. The atomic energy and other ground state properties are determined through the solution of the Schrödinger Equation which is the quantum mechanics counterpart of the law of conservation of energy. The time independent Schrödinger Equation is given below:

$$\hat{H}\psi(\vec{R},\vec{r}) = E\psi(\vec{R},\vec{r}) \tag{2.1}$$

where $\psi(\vec{R},\vec{r})$ represents the wavefunction of the system and $\hat{H}$ represents the Hamiltonian operator containing the kinetic and the potential energy of the system. Determination of the Hamiltonian is the initial step for solving a Schrödinger Equation. The electronic Hamiltonian for a many-body system with N electrons and M nuclei written in atomic units is:

$$\hat{H} = -\frac{1}{2}\sum_{i=1}^{N}\nabla_i^2 - \frac{1}{2M_A}\sum_{A=1}^{M}\nabla_A^2 - \sum_{i=1}^{N}\sum_{A=1}^{M}\frac{Z_A}{r_{iA}} + \sum_{I=1}^{N}\sum_{j>i}^{N}\frac{1}{r_{ij}} + \sum_{A=1}^{M}\sum_{B>A}^{M}\frac{Z_A Z_B}{R_{AB}} \tag{2.2}$$

Equation 2.2 illustrates that Hamiltonian operator includes terms for kinetic and potential energies of atomic particles (electrons and neutrons).

2.2 Born-Oppenheimer Approximation

The exact solution of Schrödinger equation can be obtained only for the hydrogen atom. In fact, for practical materials solving the many-body Schrödinger equation is very complicated and impractical which has lead to development of several approximations.
One of the first simplification towards the solution is separation of electrons and nucleus into separate mathematical problems. The lightest existing nucleus, which is a proton, is almost 2000 times heavier than an electron, the movement of electrons can be separated from that of the nucleus. This is known as Born-Oppenheimer approximation [45].
Although the Born-Oppenheimer approximation simplifies the Schrödinger equation by making the wave functions independent of nuclear co-ordinates, the solution of the many-body Schrödinger equation requires enormous amount of computational resources. The interaction between the electrons by electrostatic forces further complicates the electronic Schrödinger equation. In order to further simplify the calculations, DFT solves the Schrödinger equation in terms of electronic density ρ(r) instead of electronic wavefunction $\psi(\mathsf{r}_1, \mathsf{r}_2, \ldots, \mathsf{r}_n)$.

2.3 Density Functional Theory

Over past years Density Functional Theory (DFT) has become a standard tool that is widely used in material sciences for modelling materials at atomic scale and predicting

their properties. One of the uses of DFT is the study of surface reactions at atomic level through analyses on the surface structure and calculation of adsorption energies. Thus, in this theses, DFT is used as a theoretical tool to investigate Oxygen Reduction Reaction (ORR) on zirconium based electrocatalysts.

2.4 Hohenberg-Kohn Theorem

Hohenberg-Kohn theorems,in their approximate form, are very extensively employed in quantum chemistry and condensed matter physics to determine electronic structure.
First Theorem: The external potential V_{ext}(**r**) is, within a constant, an unique functional of electron density, ρ(**r**). Since external potential fixes Hamiltonian $\hat{H}$, the full many particle ground state is a unique functional of n(**r**). Mathematically it can be represented as follows:

$$E[\vec{r}] = \int n(\mathbf{r}) V_{ext} d\mathbf{x} + F_{HK} \tag{2.3}$$

Second Theorem: The Hohenberg-Kohn functional F_{HK}(**r**) delivers the lowers energy if and only if the input density is the true ground state density, $\rho(\mathbf{r}_0)$. The above statement is also called variational principle.

$$E[n(r_o)] \leq E[n(\vec{r})] = \int n(\mathbf{r}) V_{ext} d\mathbf{x} + T_e[n(\mathbf{r})] + V_{ee}[n(\mathbf{r})] \tag{2.4}$$

2.5 Kohn-Sham Equations

Following the Hohenberg-Kohn theorems, the electronic structure problem can be constructed with the electron density as the fundamental variable. In the Hatree-Frock approach, the molecular wavefunction was a Slater determinant ϕ_{SD} constructed out of N-spin orbitals. The single Slater determinat actually is an exact N-electron wavefunction of non-interacting electrons moving in an effective potential V_{HF}. The kinetic energy of such a system is recovered by

$$T_{HF} = -\frac{1}{2} \sum_{i=1}^{N} \langle \chi_i | \nabla^2 | \chi_i \rangle \tag{2.5}$$

In DFT, we set up a non-interacting reference system with a Hamiltonian in which we have an effective potential V_s(r)

$$\hat{H}_s = -\frac{1}{2} \sum_{i=1}^{N} \nabla^2 + \sum_{i=1}^{N} V_s(r_i) \tag{2.6}$$

It is important to note that the above Hamiltonian contains the contributions from kinetic energy of electrons and effective potential. Hence, the operator does not contain electron-electron interactions making it a non-interacting system.
The problem of determining the kinetic energy of the system in Kohn-Sham approach is fragmented into determining the majority of the kinetic energy as much exactly as possible and the rest is then recovered in an approximate manner. The exact kinetic energy of a non-interacting reference system with the same density as the real one is obtained from Kohn-Sham orbitals as

$$T_S = -\frac{1}{2} \sum_{i=1}^{N} \langle \chi_i | \nabla^2 | \chi_i \rangle \tag{2.7}$$

This kinetic energy is not equal to the true kinetic energy of the interacting system even if the densities are the same. In the Kohn-Sham approach, this is handled by separating the universal functional as follows:

$$F[f(r)] = T_S[f(r)] + J[f(r)] + E_{XC}[f(r)] \tag{2.8}$$

where $T_S[f(r)]$ is the kinetic energy term for non-interacting system, $J[f(r)]$ is the columbic potential term and $E_{XC}[f(r)$ is the exchange correlation energy term.

2.6 Exchange correlation functionals

The exchange correlation energy is defined as follows:

$$E_{XC}[f(r)] = (T[f(r)] - T_S[f(r)]) + (E_{ee}(f) + J[f(r)]) \tag{2.9}$$

$$Or E_{XC}[f(r)] = T_C[f(r)] + E_{ncl}[f(r)] \tag{2.10}$$

$E_{ncl}[f(r)]$ is the non-classical electrostatic contribution. Therefore, it can be seen that the residual part of the kinetic energy is simply added to the non-classical part, altogether defined as exchange correlation energy. In other words, everything which is unknown is lumped in exchange correlation functional.
Now we focus on determining the Kohn-Sham orbitals of non-interacting reference system. For this we need to determine V_S which would provide us with a Slater determinant with exactly the same density as that of our real system. The energy of the interacting real system is given as

$$E[f] = T_S[f] + J[f] + E_{XC}[f] + E_N[f] \tag{2.11}$$

The individual terms can be written as:

$$T_S[f] = -\frac{1}{2}\sum_{i=1}^{N}\langle\chi_i|\nabla^2|\chi_i\rangle \tag{2.12}$$

$$J[f] = -\frac{1}{2}\sum_{i=1}^{N}\sum_{j=1}^{N}\int\int|\phi_i r_1|^2\frac{1}{r_{12}}|\phi_j r_2|^2 dr_1 dr_2 \tag{2.13}$$

$$E_N[f] = -\sum_{i=1}^{N}\int\sum_{A=1}^{M}\frac{Z_A}{r_{1A}}|\phi_i r_1|^2 dr_1 \tag{2.14}$$

No explicit form of $E_{XC}(f)$ is known. Now, the variational principle can be applied. Following this procedure it would be possible to identify orbitals (ϕ_i) which minimize energy expression under constraint $\langle\chi_i|\chi_j\rangle = \delta_{ij}$. As a result a set of equations is obtained which on comparison with one electron Kohn-Sham equation, we find that that V_{eff} = V_S.
the effective potential V_{eff} is a functional of density. Therefore, like Hatree-Frock equations, Kohn -Sham equations are also solved iteratively so as to attain self-consistency.

2.7 Crystal Orbital Hamiltonian Population

As compared to molecules, local bonding configurations in extended systems has recieved limited attention. Hughbanks and Hoffmann introduced a highly valuable and widely used tool within the framework of semi-empirical extended Hückel theory,[46, 47] specifically, a specialized tight-binding method with overlap. Once the electronic band

structure is computed, the Mulliken overlap population technique is employed for the crystal analysis. This involves investigating all energy levels within a specific energy range to determine their bonding tendencies[48]. Through this method, overlap population-weighted densities of states are established by assessing pairwise orbital interactions between two atoms using the product of the overlap matrix and density-of-states (DOS) matrix elements. As the energy levels progress through the bands, the bonding characteristics become apparent as a function of energy. The approach, known as the Crystal Orbital Overlap Population (COOP) method, functions as the solid-state counterpart to molecular bond order. COOP has discovered numerous intriguing applications in the analysis of bonding within extended materials and has become a standard tool for tight-binding Extended Hückel (EH) calculations [49]. When the weighing of the density of states is done by corresponding element of the Hamiltonian instead of the overlap population, the method is known as crystal Hamiltonian orbital population (COHP) [50].

3 Introduction Bending ORR Scaling Relations

This chapter presents the work in paper 1 - *Bending the ORR Scaling Relations on Zirconium Oxynitride for Enhanced Oxygen Electrocatalysis* . The paper is included in this thesis. The text is taken directly from the paper with minor changes for the purpose of the thesis. The corresponding supporting information can be found in Appendix A.

3.1 Introduction

Ideal electrocatalysts for hydrogen fuel cells should allow reversible reaction. For ORR to be reversible the adsorption Gibbs energy (ΔG_{ads}) profile plotted along the reduction steps should be flat [34, 51]. None of the currently identified catalysts, however, satisfy the ideal ORR condition. Even on a platinum surface, the ORR intermediates HOO* is adsorbed too weakly and HO* too strongly.
Nevertheless, finding a material with larger (ΔG_{OOH}) and smaller (ΔG_{OH}) is restricted by the linear scaling existing within the (ΔG_{ads}) of the reaction intermediates which is observed almost universally for many materials [51, 52]. Scaling relations refer to the correlation between binding energies of different reaction intermediates. One can explain universal scaling of ORR as strong adsorption of HOO* on a metal surface being associated with similarly strong adsorption of HO* on the same when both adsorbates have similar bonding configuration with the surface. However, this might not hold true for complex oxides and oxynitrides of transition metals since they allow various bonding configurations. These oxides and oxynitrides can provide different adsorption sites like the lattice oxygen, metal sites, oxygen vacancy or impurity sites [53]. Computational investigations of ORR on defective titanium oxide surfaces indicate possible deviations from the standard scaling relations [53]. Experimental investigations also reveal that several transition metal complex oxides and oxynitrides, like that of zirconium, titanium and tantalum, show promising activity as ORR catalysts in terms of lower overpotential than platinum ORR catalysts [31, 53, 54]. Hence, we would like to explore the possibility of oxynitride of another transition metal, i.e. zirconium, exhibiting deviations from standard scaling relations while showing lower overpotential than the standard platinum catalysts.

3.2 Computational Details

All density functional theory (DFT) calculations are done using the Vienna Ab Initio Simulation Package (VASP) and the core electrons are described with the projector augmented wave (PAW) method [55, 56]. The Perdew-Burke-Ernzerhof functional (PBE) is used to describe the exchange and correlation energy [57]. The Atomic Simulation Environment (ASE) is used to set up and analyse the structures, which are optimised with a plane wave cutoff of 500 eV and Brillouin-zone integration is performed with a Monkhorst-Pack k-point mesh of 2x2x1 [58, 59]. The self-consistent electron density loop is converged to 10^{-6} eV and the structures are relaxed until all forces are below 0.02 eV $\mathring{A}^{-1}$.
We have studied the (111) surface of zirconium oxynitride (Zr_2ON_2) which is modeled by a periodic non-polar slab. The model includes 3 cationic layers with the bottom layer fixed in its position and the upper two layers allowed to relax. The associative mechanism for ORR, given below, is well established, where the reaction proceeds through four electron-proton transfer steps [35].

$$* + O_2 + H^+ + e^- \longrightarrow *OOH \tag{3.1}$$

$$*OOH + H^+ + e^- \longrightarrow *O + H_2O \tag{3.2}$$

$$*O + H^+ + e^- \longrightarrow *OH \tag{3.3}$$

$$*OH + H^+ + e^- \longrightarrow * + H_2O \tag{3.4}$$

where * denotes the active sites on the catalyst surface.

3.2.1 Adsorption Free Energy

The standard computational hydrogen electrode (CHE) approach is used to calculate the reaction free energies of electrochemical reaction steps.[34] Using the CHE, the reaction free energy, ΔG_i, of a reduction step can be written as

$$\Delta G_i = \Delta G_i^0 + eU \tag{3.5}$$

where ΔG_i^0 is the reaction free energy at 0 V versus the reversible hydrogen electrode (RHE) and U_L is the potential measured against the reversible hydrogen electrode. The DFT reaction energy corresponding to the following reactions are defined here as the adsorption energies.

$$* + H_2O \longrightarrow *O + H_2, \qquad \Delta_{ads}\ E(O*) \tag{3.6}$$

$$* + H_2O \longrightarrow *OH + 0.5H_2, \qquad \Delta_{ads}\ E(OH) \tag{3.7}$$

$$* + 2H_2O \longrightarrow *OOH + 1.5H_2, \qquad \Delta_{ads}\ E(OOH) \tag{3.8}$$

For the adsorbed species, the Gibb's free energies are calculated using the ASE package with the assumption that adsorbate degrees of freedom can be approximated by independent quantum mechanical harmonic oscillators and the vibrational frequencies of only the adsorbates are calculated. The free energy calculations for gas molecules are carried out with the ideal gas approximation [60] and those for adsorbates are carried out with harmonic approximation [61, 62, 63] where finite differences with 2 displacements of 0.01 $\mathring{A}$ are used to calculate force constants. The Gibb's free energy includes the zero point energy and entropy. For the gas phase molecules, Gibb's free energies are calculated assuming them to be ideal gas molecules.

$$\Delta\ G(U=0) = \Delta\ E_{DFT} + \Delta\ E_{ZPE} + \Delta\ U_{vib}(T) - T\Delta\ S_{vib}(T) \tag{3.9}$$

Here, the Δ G is calculated from DFT and it includes changes in electronic energy (Δ E_{DFT}) along with contributions from zero-point energy (Δ E_{ZPE}), vibration energy (Δ U_{vib}(T)) and entropy (Δ S_{vib}(T)) at T=298.15K.

We use the equilibrium potential derived from DFT calculations in this study which is determined to be 1.15V, slightly lower than the experimentally determined one of 1.23 V. The experimentally determined equilibrium potential corresponds to the value of reaction free energy of the overall reaction ($O_2 + 2H_2 \rightarrow 2H_2O$) that is 4.92 eV. However, the calculated value of equilibrium potential of 1.15 V is determined for our calculations of the H_2O formation free energy of 2.3 eV with the PBE functional. A simple one-to-one correspondence between equilibrium potential and adsorption free energy helps us determine the theoretical equilibrium potential of 1.15 V. Difference is due to DFT error on the reaction energy.

3.3 Results and Discussion

3.3.1 Structure of Zirconium Oxynitride

Zirconium Oxynitride are compounds with structure similar to fluorite type crystal in which part of oxygen of zirconia is replaced by nitrogen and anion vacancies. Zr_2ON_2 crystal belongs to space group Ia-3 (206) or according to the Pearson notation has the Pearson

symbol of cI80 [64, 65]. The Pauling electronegativity difference between for oxygen (3.50) and nitrogen (3.07) gives the oxynitride covalent characteristics, which different from oxides with ionic characteristics [66], Bulk optimisation of the representative structure of Zr_2ON_2 gives us a cubic lattice crystal structure with lattice constant of 1.01 nm which agrees very well with the experimental value of 1.0135 nm [64]. In our study we are exploring ORR on the (111) surface of Zr_2ON_2 slab [67, 68, 69]. It has a hexagonal lattice structure with lattice parameter a=1.42 nm and a total vacuum of 1.6 nm (with 0.8 nm on both side of the slab).

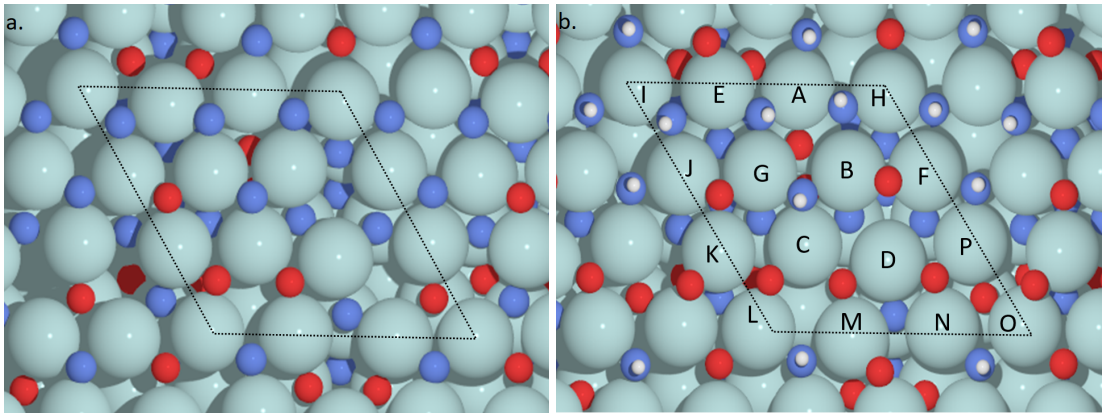

Figure 3.1: Geometries of Zirconium OxyNitride. (The light cyan atom is Zr, red is O, blue is N and white is H) a) Stoichiometric slab b) Hydrated slab: Stoichiometric slab with dissociated water adsorbed on the surface. The letters on the zirconium atoms indicate the nomenclature of the ontop-Zr sites.

Water, being one of the products of the ORR, is expected to be present in the fuel cell, hence we investigate the possibility of water molecule(s) interacting with and dissociating on the catalyst surface. From Pourbaix stability analysis [70], we conclude that water molecules interacts with the catalyst surface, dissociates over it and gets adsorbed on the surface. Various dissociation and the subsequent adsorption mechanism is studied as illustrated in Figure 3.1c. We presumed the water molecule could, potentially, split in different ways, either into an O atom and an OH ion or an O atom and two H atoms. These species, so formed, could further be adsorbed on the surface in many different ways. For example, the OH ion could be adsorbed into an intrinsic vacancy site and H on a surface N. Further, we have also tested low coverage ('1 site') and high coverage ('4 sites') configuration. The entries in the legend of Fig3.1c represent the different configurations tested. The subscript V denotes an interstitial vacancy site, and the subscript L denotes a lattice site; for example, N_L and O_L represents nitrogen and oxygen lattice adsorption site. O_V in the label stands for an oxygen atom getting adsorbed in an intrinsic vacancy site. In contrast, an N_L and O_L associated with H is a hydrogen atom getting adsorbed over an oxygen or nitrogen atom lattice. For example, the (O_V+N_LH+$N_L H_2$) would stand for the configuration where, after the water split, the O atom has adsorbed into an intrinsic vacancy site. In contrast, one H atom has adsorbed onto a surface N while two have adsorbed onto another N. According to the stability plot for water splitting over Zr_2ON_2 slab, the energetically most favorable configuration is water dissociating into an O atom and two H atoms with the O getting adsorbed in the intrinsic anion vacancy sites and the H on surface N, the configuration of the same is illustrated in 3.1b. The structural illustration for the rest of the configurations of water splitting has been provided in Appendix A. The catalytic activity of the hydrated Zr_2ON_2 towards ORR is evaluated systematically by

studying all the Zr-ontop site for their ORR activity.

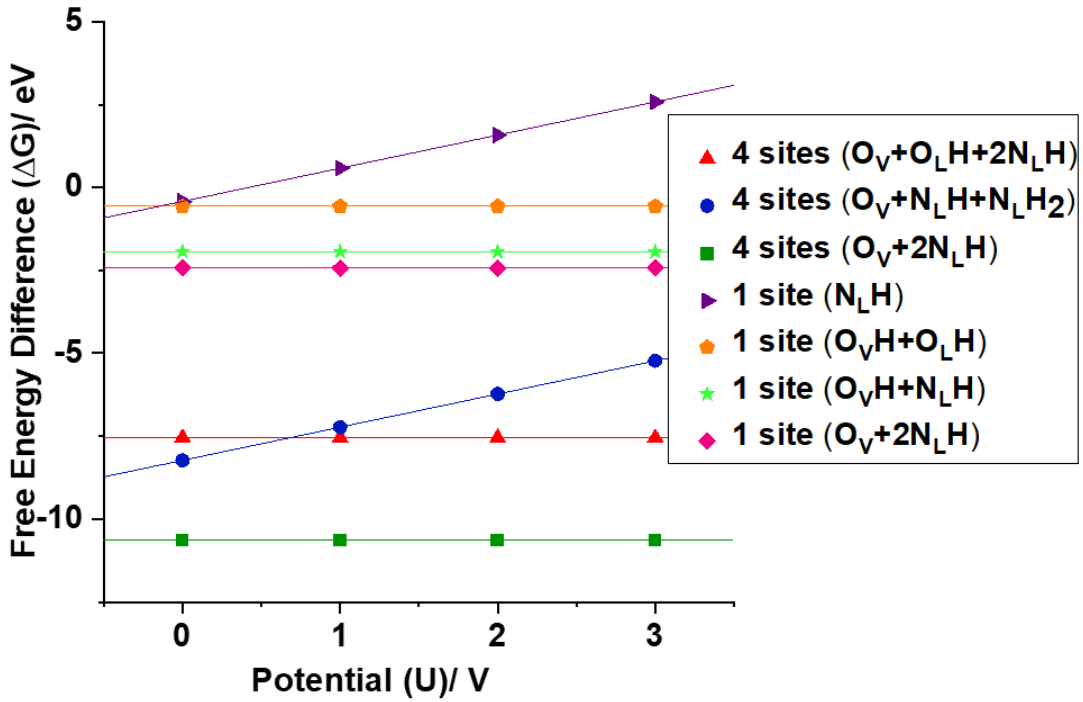

Figure 3.2: Stability plot for water splitting over Zr_2ON_2 slab

3.3.2 Free Energy Diagram

It is assumed the ORR catalysed by Zr_2ON_2 proceeds through an associative mechanism, which involves hydrogenation of adsorbed molecular oxygen on the catalytic surface [71] which is evidenced from the free energy diagrams (FED) in figure 3.3. The possibility of ORR on stoichiometric Zr_2ON_2 surface taking place through dissociative mechanism was also investigated. Since the dissociative mechanism involves direct dissociation of O_2 without the formation of the OOH* intermediate, the energy barrier of O_2 dissociation is relevant in this scenario. Our test calculations found a high O_2 dissociation barrier in the range of 1.2 to 1.55 eV. A barrier of more than 0.8 eV is generally considered unfavorable for the dissociative mechanism at low temperature; therefore, we concluded that the Zr_2ON_2 surface favours the associative mechanism for ORR.

We calculated the Gibb's free energy of adsorption for the three ORR intermediates i.e. hydroxyl (OH*), hydroperoxyl (OOH*) and oxide (O*) using the computational hydrogen electrode (CHE) approach and have investigated all the Zr-ontop sites as potential catalytic sites and the free energy diagrams (FED) show that majority of them provide stable binding sites for these ORR intermediates. We had also sampled various orientations of the adsorbates over the Zr_2ON_2 slab and the reported adsorption energies correspond to the geometric configurations that give us the lowest adsorption energy. With respect to adsorption of different intermediates on the catalytic sites of the hydrated Zr_2ON_2(111) slab, we can make certain observations. During adsorption of OH and OOH intermediates; they adsorb directly on all of the ontop Zr sites. Although for most of the ontop-Zr catalytic sites, direct adsorption of the O* intermediate also takes place, for certain sites they form NHO* or O-O* peroxide-like intermediates upon adsorption. Even in the cases where there is no complex formation, we can see some of the O* adsorbs on the Zr-ontop sites while others move towards a bridge site.

The FEDs for each adsorption sites are initially constructed at the equilibrium potential. (All the FEDs are provided in Appendix A). The favourable ORR catalytic sites are the ones for which the constructed FEDs have reaction steps have potential energy that are downhill at the highest possible potential. Within the CHE model the highest potential at which all the reaction steps are downhill in free energy is called the thermodynamic limiting potential, (U_L). The theoretical overpotential (η) is defined as the difference between the equilibrium potential and the values of U_L. The η as well as the U_L gives us the measure of the activity of a catalyst. Higher the U_L and correspondingly lower the η implies higher catalytic activity.
In figure 3.3, the FEDs have been drawn at an overpotential of 0.4V. A FED constructed at equilibrium potential is provided in Appendix A for reference. In figure 3.3, we have different subfigures corresponding to different adsorption configuration of the O* intermediates. Since adsorption of OH* and OOH* intermediates are similar, directly on the ontop-Zr sites, we have chosen adsorption of O* intermediate as the differentiating factor to group different FEDs. Hence we have a subfigures which are FEDs corresponding to situations where formation of NHO* complex, O-O peroxide like complex or no complex forms upon adsorption of O*.
When we observe all the FEDs together, we can observe that there are different values of U_L corresponding to every Zr-ontop sites. The values for the U_L and η corresponding to every Zr-ontop sites is given in Table 1 of Appendix A. This brings us to the conclusion that different catalytic sites possess different catalytic activity, where the sites with higher U_L are more active. We observe the presence of two catalytic sites where the U_L is negative; this means those two sites are unfavorable for the ORR in an H_2 fuel cell. These two sites, site A and C, along with another site, G, with very low limiting potential (U_L=0.1), are the ones where formation of a NHO* complex takes place upon O* adsorption. The FED corresponding to site A is illustrated in figure 3.3a. Hence this leads us to believe that the formation of this NHO* complex leads to deactivation or very low activity of the catalytic sites. We also notice the formation of a peroxide-like complex upon O* adsorption on certain sites. For sites B, F, and K the value of U_L is high (<0.5V) while for other site E it is low (>0.15V) Hence it can be concluded that the O-O peroxide-like complex formation does not seem to have any effect on the catalytic activity of those sites. For most of the sites, however, the adsorption of O* does not give rise to formation of any complex.
We have also, very briefly, explored the possibility of Zr_2ON_2 surface as a catalyst for oxygen evolution reaction (OER). The reader can refer to Appendix A regarding the same.
We had investigated the possibility of the Zr_2ON_2 surface undergoing a Mars van-Krevelen mechanism [72] involving N or O vacancies and computed the O and N vacancy formation energies for the same. However the O and N vacancy formation energies were quite high, in the range of more than 2 eV for N-vacancy formation and around 3.5 eV for O-vacancy formation. These values lead us to conclude that such a mechanism was unlikely to take place on the Zr_2ON_2 surface. A detailed table with all the vacancy formation energies is given in Appendix A. Additionally, vacancy formation energy values indicate the stability of the Zr_2ON_2 surface. This conclusion is also corroborated by various experimental studies.[73, 74]

3.3.3 Scaling Relations

Observing figure 3.4a and 3.4b, we can conclude that scaling relations exist between the ORR intermediates on Zr_2ON_2 catalyst. The OOH* or O* vs OH* scaling relations imply that there exists a single independent variable that can be used to describe the binding energies of all the ORR intermediates on the catalyst surface. We have used OH adsorption free energy as the descriptor for our scaling relations. (Note: The O* adsorption energies corresponding sites where NHO* complex formation takes place are not included in the

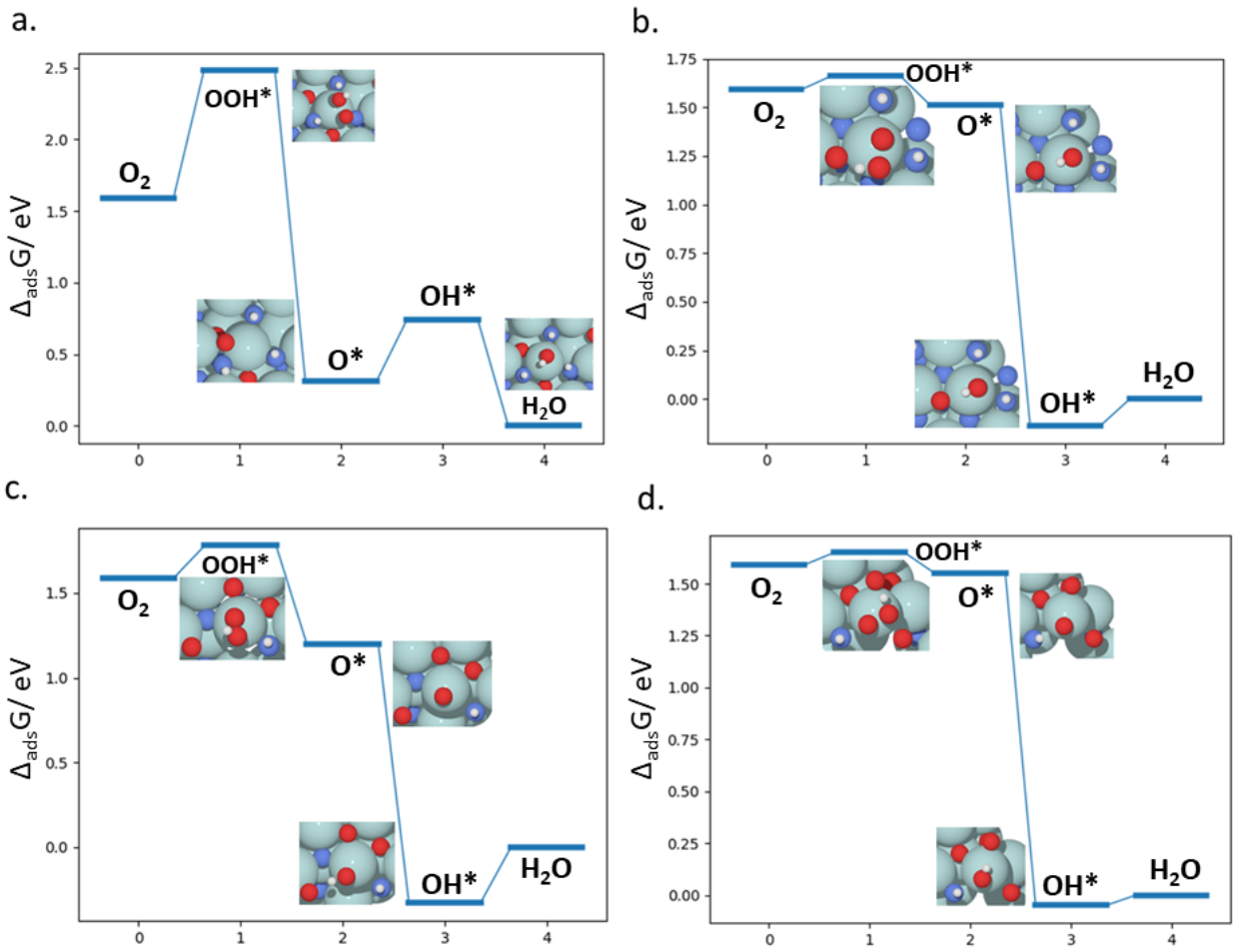

Figure 3.3: Free energy diagrams for the ORR taking place over selected catalytic sites (The light cyan atom is Zr, red is O, blue is N and white is H) A) Site A where NHO* complex formation takes place. B) Site F where O-O peroxide like complex formation takes place. C) Site N with no complex formation. D) Site O with no complex formation.

G_{O*}-G_{OH} scaling relation since they form outliers.) Since the theoretical overpotential is a function of free energy and correspondingly that of binding energy, scaling relations are also used to determine the limiting potential. From the scaling relation plots in Figure 3.4, it can be seen that there exists a linear correlation between the the adsorption energies of OOH* and O* vs OH*. The scaling relations that are determined for the Zr_2ON_2 catalyst from the adsorption energies of the intermediates are as follows:

$$\Delta G_{OOH} = 0.78\Delta G_{OH} + 3.52 \text{ eV} \tag{3.10}$$

$$\Delta G_{O*} = 1.04\Delta G_{OH} + 2.16 \text{ eV} \tag{3.11}$$

The determined scaling relation for G_{OH}-G_{OOH} is comparable to that of the standard ORR scaling relation

$$\Delta G_{OOH} = \Delta G_{OH} + 3.2 \text{ eV} \tag{3.12}$$

however the one for G_{O*}-G_{OOH} deviates dramatically from the typical ORR scaling relation

$$\Delta G_{O*} = 2\Delta G_{OH} \tag{3.13}$$

The standard scaling relation is typically observed for a wide range of materials like porphyrins [75], boron nitride [76], MoS_2 [76], ultrathin metal oxide sheets,[76] MN_4 motifs in graphene[76], carbons and HAB-based coordination polymers [51, 77]. A previous study [35] reports scaling relations for platinum slab with explicit solvation with no significant deviation from the standard scaling relation. This leads makes us believe hydration is not the reason for the dramatic deviation of the G_{O*}-G_{OH} scaling that we observe here.
As we have discussed earlier, the OH and OOH intermediates adsorb directly on all of the ontop Zr sites without exception. However this is not true for the O* intermediate. On few sites it forms complexes like the NHO* complex or O-O* peroxide-like complex. Even in absence of complex formation, adsorption on bridge sites is observed for some sites while for others absorption on ontop sites is observed. We refer to this phenomena as the atypical adsorption of O* intermediate on the Zr_2ON_2 surface and believe this is the cause for deviation in OOH vs O* scaling relation. This is evident from 3.4b where we can see the outliers circled in blue corresponding to sites where NHO* formation takes place. Hence we believe the atypical adsorption of O* intermediate also causes the deviation in $\Delta G_{O*} = 2\Delta G_{OH}$ scaling relation.

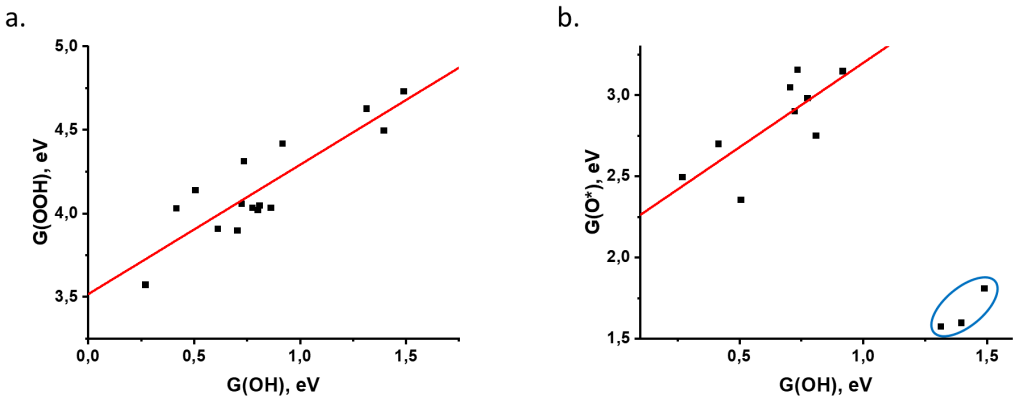

Figure 3.4: Scaling relations for adsorption energies of ORR intermediates at ontop Zr sites. A) Scaling relation between OH and OOH intermediates. B) Scaling relation between OH and O* intermediates.

3.3.4 Volcano Plot

While discussing the binding energies of the ORR intermediates to the catalytic sites on the Zr_2ON_2 surface it is worth mentioning that most sites bind the ORR intermediates too weakly. Hence, contrary to many transition metal ORR catalysts where *OH $\longrightarrow$ *H_2O is the potential limiting step [78, 70], in case of Zr_2ON_2 catalyst O_2 activation, O_2 $\longrightarrow$ *OOH, is the potential limiting step for majority of the catalytic sites. To maximise the descriptive power of the volcano plot, we therefore use *OOH adsorption free energy as the descriptor instead of using *OH adsorption free energy. The volcano plot with the commonly used *OH descriptor is shown in Appendix A. The volcano indicates that the minimum theoretical overpotential of the Zr_2ON_2 catalyst is around 0.45 eV. This value of overpotential is in agreement with the experimentally determined values for ZrO_xN_y-MWCNT catalyst at a current density of 0.1 A cm$^-2$ [31]. Similar values have been reported by other experimental studies as well [79, 80, 81]. The weak binding of ORR intermediates further agrees with the experimentally observed O_2 reduction [82]. The weak binding of reaction intermediates also indicates that several sites are also selective for the 2 electron pathway of ORR [82].

The scope of our study is limited to the thermodynamics of reaction intermediates, which have been found to well describe trends in ORR activity on the terraces of metal surfaces well. Incorporating surface kinetics is expected to provide similar trends as the thermodynamic analysis while suppressing the activity around the apex of the volcano [83].

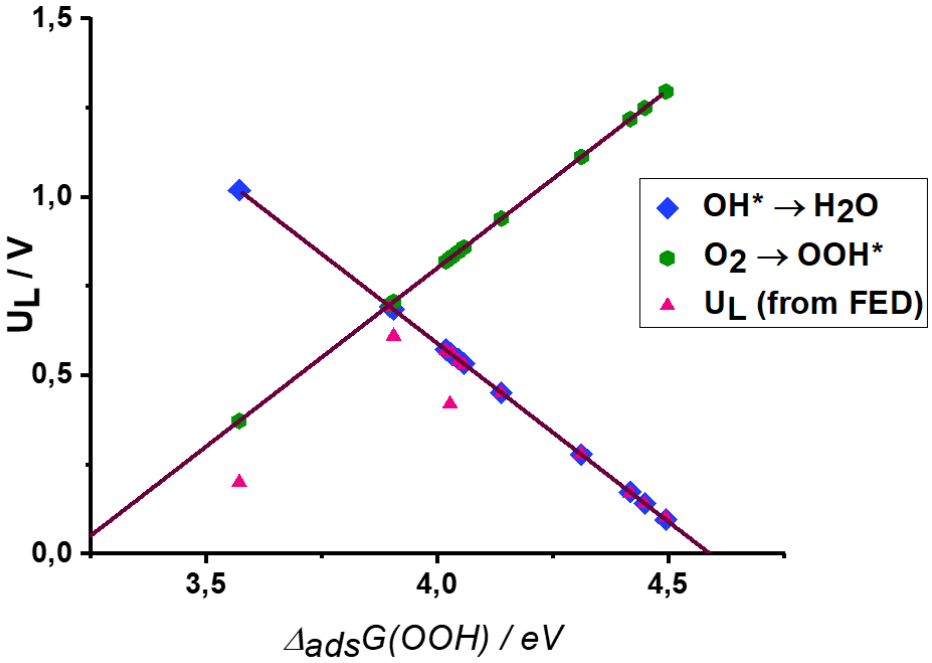

Figure 3.5: Volcano plot with OOH adsorption free energy as the descriptor.

3.3.5 Density of States

The total and partial density of states (TDOS and pDOS) are plotted to clarify the bond formation. As SCAN functional is better suited for computing band gaps, we use it for our density of states calculations [84]. In our DOS plot the Fermi level (E_f) is at 0 eV. Fig. 3.6 shows the total and partial density of states of stoichiometric Zr_2ON_2 slab.

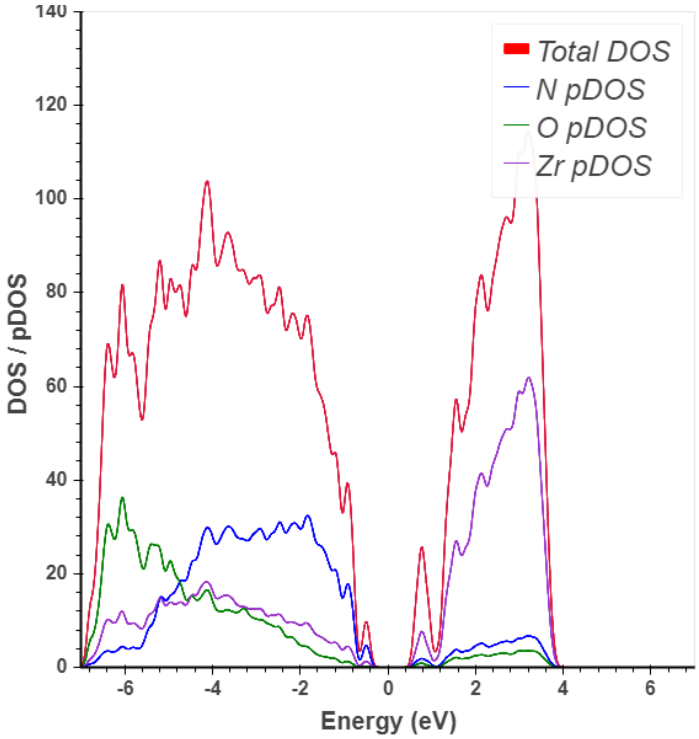

Figure 3.6: Calculated total and projected density of states for Zirconium Oxynitride for Stoichiometric slab

Fig. 3.7 shows the total and partial density of states of hydrated Zr_2ON_2 slab and a hydrated Zr_2ON_2 slab with an O* adsorbate. From the figure 3.6 and 3.7a, we can see that the there is a reduction of band gap upon hydration of the Zr_2ON_2 slab. The stoichiometric slab has a band gap of 0.8 eV which reduces to 0.4 eV when the slab is hydrated. This implies that the hydration of the slab makes it a better conductor. The fermi level is within the band gap, and the top of the valence band is formed mainly by N 2p states and to a lesser extend O 2p and Zr states. The conduction band has mainly Zr 3d character. As we can see from 3.7a and 3.7b, there is a increase in DOS and N pDOS intensity around the E_f upon adsorption of O* on the hydrated Zr_2ON_2 slab. Upon adsorption of O*, the fermi level moves below the top of the valence band indicating that N, O, and Zr contributes with charge to bind the O* adsorbate. The magnitude of DOS at E_f can serve as indicator for the ability to form bonds with adsorbed species [85]. Along with the DOS and pDOS plots, we have also studied several electronic properties like band centre, band-width and fractional band filling [86, 87, 88]. We have also tried to find out if relationships between electronic properties and binding energies exist. However none of the analysis carried out could capture the complexity of the Zr_2ON_2 catalyst.

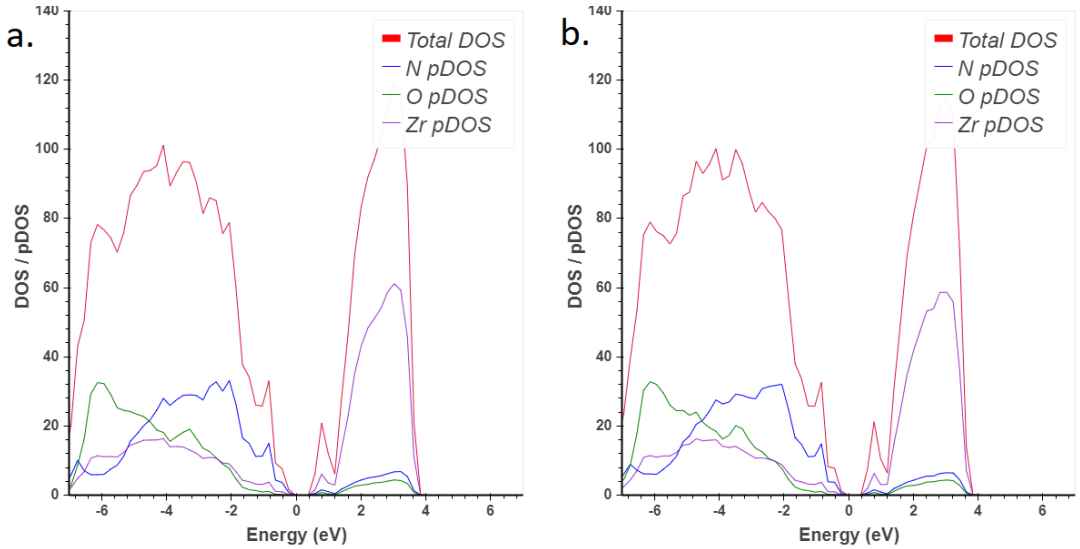

Figure 3.7: Calculated total and projected density of states for Zirconium Oxynitride. A) Hydrated slab: Stoichiometric slab with dissociated water adsorbed on the surface B) Hydrated slab with O* adsorbate on ontop Zr site O.

In charge density difference maps (present in Appendix A) we can see two different kinds of spatial distribution of electronic charge density denoted by different colours. The yellow regions signify increase in electronic charge density and blue region signify decrease in electronic charge density in those regions. This helps us to draw the conclusion that the charge transfer occurs at the adsorption site. Most significant charge transfer is near the surface with the charge being transferred from the zirconium atom to the O* adsorbate. Some charge transfer is also observed for the neighbouring nitrogen and oxygen atoms near the ontop-Zr sites.

3.4 Conclusion

Our DFT calculations show that Zr_2ON_2 is a viable candidate as an ORR catalyst with Zr-ontop sites acting as the active catalytic sites. However, the sites that shows NHO* complex formation during O* adsorption are either inactive or very mildly active sites. Ideal electrocatalysts for ORR must allow it to occur reversibly and complex oxides of transition metals are viable candidates for the same [89]. Our calculations also revealed that the universal scaling line between O* and OH* adsorption free energy can be broken by using a complex oxide surface of a transition metal oxynitride. This does, however, not lead to improved ORR activity. On the basis of scaling relations, we also plot the activity volcano which helps us draw the conclusion that the maximum limiting potential for the Zr_2ON_2 catalyst is approximately 0.70V which agrees with the experimentally determined onset potential [31, 79, 80]. From the ORR kinetics and FEDs of individual catalytic sites we also understand that all sites are not equally active.

4 Electronic and Structural Effects of ORR catalyst on Intermediate Binding

This chapter presents the work in paper 2 - *Understanding the electronic and structural effects in ORR intermediate binding on anion-substituted zirconia surfaces*. The paper is included in this thesis. The text is taken directly from the paper with minor changes for the purpose of the thesis. The corresponding supporting information can be found in Appendix B.

4.1 Introduction

In the PEMFCs, oxygen reduction reaction can take place through two different pathways at the fuel cell cathode, the two-electron pathway and the four-electron pathway [82]. However, for the PEMFC cathodic catalyst, the two-electron pathway is not desirable; it is the four-electron pathway which is preferred for the long-term operation of PEMFC. The four-electron pathway can involve two different mechanisms [34].

One is the 'associative mechanism' which involving three intermediates hydroperoxyl ion (OOH), hydroxyl ion (OH) and oxygen radical (O*). While the other mechanism is called the 'dissociative mechanism' where only two intermediates are involved OH and O* intermediates [35].

Previous studies have demonstrated O* and OH intermediates are the key descriptors that can help in predicting the ORR activity of catalysts [34, 51, 83]. While there are a number of studies which has studied the relative binding energies of these two species in terms of scaling relations [90, 91], their underlying descriptors are not very well-understood [51, 92]. Fung et al showed that the integrated crystal orbital Hamiltonian population (ICOHP) [50] of the bond between lattice metal and oxygen is a good descriptor for the adsorption energy of hydrogen on lattice oxygen in perovskites [93]. More recently Winther et al demonstrated that the O and OH adsorption energies on transition metal MO_2 surfaces is well captured by the metal-oxygen ICOHP of the bulk oxide [94]. In this work, we are studying the trends in the adsorption energy of O* and OH adsorbates on the surface of anion-substituted zirconia. We find that in the absence of structural reorganization in the zirconia slabs the adsorption energies are captured by the integrated COHP with a high accuracy.

While a number of studies has previously reported zirconium oxynitride (Zr_2ON_2) as an promising alternative to platinum based ORR catalysts [31, 80], the reason behind the favourable ORR activity of the same is not well understood. A number of transition metal-based ORR catalysts which show promising ORR activity [29, 30, 31] also exhibits deviations from standard scaling relations [53]. It is generally accepted that deviation from these scaling relations is the key to enhanced ORR electrocatalysis [95]. In our previous work we have explored the possibility of enhanced ORR activity due to bending of ORR scaling relations [43]. We concluded that the G_{O*}-G_{OH} scaling relation for ORR on Zr_2ON_2 catalyst indeed shows deviation from the standard scaling relation, however, there was no indication that it necessarily results in enhanced electrocatalysis. Several electronic descriptors failed to capture the complexity of the Zr_2ON_2 catalyst surface that arises from presence of two different anions i.e. oxygen and nitrogen in the anionic layers. Hence, in order to simplify the system, we have created model systems where we substitute one or two lattice oxygen for a carbon or two nitrogen atoms for this study. Further, we use ICOHP as an electronic descriptor for describing trends in the adsorption energies

of the O* and OH adsorbates as well as to gain insights into bonding configurations of the same.

4.2 Computational Details

All the DFT calculations have been performed using the Vienna Ab Initio Simulation Package (VASP) [55] and the core electrons are described with the projector augmented wave (PAW) method [56]. To describe the correlation and exchange energy the Perdew-Burke-Ernzerhof functional (PBE) [57] is used. The Atomic Simulation Environment (ASE) [58] is used to set up and analyse the structures, which are optimised with a plane wave cutoff of 500 eV and Brillouin-zone integration is performed with a Monkhorst-Pack k-point mesh [59] of 2x2x1. All the calculations were done with spin polarization. The self-consistent electron density loop is converged to 10^{-6} eV and the structures are relaxed until all forces are below 0.02 eV $\mathring{A}^{-1}$.

We have studied nitrogen and carbon substituted zirconia slabs. The model includes three cationic layers with the bottom layer fixed in its bulk position and the upper two layers are allowed to relax. A high throughput workflow was used to create the nitrogen and carbon substituted zirconia slabs. Another similar high throughput workflow was used to optimize the slabs and carry out the adsorption calculations for the different ORR intermediates. The workflow was interfaced with the Atomic Simulation Environment (ASE) and was managed with the workflow management software, MyQueue [58, 96].

The Lobster package [97] was used to perform COHP calculations. The calculations were started from re-converging electronic structure with symmetry being disabled. ICOHP between all pairs of atoms were included in the Lobster calculation up to a radial cutoff of 3 $\mathring{A}$ were investigated. More specifically we focus on the bond between the adsorbed oxygen, and the surface Zr, C and N atomic species.

4.3 Results and discussion

4.3.1 Nitrogen and Carbon substituted Zirconia

Zirconia is a crystalline compound with polymorphic crystal structure and exhibits three different crystalline forms: monoclinic, tetragonal and cubic form [98, 99]. Previous studies have demonstrated the tetragonal phase shows the highest ORR activity among all three, hence that is the phase we have selected for our study [100]. Our selected ZrO_2 crystal belongs to space group $P4_2/nmc$ (137) or according to the Fedorov notation has the Fedorov symbol of 67a [101]. In our study we are exploring adsorption of ORR intermediates on the (011) surface of a ZrO_2 slab. It has a hexagonal lattice structure with a total vacuum of 1.6 nm (with 0.8 nm on both sides of the slab). The model structures that has been studied in this work are two different types of anion-substituted zirconia; nitrogen substituted zirconia and carbon substituted zirconia slabs. In order to prepare the model structure for nitrogen substituted zirconia, two lattice oxygen atoms were substituted with two nitrogen atoms. The nitrogen atom has a formal oxidation state of -3 while oxygen has a oxidation state of -2. Therefore, to preserve the charge neutrality of the system an oxygen vacancy is introduced. For preparing the model structure of carbon substituted zirconia, a similar strategy is used, one lattice oxygen atom was substituted with a carbon atom. In order to maintain charge neutrality of the model system, since carbon has a formal oxidation state of -4 while oxygen has an oxidation state of -2, we introduced an oxygen vacancy. The anionic substitutions were carried out on the surface and/or the sub-surface anion layers. However, the oxygen vacancy was introduced only in the sub-surface anion layer. This was done since our test calculations show surface vacancies are unstable. Hence, we have 8 lattice oxygen atoms in the surface and sub-surface anion layer, where potential anionic substitutions could be carried out and 4 lattice oxygen

atoms, in sub-surface anion layer, where potential oxygen vacancies can be introduced. Different combinations of anionic substitutions and introduction of oxygen vacancy to the zirconia slab leads to creation of 84 different nitrogen-substituted slabs and 28 different carbon-substituted slabs. 4.1 illustrates two such anion-substituted zirconia structures, a nitrogen substituted zirconia and a carbon substituted zirconia slab. High throughput workflows were used to create and optimize the anion substituted zirconia slabs in addition to carrying out the adsorption calculations for the adsorption of the ORR intermediates. The structural and electronic trends for the adsorption of the O*, *OH and *OOH intermediates on the anion substituted ZrO_2 slab is evaluated systematically by studying the adsorption over all the Zr-ontop sites. The adsorption energies of the ORR adsorbates are calculated relative to the gas phase water and hydrogen in molecular form.

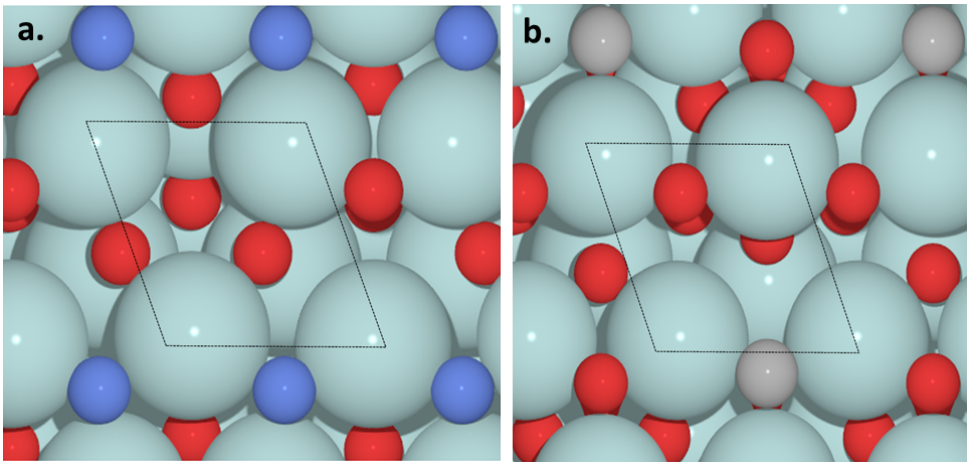

Figure 4.1: Geometries of anion substituted zirconia slab. a) Nitrogen substituted zirconia slab b) Carbon substituted zirconia slab

4.3.2 Adsorption Energy and Limiting Potential Distribution

The range of distribution of adsorption energies can help us understand the adsorption configurations of ORR adsorbates (O*, OH or OOH) on nitrogen or carbon substituted zirconia surface. From the histogram of O*, OH and OOH adsorption energies, shown in Figure 4.2, one can observe the OOH adsorption energies for both nitrogen and carbon substituted slabs are spread over a modest range of around 4 eV. The variation of OOH adsorption energy is largely due to variation in the alignment of the OOH adsorbate with the anion-substituted zirconia surface. The OH adsorption energy show a narrow range of 2 eV which is due to OH adsorption taking place mainly on the ontop zirconia site. However we noted the most surprising observation for O* adsorption energy. For both nitrogen and carbon substituted slabs, they are spread over a large range of around 5 eV. We attribute the reason for this large range of adsorption energy to the wide variety of configurations of O* adsorption. The O* adsorbate adsorbs on ontop zirconia sites, bridge sites and in some cases forms a complex with the substituent anion, nitrogen or carbon. There are different ranges of adsorption energy associated with each adsorption configuration; the adsorption on ontop zirconia sites being the weakest followed by adsorption on the bridge sites and the strongest adsorption configuration being the anionic complex formation.

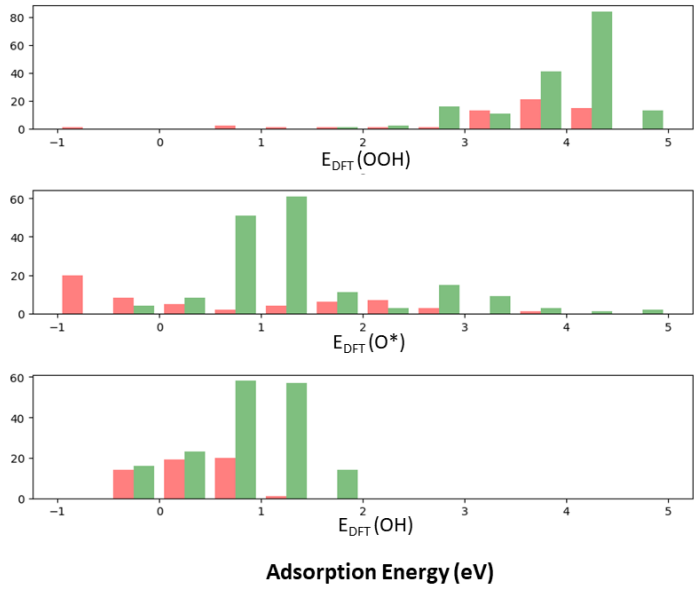

Figure 4.2: Histogram of adsorption energies of ORR intermediates i.e. OOH, O* and OH. The red bars represent adsorption energies for carbon substituted slabs while green represents adsorption energies for nitrogen substituted slabs.

For most of the materials the adsorption of ORR intermediates are restricted by a linear scaling [51, 52, 95]. Hence we wanted to explore whether such scaling relations exist for the systems explored in this study. The OOH-OH and O*-OH scaling relations are provided in the Supporting Information. From these plots of scaling relations, we can understand the adsorption energies do not scale well with each other for nitrogen and carbon substituted zirconia systems.
Within the CHE model the highest potential at which all the reaction steps are downhill in free energy is called the thermodynamic limiting potential, (U_L). The U_L gives us a measure of the activity of a catalyst. Higher U_L implies higher catalytic activity. A negative value of U_L implies catalytic inactivity. From the histogram of limiting potentials in 4.3, we can observe the U_L for most of the carbon substituted slabs is negative. On the other hand U_L for most of the nitrogen substituted slabs are positive and the peak is obtained at 0.25V with some of the values reaching upto 0.65V. Hence we can conclude that anionic substitution with nitrogen on zirconia is more favorable to ORR activity than that with carbon.

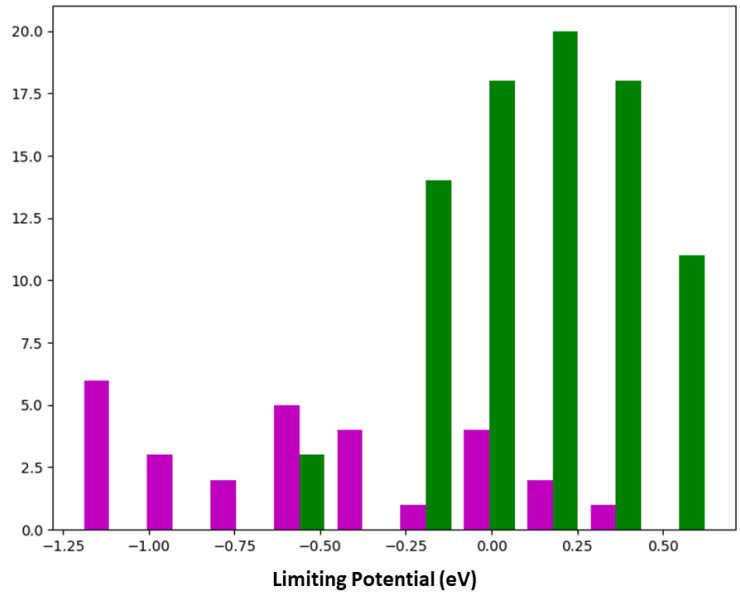

Figure 4.3: Histogram of limiting potentials for both carbon and nitrogen substituted zirconia slabs. The magenta bars represent limiting potentials for carbon substituted slabs while green represents limiting potentials for nitrogen substituted slabs.

We have also explored potential correlation between U_L and relative slab stability by plotting them in form of a scatter plot. It has been provided in the Supporting Information. From the plot, we can conclude that the U_L does not show any correlation with the relative slab stability of the anion substituted zirconia slabs.

4.3.3 ICOHP as a Electronic Descriptor for O* Adsorption

The bonding and anti-bonding interactions in a chemical system can be studied with a method known as crystal orbital Hamiltonian population (COHP) [49, 102]. In our study, we have found that the integrated crystal orbital Hamiltonian populations (ICOHP) [50] can provide valuable insights to the origin of adsorption energy variations. The calculation of ICOHP involves projection of plane wave basis sets solution, which is obtained from calculations carried out using ground state DFT method, into LCAO basis functions. We can calculate the Hamiltonian between two projected orbitals from the basis functions, which would indicate whether the net interaction is bonding or anti-bonding at a particular band energy [50, 103]. Hence, the ICOHP can be considered as energy contribution from overlap of two orbitals. Such an energy contribution can be negative (bonding) or positive (anti-bonding).

One of the aims of our study is to gain an understanding of the structural and electronic effects on the adsorption of ORR intermediates on anion-substituted zirconia slabs. In order to achieve this, we create two types of structural models, the unconstrained model and the constrained model. In the unconstrained model, the top two layers of the slab and the adsorbate is relaxed during the optimisation calculations (the bottom layer is constrained) while in the constrained model, the entire slab is constrained during the optimization calculation with only the adsorbates being free to move (where the two top layers of the slab are relaxed for the slab without adsorbates). The adsorption of O* species is carried out on the ontop-Zr sites on nitrogen and carbon-substituted slabs (both unconstrained and constrained). Our adsorption calculations over the unconstrained slab reveal that the incoming adsorbates introduce significant structural changes in the anion-substituted slabs which implies that there are both structural and electronic effects that influences the

adsorption energy. In terms of structural change, the displacement of lattice anions i.e. oxygen , nitrogen and carbon is much more significant than that of the zirconium.

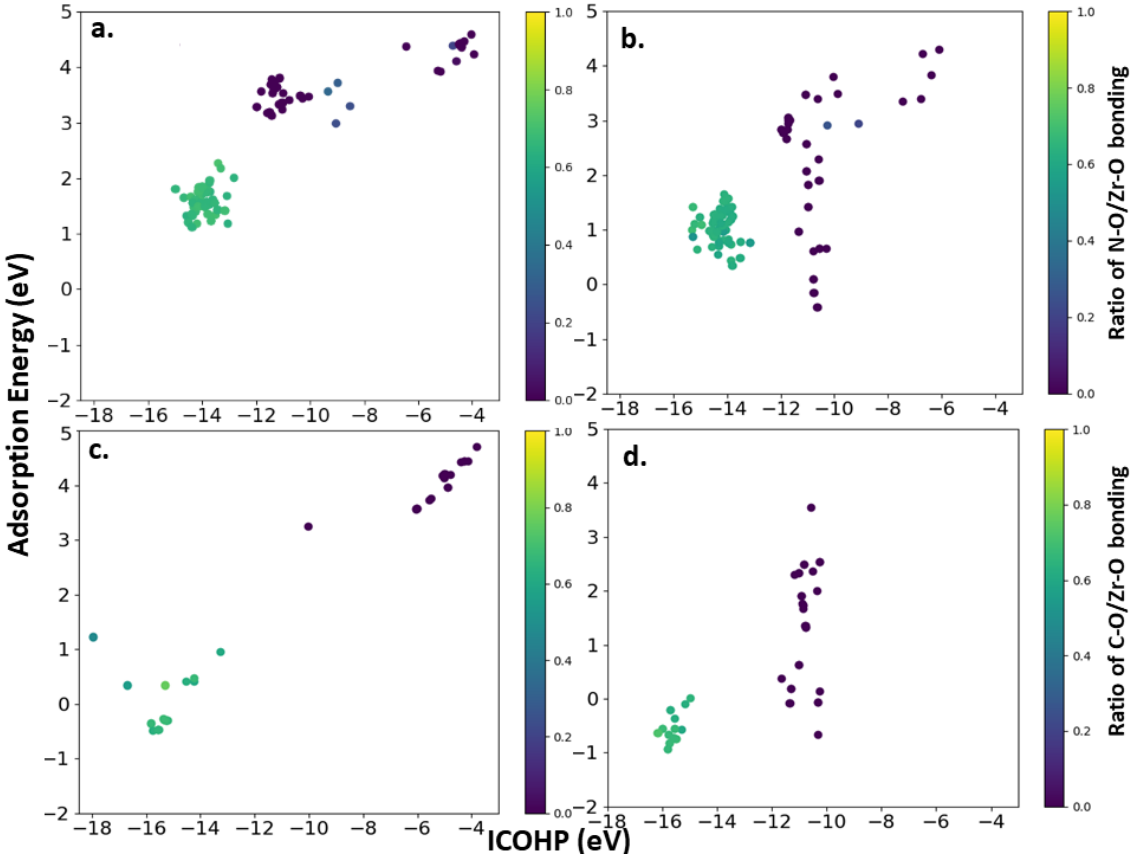

Figure 4.4: ICOHP vs Adsorption energy plots a) Constrained Nitrogen substituted zirconia slab b) Nitrogen substituted zirconia slab c) Constrained Carbon substituted zirconia slab d) Carbon substituted zirconia slab

Previous studies report similar influence of structural and electronic effects on different electrocatalysts [104, 105, 106]. Fig 4.4a and 4.4c shows the correlation between the total ICOHP of the O* adsorbate (considering bonds to all nearest Zr, N and C neighbours) and O* adsorption energy over constrained slabs. Since the constrained slab cannot move during O* adsorption, the adsorption energy in this case is affected by electronic effects only. Thus, in the constrained case the adsorption energy is expected to be proportional to the O-surface bond energy, captured by the ICOHP. As such we can observe quite a linear dependence of adsorption energy on ICOHP, except for in the weak binding limit ($\Delta E \approx 4.6$)eV. However in the unconstrained case shown in fig 4.4b and 4.4d, we see a strong deviation from the linear trend. We therefore conclude that, in addition to electronic effects, structural reorganization effects in the zirconia slab play a major role in adsorption of O* intermediate.

4.3.4 ICOHP as a Electronic Descriptor for OH Adsorption

Similar adsorption calculations are carried out with OH adsorbate on ontop-Zr sites on the nitrogen and carbon substituted zirconia slabs (both unconstrained and constrained). Since adsorption of OH over the constrained slab is influenced only by the electronic effects, in the Fig 4.5a and Fig 4.5c we can observe a linear dependence of adsorption energy on ICOHP. Since ICOHP magnitude is an indicator of bond strength, higher ICOHP

magnitude indicates a stronger bond. As higher adsorption energy also indicates stronger bond, ICOHP shows a strong correlation with adsorption energy in this case. However, when the slab is unconstrained, the adsorption energy is influenced not only by the electronic effects but also the structural effects. The structural effects are caused, mainly, by the reorganisation of the anion-substituted zirconia lattice caused by the incoming adsorbate species. The synergistic effect of the structural and electronic changes cause a deviation from the linear trend between the adsorption energy and ICOHP which can be observed in Fig 4.5b and 4.5d. This is similar to the deviation from the linear dependence of O* adsorption energy on ICOHP we observe in figure 4.4b and 4.4d.

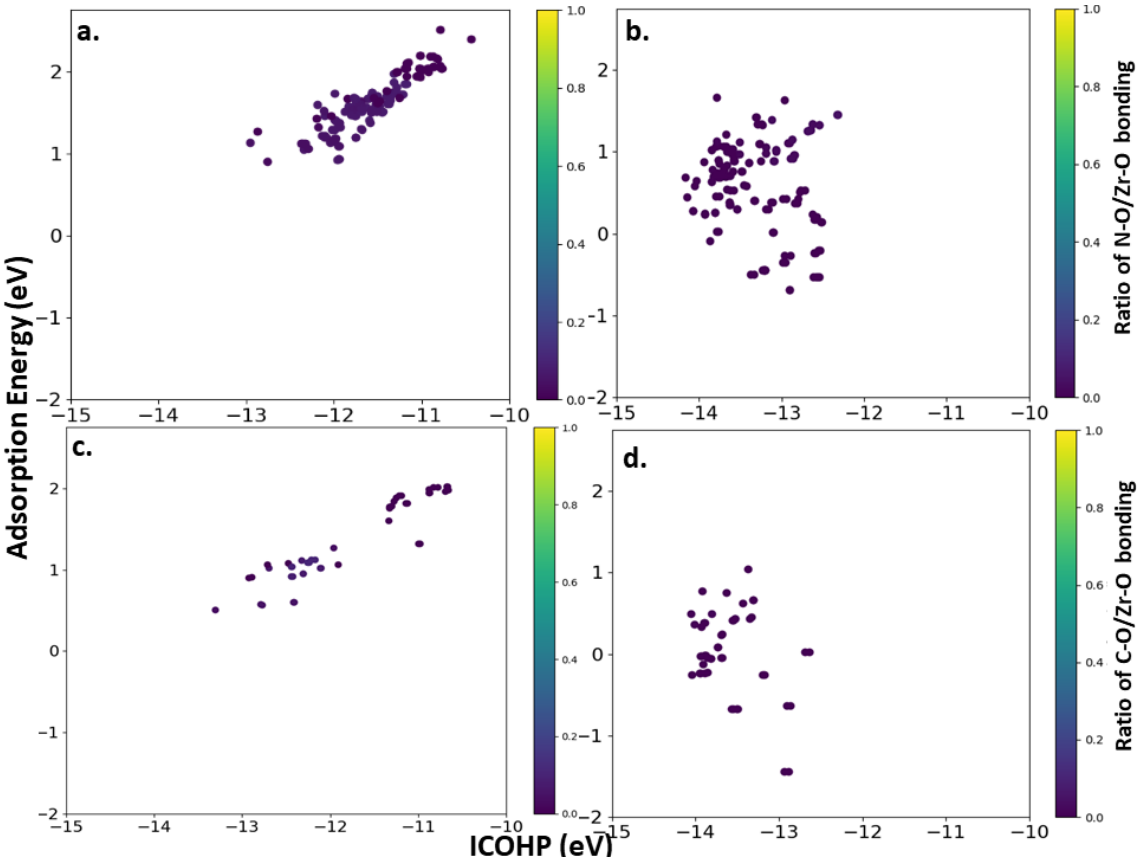

Figure 4.5: ICOHP vs Adsorption energy plots a) Constrained Nitrogen substituted zirconia slab b) Nitrogen substituted zirconia slab c) Constrained Carbon substituted zirconia slab d) Carbon substituted zirconia slab

We have quantified the the effect of structural changes only on the adsorption energies by computing the differences in the adsorption energies of the constrained and unconstrained slabs and have presenting them in form of a histogram which is provided in Appendix B. From the histogram we can understand adsorption of O* intermediate induces structural changes in the slab to a greater degree than the OH intermediate.

4.3.5 Insights into Bond Configurations

As ICOHP is an indication of bond strength, there exists a correlation between bond length and ICOHP. Fig 6 gives us an overview of the relation between bond lengths between different pairs of atoms for O* adsorption over nitrogen and carbon substituted zirconia slabs (unconstrained and constrained). Similar plots have been made for OH adsorption have been provided in Appendix B.

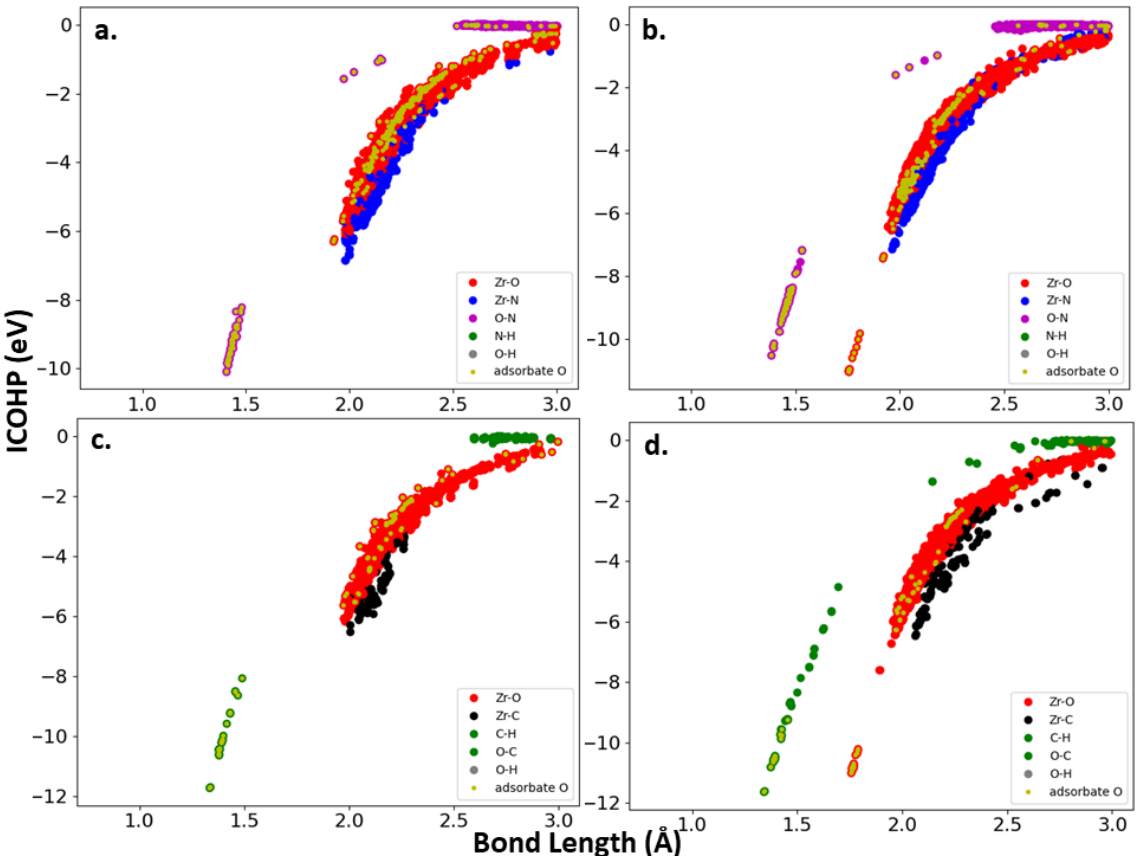

Figure 4.6: ICOHP vs bond length plots a) Constrained Nitrogen substituted zirconia slab b) Nitrogen substituted zirconia slab c) Constrained Carbon substituted zirconia slab d) Carbon substituted zirconia slab

The yellow overlay indicates the bonds that are formed between an atom (zirconia, nitrogen or carbon) and the adsorbate oxygen. The trend that we observe across the unconstrained system versus the constrained system is that the adsorbate oxygen and zirconium tend to bond more strongly in the unconstrained system as opposed to the constrained system. In order for the O* adsorbate to adsorb over the unconstrained system, the lattice zirconium atoms have to rearrange themselves. This is so as to change the bond order to accommodate the incoming O* species. If such a structural rearrangement is not possible or it does not change the bond order enough, then it is more favorable for the O* adsorbate to adsorb over the lattice nitrogen or carbon. The change in bond order is also evident from the fact that for the unconstrained system, the ICHOP for the zirconium-adsorbate oxygen bond is distributed over a larger range than in the constrained system. From Fig 4.6 it is also clear that only ICOHP, as a descriptor, is not enough to capture the trend in the adsorption energies.

4.4 Conclusion

ICOHP is a very useful electronic descriptor for prediction of O* and OH adsorption energies on zirconia-based catalytic systems. From our comparative study of constrained and unconstrained anion-substituted zirconia slabs, we understand both the structural as well electronic effects of the slabs play a role in the adsorption of the O* and OH intermediates. The incoming adsorbates introduces structural changes in the slab, the lattice Zr atoms gets displaced to change the bond order in order to accommodate the adsorbate species

on the surface of the slab. The structural reorganisation of the nitrogen and carbon substituted zirconia slabs partially contributes to the bond strength between the active sites and the adsorbates.
Additionally, we can also state that anionic substitution on zirconia catalyst with nitrogen is a better choice than that by carbon in terms of ORR activity. We draw this conclusion from the values of limiting potential calculated for the anion-substituted zirconia slabs illustrated in figure 4.3. The predominantly positive values of U_L with the peak at 0.25V and values reaching as high as 0.65V is indicative of the same. However, there was no correlation found between the stability of the slabs and their ORR activity.

5 Conclusion and Outlook

5.1 Conclusion

This thesis presents the outcome of the studies on non platinum group metal (non-PGM) zirconium-based catalysts for Oxygen Reduction Reaction (ORR). This includes investigations into zirconium oxynitride and anion substituted zirconia, the substituent anions being nitrogen and carbon, as cost effective and efficient catalysts for ORR.

In the first study, we investigated transition metal based catalyst namely zirconium oxynitride (Zr_2ON_2) as a cost effective alternative to the expensive platinum based catalysts for ORR. Our calculations reveal that Zr_2ON_2 is indeed an effective ORR catalyst where the ontop-Zr sites acts as the active sites. However, the site activity also depended on the formation of complexes, for instance, the sites where NHO* complex formation occurs during O* adsorption are generally either inactive or exhibit very low levels of activity. Our calculations also indicate that the conventional scaling relationship between the adsorption free energies of O* and OH* can be broken when ORR takes place on the complex surface of a transition metal oxynitride. Nevertheless, this does not result in enhanced ORR activity. Utilizing scaling relations, we construct an activity volcano plot, leading us to the conclusion that the Zr_2ON_2 catalyst exhibits a maximum limiting potential of around 0.70 V, a finding consistent with the experimentally determined onset potential.

In the second study, we explored integrated crystal orbital Hamiltonian population as an effective descriptor for adsorption energies of ORR intermediates on anion substituted zirconia surface. our comparative study of constrained and unconstrained anion-substituted zirconia slabs, has revealed that both the structural and electronic characteristics of these slabs have a significant impact on the adsorption of O* and OH intermediates. When adsorbates are introduced, they induce structural modifications within the slab. This leads to the displacement of Zr atoms within the lattice, resulting in changes to bond orders to accommodate the adsorbate species on the surface of the slab. The structural reorganisation of the nitrogen and carbon substituted zirconia slabs also contributes, to some extent, to the strength of the bonds between active sites and adsorbates. Furthermore, it can be asserted that substituting anions with nitrogen in zirconia catalysts yields better results in terms of ORR activity compared to carbon substitution. This conclusion is drawn based on the calculated values of the limiting potential for the anion-substituted zirconia slabs. The consistently positive limiting potential values, with a prominent peak at 0.25V and some values reaching as high as 0.65V is also indicative of nitrogen being a better substituent in zirconia than carbon in terms of enhanced ORR activity. However, it is important to note that no correlation was observed between the stability of the slabs and their ORR activity.

Overall, through the above studies, the insights gained into the zirconium based non-PGM ORR catalysts, the deviations from the standard correlations between different ORR intermediates, the catalyst-adsorbate interactions among others can guide the design of future ORR catalysts.

5.2 Outlook

While zirconium based non-PGM catalysts exhibited favourable catalytic activity towards ORR, there are aspects that can be explored further regarding this class of catalysts. Particularly the effect of nitrogen content and cation substitution in zirconia on ORR activity can be explored further.

- **Effect of nitrogen content on ORR activity**: In our second study on anion substituted zirconia explored ORR on zirconia surface we introduced two nitrogen anions in the zirconia structure by replacing lattice oxygen. Most of the limiting potential value for the nitrogen substituted zirconia catalysts are found in 0.1 to 0.4V range. Our first study explores ORR taking place on zirconium oxynitride surface, which is a material with higher nitrogen content than nitrogen-substituted zirconia. The limiting potential in this case is found to be around 0.7V. Seemingly, the ORR activity increases with increase in nitrogen content. In future, the effect of nitrogen content in zirconia on ORR activity can be further explored.
- **Effect of cation substitution**: There has been previous studies which has explored doped transition metal ORR catalysts, for example phosphor and nitrogen co-doped titanium dioxide [107] or cation substituted lanthanum cobaltite [108]. They report enhanced electrocatalytic activity after introduction of cationic dopant. Similarly, the effect of cation substitution in zirconia by transition metals is an aspect that can be studied in future.

Bibliography

[1] John Twidell. *Renewable energy resources*. Routledge, 2021.

[2] Muvva V Ramana. “Technical and social problems of nuclear waste”. In: *Wiley Interdisciplinary Reviews: Energy and Environment* 7.4 (2018), e289.

[3] N L□ Panwar, S C□ Kaushik, and Surendra Kothari. “Role of renewable energy sources in environmental protection: A review”. In: *Renewable and sustainable energy reviews* 15.3 (2011), pp. 1513–1524.

[4] sustainable.dk. *Klima Ambassaden*. http://sustainable.dk/naturvidenskabeligt-grundforlob/transport/4-elbiler/. Accessed: 2023-07-17. 2023.

[5] AR Dehghani-Sanij et al. “Study of energy storage systems and environmental challenges of batteries”. In: *Renewable and Sustainable Energy Reviews* 104 (2019), pp. 192–208.

[6] Patrick Moriarty and Damon Honnery. “Global transport energy consumption”. In: *Alternative energy and shale gas encyclopedia* (2016), pp. 651–656.

[7] Yoshio Hori, Akira Murata, and Ryutaro Takahashi. “Formation of hydrocarbons in the electrochemical reduction of carbon dioxide at a copper electrode in aqueous solution”. In: *Journal of the Chemical Society, Faraday Transactions 1: Physical Chemistry in Condensed Phases* 85.8 (1989), pp. 2309–2326.

[8] Andrew A Peterson et al. “How copper catalyzes the electroreduction of carbon dioxide into hydrocarbon fuels”. In: *Energy & Environmental Science* 3.9 (2010), pp. 1311–1315.

[9] Andrew A Peterson and Jens K Nørskov. “Activity descriptors for CO2 electroreduction to methane on transition-metal catalysts”. In: *The Journal of Physical Chemistry Letters* 3.2 (2012), pp. 251–258.

[10] Yin-Jia Zhang and Andrew A Peterson. “Oxygen-induced changes to selectivity-determining steps in electrocatalytic CO 2 reduction”. In: *Physical Chemistry Chemical Physics* 17.6 (2015), pp. 4505–4515.

[11] Joseph H Montoya et al. “Theoretical insights into a CO dimerization mechanism in CO2 electroreduction”. In: *The journal of physical chemistry letters* 6.11 (2015), pp. 2032–2037.

[12] Mohammadreza Karamad et al. “Mechanistic pathway in the electrochemical reduction of CO2 on RuO2”. In: *Acs Catalysis* 5.7 (2015), pp. 4075–4081.

[13] VL Kuznetsov and PP Edwards. “Functional materials for sustainable energy technologies: Four case studies”. In: *ChemSusChem: Chemistry & Sustainability Energy & Materials* 3.1 (2010), pp. 44–58.

[14] Manish Kumar Singla, Parag Nijhawan, and Amandeep Singh Oberoi. “Hydrogen fuel and fuel cell technology for cleaner future: a review”. In: *Environmental Science and Pollution Research* 28 (2021), pp. 15607–15626.

[15] Alberto A Boretti. “Energy recovery in passenger cars”. In: (2012).

[16] Wolf Vielstich, Arnold Lamm, and Hubert Gasteiger. “Handbook of fuel cells. Fundamentals, technology, applications”. In: (2003).

[17] Anca Faur Ghenciu. “Review of fuel processing catalysts for hydrogen production in PEM fuel cell systems”. In: *Current opinion in solid state and materials science* 6.5 (2002), pp. 389–399.

[18] P Costamagna and S Srinivasan. “Quantum jumps in the PEMFC science and technology from the 1960s to the year 2000, Part I”. In: *Fundamental scientific aspects* 84 (1999), pp. 167–172.

[19] F Barbir and T Gomez. “Efficiency and economics of proton exchange membrane (PEM) fuel cells”. In: *international journal of hydrogen energy* 22.10-11 (1997), pp. 1027–1037.
[20] Steven G Chalk, James F Miller, and Fred W Wagner. “Challenges for fuel cells in transport applications”. In: *Journal of Power sources* 86.1-2 (2000), pp. 40–51.
[21] G Cacciola, V Antonucci, and S Freni. “Technology up date and new strategies on fuel cells”. In: *Journal of power sources* 100.1-2 (2001), pp. 67–79.
[22] Sergei Gamburzev and A John Appleby. “Recent progress in performance improvement of the proton exchange membrane fuel cell (PEMFC)”. In: *Journal of power sources* 107.1 (2002), pp. 5–12.
[23] Yonghong Bing et al. “Nanostructured Pt-alloy electrocatalysts for PEM fuel cell oxygen reduction reaction”. In: *Chem. Soc. Rev.* 39.6 (2010), pp. 2184–2202.
[24] Michael J Janik, Christopher D Taylor, and Matthew Neurock. “First-principles analysis of the initial electroreduction steps of oxygen over Pt (111)”. In: *J. Electrochem. Soc.* 156.1 (2008), B126.
[25] Gang Wu et al. “High-performance electrocatalysts for oxygen reduction derived from polyaniline, iron, and cobalt”. In: *Science* 332.6028 (2011), pp. 443–447.
[26] Azhagumuthu Muthukrishnan et al. “Fe-containing polyimide-based high-performance ORR catalysts in acidic medium: a kinetic approach to study the durability of catalysts”. In: *Catal. Sci. Technol.* 5.1 (2015), pp. 475–483.
[27] Michel Lefèvre et al. “Iron-based catalysts with improved oxygen reduction activity in polymer electrolyte fuel cells”. In: *Science* 324.5923 (2009), pp. 71–74.
[28] Jianglan Shui et al. “N-doped carbon nanomaterials are durable catalysts for oxygen reduction reaction in acidic fuel cells”. In: *Sci. Adv.* 1.1 (2015), e1400129.
[29] Akimitsu Ishihara et al. “Tantalum (oxy) nitrides prepared using reactive sputtering for new nonplatinum cathodes of polymer electrolyte fuel cell”. In: *Electrochim. Acta* 53.16 (2008), pp. 5442–5450.
[30] N Uehara et al. “Kinetic study of oxygen reduction reaction on tantalum oxide-based electrocatalysts produced from oxy-tantalum phthalocyanines in acidic media”. In: *Electrochim. Acta* 182 (2015), pp. 789–794.
[31] Mitsuharu Chisaka et al. “Zirconium oxynitride-catalyzed oxygen reduction reaction at polymer electrolyte fuel cell cathodes”. In: *ACS Omega* 2.2 (2017), pp. 678–684.
[32] Makoto Hamazaki et al. “Durability of titanium-niobium oxides mixed with Ti4O7 as non-precious-and carbon-free cathodes for PEFCs in H2SO4 at 80 C”. In: *Electrochemistry* 83.10 (2015), pp. 817–819.
[33] Chaojie Song and Jiujun Zhang. “Electrocatalytic oxygen reduction reaction”. In: *PEM fuel cell electrocatalysts and catalyst layers: fundamentals and applications*. Springer, 2008, pp. 89–134.
[34] Jens Kehlet Nørskov et al. “Origin of the overpotential for oxygen reduction at a fuel-cell cathode”. In: *The Journal of Physical Chemistry B* 108.46 (2004), pp. 17886–17892.
[35] Heine A Hansen, Venkatasubramanian Viswanathan, and Jens K Nørskov. “Unifying kinetic and thermodynamic analysis of 2 e–and 4 e–reduction of oxygen on metal surfaces”. In: *J. Phys. Chem. C* 118.13 (2014), pp. 6706–6718.
[36] Ifan EL Stephens et al. “Understanding the electrocatalysis of oxygen reduction on platinum and its alloys”. In: *Energy & Environmental Science* 5.5 (2012), pp. 6744–6762.
[37] Jianbo Wu and Hong Yang. “Platinum-based oxygen reduction electrocatalysts”. In: *Accounts of chemical research* 46.8 (2013), pp. 1848–1857.

[38] Yao Nie, Li Li, and Zidong Wei. “Recent advancements in Pt and Pt-free catalysts for oxygen reduction reaction”. In: *Chemical Society Reviews* 44.8 (2015), pp. 2168–2201.
[39] Joseph H Montoya et al. “Materials for solar fuels and chemicals”. In: *Nature materials* 16.1 (2017), pp. 70–81.
[40] Yun Wang et al. “A review of polymer electrolyte membrane fuel cells: Technology, applications, and needs on fundamental research”. In: *Applied energy* 88.4 (2011), pp. 981–1007.
[41] Tipaporn Patniboon and Heine Anton Hansen. “N-Doped Graphene Supported on Metal-Iron Carbide as a Catalyst for the Oxygen Reduction Reaction: Density Functional Theory Study”. In: *ChemSusChem* 13.5 (2020), pp. 996–1005.
[42] Yiran Wang et al. “High-throughput screening of carbon-supported single metal atom catalysts for oxygen reduction reaction”. In: *Nano Research* 15 (2022), pp. 1054–1060.
[43] Sukanya Sinha, Tejs Vegge, and Heine Anton Hansen. “Bending the ORR scaling relations on zirconium oxynitride for enhanced oxygen electrocatalysis”. In: *ChemCatChem* (2023), e202300349.
[44] Mateusz Reda, Heine Anton Hansen, and Tejs Vegge. “DFT study of stabilization effects on N-doped graphene for ORR catalysis”. In: *Catalysis Today* 312 (2018), pp. 118–125.
[45] Max Born and Robert Oppenheimer. “On the quantum theory of molecules”. In: *Quantum Chemistry: Classic Scientific Papers*. World Scientific, 2000, pp. 1–24.
[46] Roald Hoffmann and William N Lipscomb. “Theory of polyhedral molecules. I. Physical factorizations of the secular equation”. In: *The Journal of Chemical Physics* 36.8 (1962), pp. 2179–2189.
[47] Roald Hoffmann. “An extended Hückel theory. I. hydrocarbons”. In: *The Journal of Chemical Physics* 39.6 (1963), pp. 1397–1412.
[48] Timothy Hughbanks and Roald Hoffmann. “Chains of trans-edge-sharing molybdenum octahedra: metal-metal bonding in extended systems”. In: *Journal of the American Chemical Society* 105.11 (1983), pp. 3528–3537.
[49] Roald Hoffmann. *Solids and surfaces: a chemist’s view of bonding in extended structures*. John Wiley & Sons, 1991.
[50] Richard Dronskowski and Peter E Blöchl. “Crystal orbital Hamilton populations (COHP): energy-resolved visualization of chemical bonding in solids based on density-functional calculations”. In: *The Journal of Physical Chemistry* 97.33 (1993), pp. 8617–8624.
[51] Ambarish Kulkarni et al. “Understanding catalytic activity trends in the oxygen reduction reaction”. In: *Chem. Rev* 118.5 (2018), pp. 2302–2312.
[52] Yasuharu Okamoto and Osamu Sugino. “Hyper-volcano surface for oxygen reduction reactions over noble metals”. In: *J. Phys. Chem. C* 114.10 (2010), pp. 4473–4478.
[53] Yoshiyuki Yamamoto, Shusuke Kasamatsu, and Osamu Sugino. “Scaling relation of oxygen reduction reaction intermediates at defective TiO2 surfaces”. In: *J. Phys. Chem. C* 123.32 (2019), pp. 19486–19492.
[54] Akimitsu Ishihara et al. “Tantalum oxynitride for a novel cathode of PEFC”. In: *Electrochem. Solid-State Lett.* 8.4 (2005), A201.
[55] Georg Kresse and Jürgen Hafner. “Ab initio molecular dynamics for liquid metals”. In: *Phys. Rev. B* 47.1 (1993), p. 558.
[56] Peter E Blöchl. “Projector augmented-wave method”. In: *Phys. Rev. B* 50.24 (1994), p. 17953.

[57] John P Perdew, Kieron Burke, and Matthias Ernzerhof. “Generalized gradient approximation made simple”. In: *Phys. Rev. Lett.* 77.18 (1996), p. 3865.
[58] Ask Hjorth Larsen et al. “The atomic simulation environment—a Python library for working with atoms”. In: *J. Phys.: Condens. Matter* 29.27 (2017), p. 273002.
[59] Hendrik J Monkhorst and James D Pack. “Special points for Brillouin-zone integrations”. In: *Phys. Rev. B* 13.12 (1976), p. 5188.
[60] Christopher J Cramer and FM Bickelhaupt. “Essentials of computational chemistry”. In: *AAngew. Chem., Int. Ed. Engl.* 42.4 (2003), pp. 381–381.
[61] Charles T Campbell, Lynza H Sprowl, and Líney Árnadóttir. “Equilibrium constants and rate constants for adsorbates: Two-dimensional (2D) ideal gas, 2D ideal lattice gas, and ideal hindered translator models”. In: *J. Phys. Chem. C* 120.19 (2016), pp. 10283–10297.
[62] Lynza H Sprowl, Charles T Campbell, and Liney Arnadottir. “Hindered translator and hindered rotor models for adsorbates: Partition functions and entropies”. In: *J. Phys. Chem. C* 120.18 (2016), pp. 9719–9731.
[63] Lynza H Sprowl, Charles T Campbell, and Liney Arnadottir. “Correction to “hindered translator and hindered rotor models for adsorbates: partition functions and entropies””. In: *J. Phys. Chem. C* 121.17 (2017), pp. 9655–9655.
[64] Pierre Villars and Karin Cenzual, eds. *Zr2ON2 (Zr2N2O cub) Crystal Structure: Datasheet from “PAULING FILE Multinaries Edition – 2012” in SpringerMaterials (https://materials.springer.com/isp/crystallographic/docs/sd_0382074)*. Copyright 2016 Springer-Verlag Berlin Heidelberg & Material Phases Data System (MPDS), Switzerland & National Institute for Materials Science (NIMS), Japan. URL: https://materials.springer.com/isp/crystallographic/docs/sd_0382074.
[65] SJ Clarke, CW Michie, and MJ Rosseinsky. “Structure of Zr2ON2 by Neutron Powder Diffraction: The Absence of Nitride–Oxide Ordering”. In: *J. Solid State Chem.* 146.2 (1999), pp. 399–405.
[66] I Bertóti. “Nitrogen modified metal oxide surfaces”. In: *Catal. Today* 181.1 (2012), pp. 95–101.
[67] GI Cubillos et al. “Synthesis and biological characterization of zirconium oxynitride thin film growth by radio-frequency sputtering”. In: *Thin Solid Films* 529 (2013), pp. 342–346.
[68] GI Cubillos et al. “Chemical composition and microstructure of zirconium oxynitride thin layers from the surface to the substrate-coating interface”. In: *Mater. Charact.* 131 (2017), pp. 450–458.
[69] J Probst, U Gbureck, and R Thull. “Binary nitride and oxynitride PVD coatings on titanium for biomedical applications”. In: *Surf. Coat. Technol.* 148.2-3 (2001), pp. 226–233.
[70] Heine A Hansen, Jan Rossmeisl, and Jens K Nørskov. “Surface Pourbaix diagrams and oxygen reduction activity of Pt, Ag and Ni (111) surfaces studied by DFT”. In: *Phys. Chem. Chem. Phys.* 10.25 (2008), pp. 3722–3730.
[71] Hui He et al. “Molecular and electronic structures of transition-metal macrocyclic complexes as related to catalyzing oxygen reduction reactions: a density functional theory study”. In: *J. Phys. Chem. C* 116.30 (2012), pp. 16038–16046.
[72] C Doornkamp and V Ponec. “The universal character of the Mars and Van Krevelen mechanism”. In: *J. Mol. Catal. A: Chem.* 162.1-2 (2000), pp. 19–32.
[73] Shotaro Doi et al. “Zirconium nitride and oxynitride for new cathode of polymer electrolyte fuel cell”. In: *ECS Trans.* 1.6 (2006), p. 17.
[74] Shotaro Doi et al. “Zirconium-based compounds for cathode of polymer electrolyte fuel cell”. In: *J. Electrochem. Soc.* 154.3 (2007), B362.

[75] Federico Calle-Vallejo, Alexander Krabbe, and Juan M García-Lastra. “How covalence breaks adsorption-energy scaling relations and solvation restores them”. In: *Chem. Sci.* 8.1 (2017), pp. 124–130.
[76] Samira Siahrostami et al. “Two-dimensional materials as catalysts for energy conversion”. In: *Catal. Lett.* 146.10 (2016), pp. 1917–1921.
[77] Guoping Gao, Eric R Waclawik, and Aijun Du. “Computational screening of two-dimensional coordination polymers as efficient catalysts for oxygen evolution and reduction reaction”. In: *J. Catal.* 352 (2017), pp. 579–585.
[78] Shyam Kattel, Plamen Atanassov, and Boris Kiefer. “A density functional theory study of oxygen reduction reaction on non-PGM Fe–N x–C electrocatalysts”. In: *Phys. Chem. Chem. Phys.* 16.27 (2014), pp. 13800–13806.
[79] Gang Liu et al. “Preparation, characterization of ZrOxNy/C and its application in PEMFC as an electrocatalyst for oxygen reduction”. In: *J. Power Sources* 172.2 (2007), pp. 503–510.
[80] Youta Maekawa et al. “Catalytic activity of zirconium oxynitride prepared by reactive sputtering for ORR in sulfuric acid”. In: *Electrochem. Solid-State Lett.* 11.7 (2008), B109.
[81] Guangjin Wang et al. “Origin of enhanced catalytic activity of oxygen reduction reaction on zirconium oxynitrides: A first-principle study”. In: *Solid State Ionics* 317 (2018), pp. 15–20.
[82] Venkatasubramanian Viswanathan et al. “Unifying the 2e–and 4e–reduction of oxygen on metal surfaces”. In: *J. Phys. Chem. Lett* 3.20 (2012), pp. 2948–2951.
[83] Venkatasubramanian Viswanathan et al. “Universality in oxygen reduction electrocatalysis on metal surfaces”. In: *ACS Catal.* 2.8 (2012), pp. 1654–1660.
[84] Jianwei Sun et al. “Accurate first-principles structures and energies of diversely bonded systems from an efficient density functional”. In: *Nat. Chem.* 8.9 (2016), pp. 831–836.
[85] David Fuks et al. “Density functional theory study of sulfur adsorption at the (001) surface of metal-rich nickel phosphides: Effect of the Ni/P ratio”. In: *J. Phys. Chem. C* 114.31 (2010), pp. 13313–13321.
[86] A Seifitokaldani, O Savadogo, and M Perrier. “Density functional theory (DFT) computation of the oxygen reduction reaction (ORR) on titanium nitride (TiN) surface”. In: *Electrochim. Acta* 141 (2014), pp. 25–32.
[87] Sandeep Nigam and Chiranjib Majumder. “ORR viability of alumina-supported platinum nanocluster: exploring oxidation behaviour by DFT”. In: *Phys. Chem. Chem. Phys.* 19.29 (2017), pp. 19308–19315.
[88] Fan Liu et al. “Systematic exploration of N, C configurational effects on the ORR performance of Fe–N doped graphene catalysts based on DFT calculations”. In: *RSC Adv.* 9.39 (2019), pp. 22656–22667.
[89] Akimitsu Ishihara et al. “Challenge of advanced low temperature fuel cells based on high degree of freedom of group 4 and 5 metal oxides”. In: *Curr. Opin. Electrochem.* 21 (2020), pp. 234–241.
[90] Rune Christensen et al. “Functional independent scaling relation for ORR/OER catalysts”. In: *The Journal of Physical Chemistry C* 120.43 (2016), pp. 24910–24916.
[91] Tyler Sours et al. “Circumventing scaling relations in oxygen electrochemistry using metal–organic frameworks”. In: *The Journal of Physical Chemistry Letters* 11.23 (2020), pp. 10029–10036.
[92] Colin F Dickens et al. “An electronic structure descriptor for oxygen reactivity at metal and metal-oxide surfaces”. In: *Surface Science* 681 (2019), pp. 122–129.

[93] Victor Fung, Zili Wu, and De-en Jiang. “New bonding model of radical adsorbate on lattice oxygen of perovskites”. In: *The Journal of Physical Chemistry Letters* 9.21 (2018), pp. 6321–6325.
[94] Benjamin M Comer et al. “Unraveling electronic trends in O* and OH* surface adsorption in the MO2 transition-metal oxide series”. In: *The Journal of Physical Chemistry C* 126.18 (2022), pp. 7903–7909.
[95] Isabela C Man et al. “Universality in oxygen evolution electrocatalysis on oxide surfaces”. In: *ChemCatChem* 3.7 (2011), pp. 1159–1165.
[96] Jens Jørgen Mortensen, Morten Gjerding, and Kristian Sommer Thygesen. “MyQueue: Task and workflow scheduling system”. In: *Journal of Open Source Software* 5.45 (2020), p. 1844.
[97] Stefan Maintz et al. *LOBSTER: A tool to extract chemical bonding from plane-wave based DFT*. 2016.
[98] Daning Wang et al. “Crystal structure of zirconia by Rietveld refinement”. In: *Science in China Series A: Mathematics* 42 (1999), pp. 80–86.
[99] Thaleia Vagkopoulou et al. “Zirconia in dentistry: Part 1. Discovering the nature of an upcoming bioceramic”. In: *Eur. J. Esthet. Dent* 4.2 (2009).
[100] Guangjin Wang et al. “Density functional studies of zirconia with different crystal phases for oxygen reduction reaction”. In: *RSC advances* 5.103 (2015), pp. 85122–85127.
[101] Hongbo Wu et al. “First-principles study of phase transition and band structure of ZrO2 under pressure”. In: *Journal of Alloys and Compounds* 645 (2015), pp. 352–357.
[102] Rutger A Van Santen, Ionut Tranca, and Emiel JM Hensen. “Theory of surface chemistry and reactivity of reducible oxides”. In: *Catalysis Today* 244 (2015), pp. 63–84.
[103] Volker L Deringer, Andrei L Tchougréeff, and Richard Dronskowski. “Crystal orbital Hamilton population (COHP) analysis as projected from plane-wave basis sets”. In: *The journal of physical chemistry A* 115.21 (2011), pp. 5461–5466.
[104] Aliaksandr S Bandarenka and Marc TM Koper. “Structural and electronic effects in heterogeneous electrocatalysis: Toward a rational design of electrocatalysts”. In: *Journal of Catalysis* 308 (2013), pp. 11–24.
[105] Flavio Colmati et al. “Direct Ethanol Fuel Cells: The influence of structural and electronic effects on Pt–Sn/C electrocatalysts”. In: *International Journal of Hydrogen Energy* 44.54 (2019), pp. 28812–28820.
[106] Shih-Hong Chang et al. “Structural and Electronic Effects of Carbon-Supported PtxPd1- x Nanoparticles on the Electrocatalytic Activity of the Oxygen-Reduction Reaction and on Methanol Tolerance”. In: *Chemistry–A European Journal* 16.36 (2010), pp. 11064–11071.
[107] Mitsuharu Chisaka and Hiroyuki Morioka. “Phosphor and nitrogen co-doped rutile TiO 2 covered on TiN for oxygen reduction reaction in acidic media”. In: *Catalysis Science & Technology* 9.3 (2019), pp. 611–619.
[108] Xingdong Jiang et al. “Cation substitution of B-site in LaCoO3 for bifunctional oxygen electrocatalytic activities”. In: *Journal of Alloys and Compounds* 878 (2021), p. 160433.

Appendix A

Supplementary material for ’Bending ORR Scaling Relations’

This appendix is the supplemantary material of Chapter 3, which is based on the supporting information of Paper I.

Supporting Information

Water Split Stability Plot

The adsorption configurations corresponding rest of the geometries sampled for Figure 1c i.e. the water split stability plot. (In the renderings of the adsorbates on the Zr_2ON_2 slabs, the light cyan atom is Zr, red is O, blue is N and white is H).

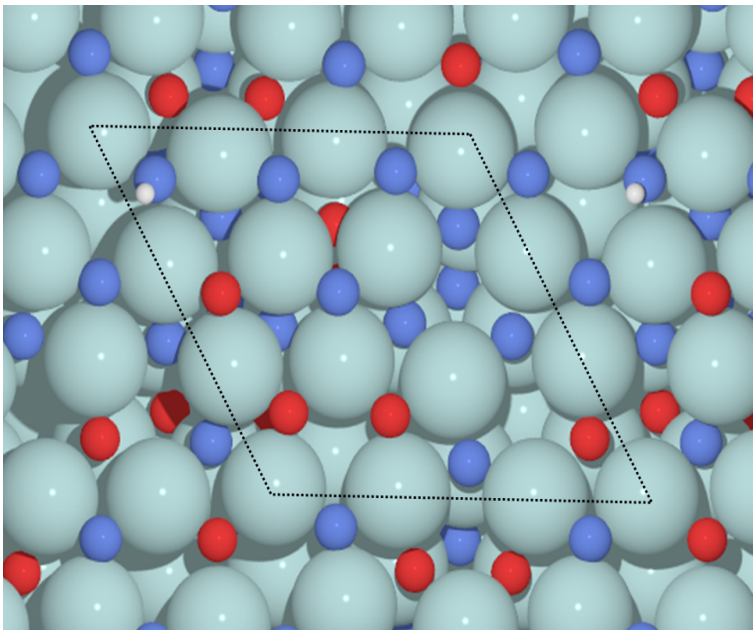

Figure 1: Water split configuration: 1 site N_LH

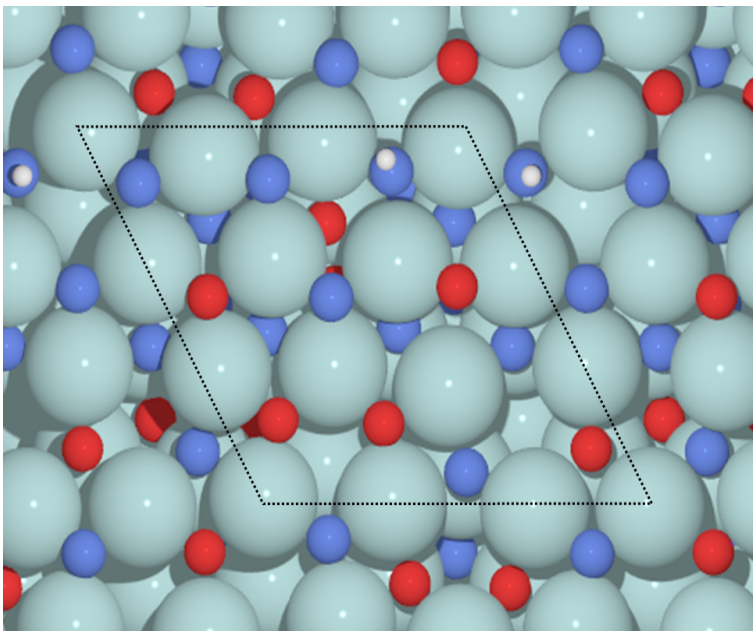

Figure 2: Water split configuration: 1 site O_V+N_LH

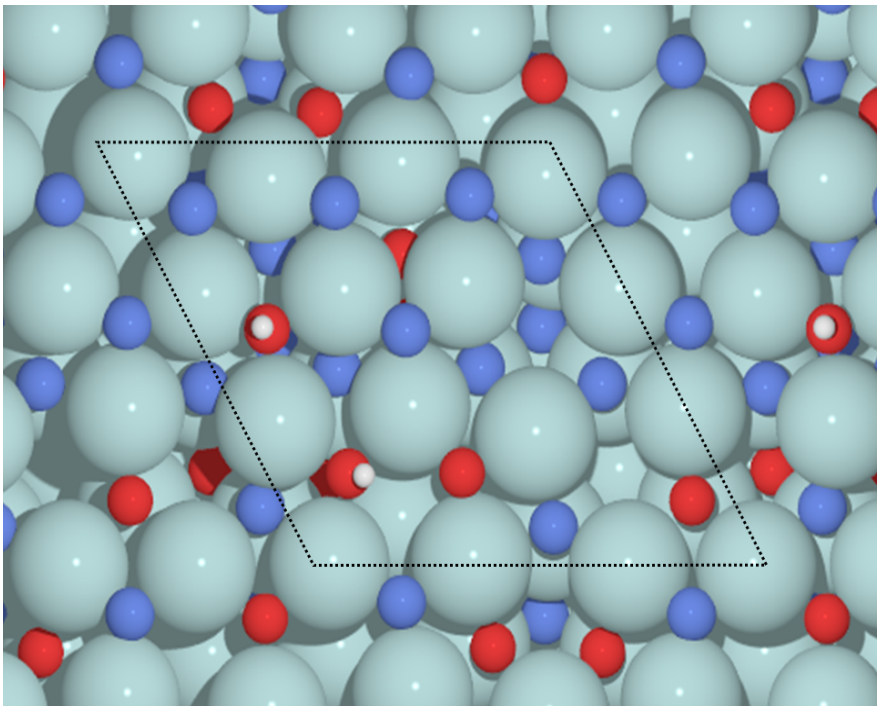

Figure 3: Water split configuration: 1 site O_VH+O_LH

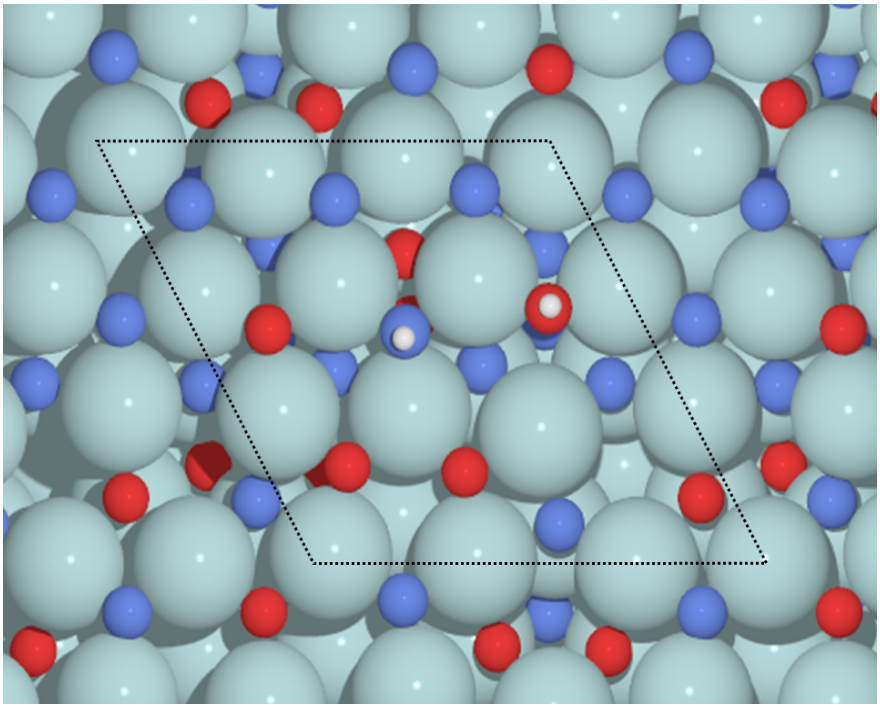

Figure 4: Water split configuration: 1 site O_VH+N_LH

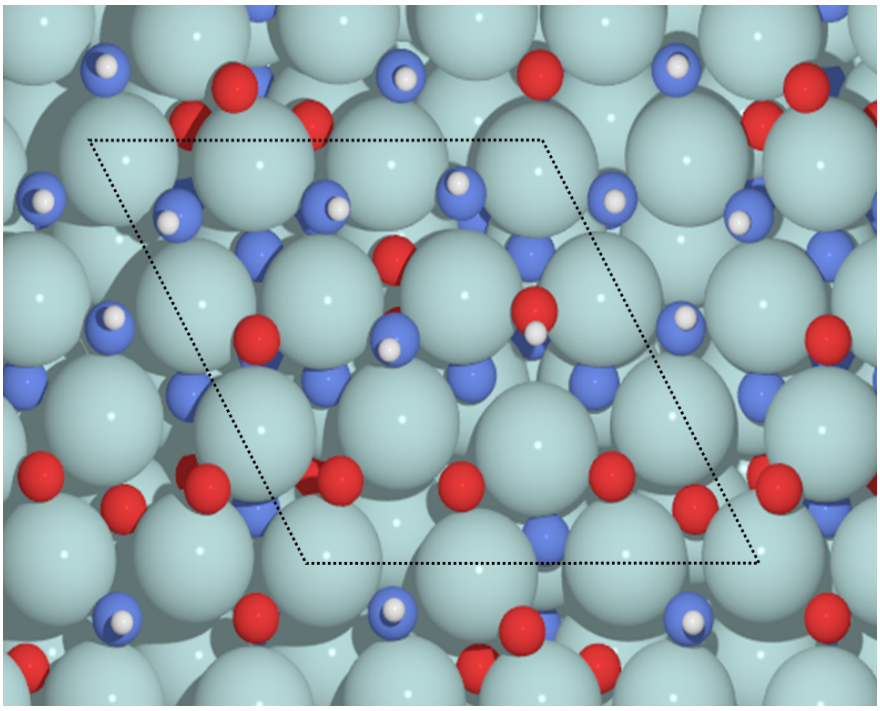

Figure 5: Water split configuration: 4 sites O_V+O_LH+2N_LH

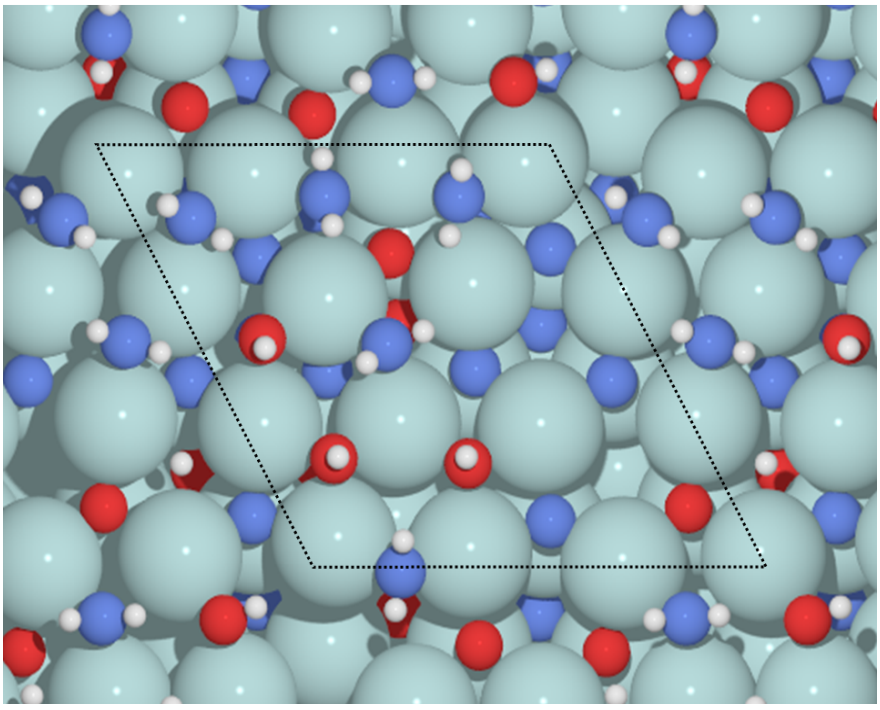

Figure 6: Water split configuration: 4 sites O_V+N_LH+$N_L$$H_2$

Free Energy Diagram

Free Energy Diagrams corresponding to rest of the sites (In the renderings of the adsorbates on the Zr_2ON_2 slabs, the light cyan atom is Zr, red is O, blue is N and white is H).

a.

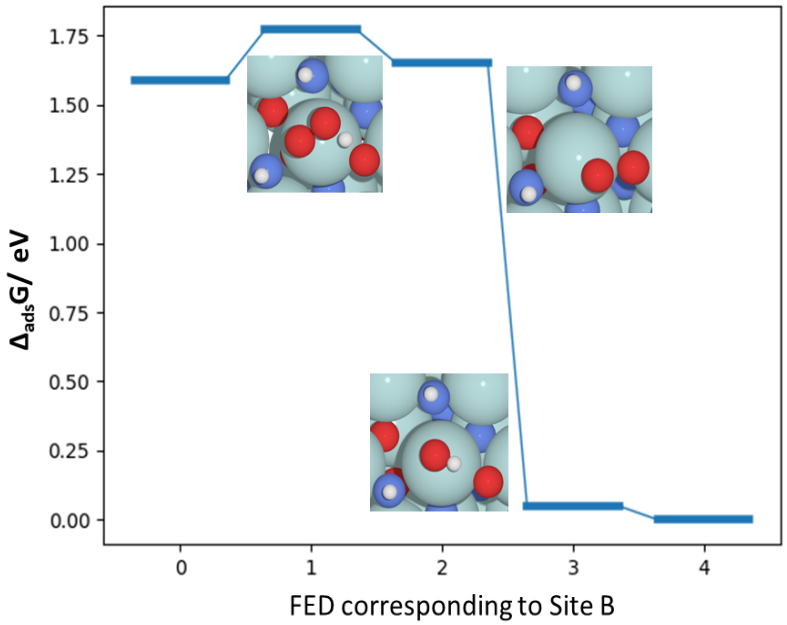

b.

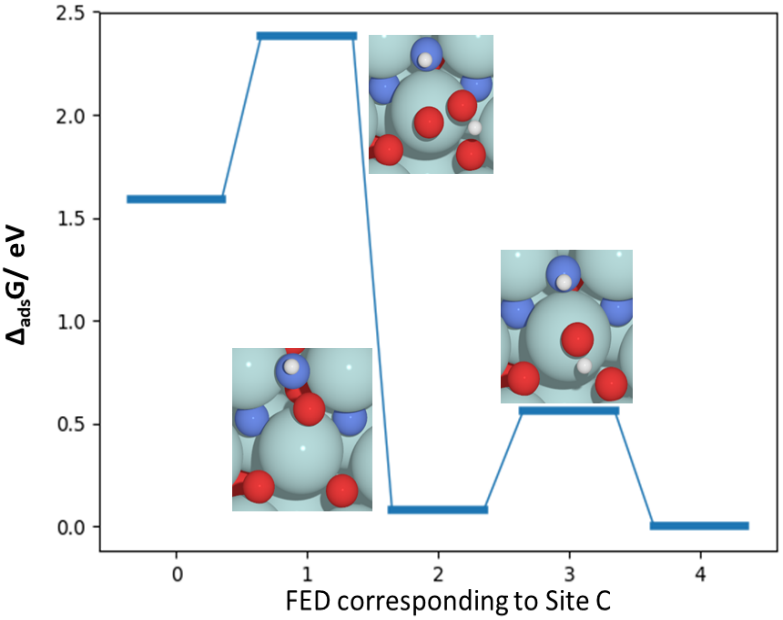

c.

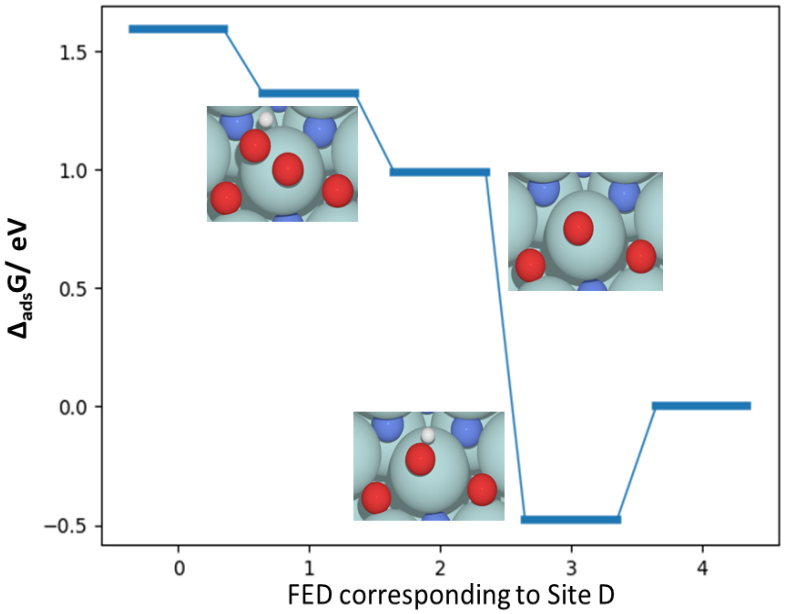
1.5
1.0
0.5
0.0
−0.5
$\Delta_{ads}G$/ eV
0
1
2
3
4
FED corresponding to Site D

d.

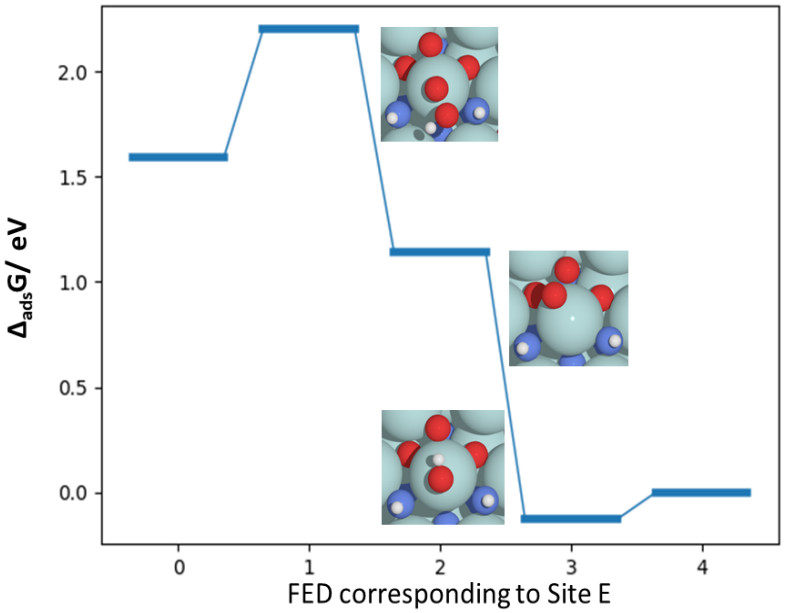
2.0
1.5
1.0
0.5
0.0
$\Delta_{ads}G$/ eV
0
1
2
3
4
FED corresponding to Site E

e.

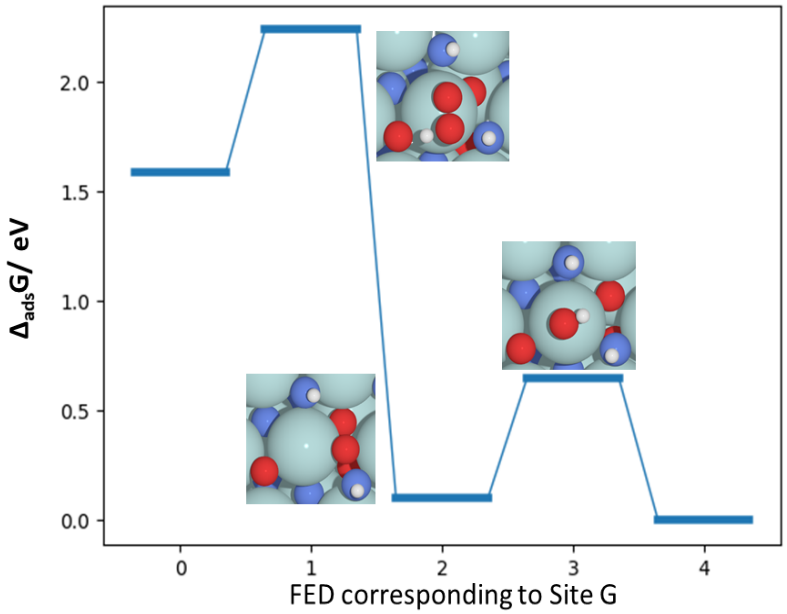
2.0
1.5
1.0
0.5
0.0
$\Delta_{ads}G$/ eV
0
1
2
3
4
FED corresponding to Site G

f.

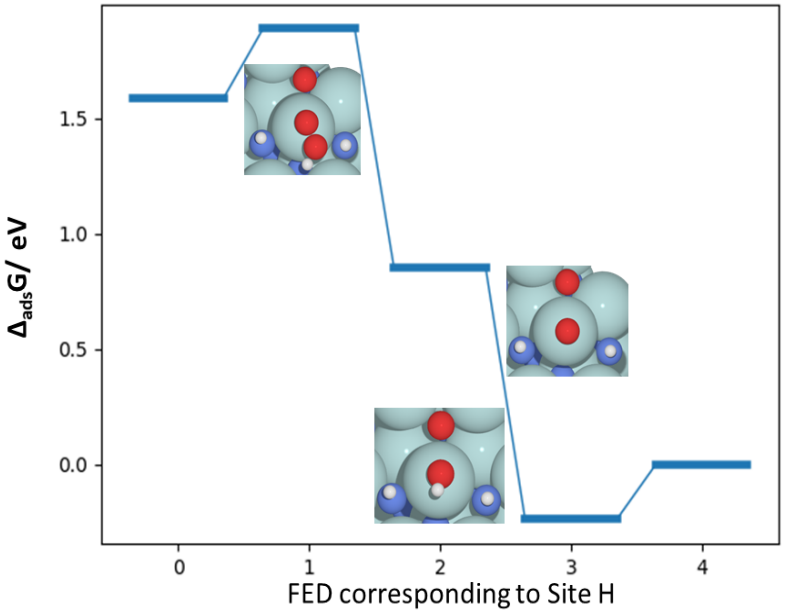
1.5
1.0
0.5
0.0
$\Delta_{ads}G$/ eV
0
1
2
3
4
FED corresponding to Site H

g.

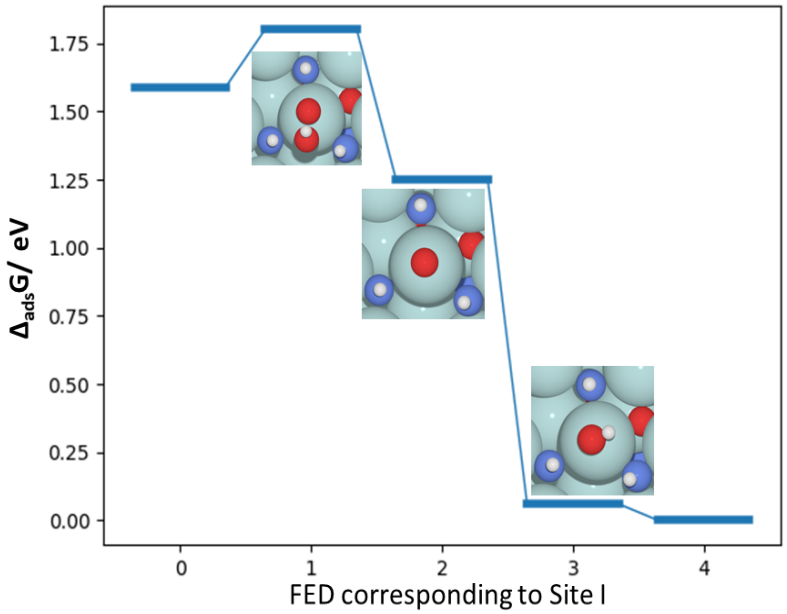
1.75
1.50
1.25
1.00
0.75
0.50
0.25
0.00
$\Delta_{ads}G$/ eV
0
1
2
3
4
FED corresponding to Site I

h.

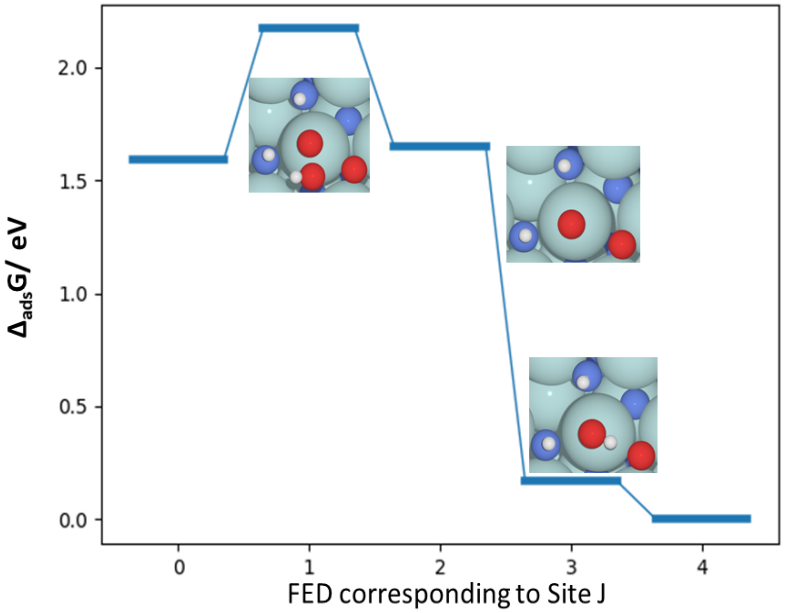
2.0
1.5
1.0
0.5
0.0
$\Delta_{ads}G$/ eV
0
1
2
3
4
FED corresponding to Site J

h.

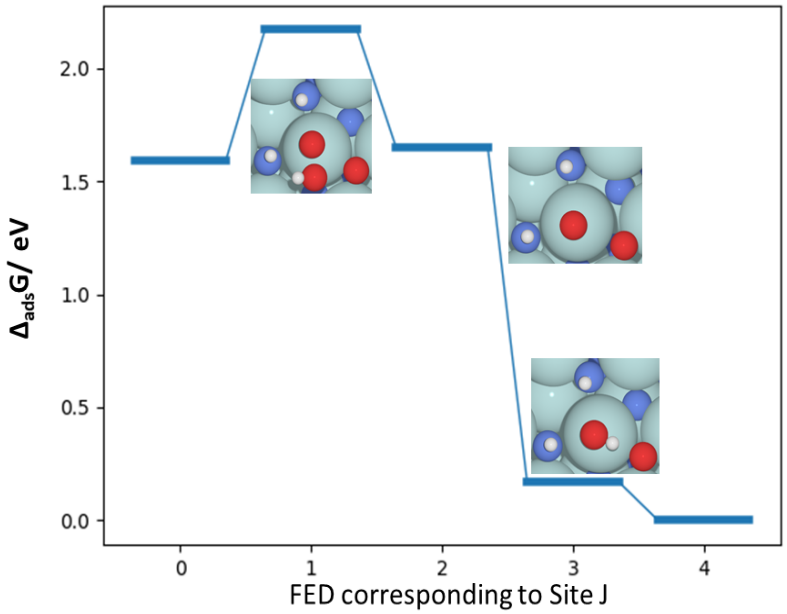
2.0
1.5
1.0
0.5
0.0
$\Delta_{ads}G$/ eV
0
1
2
3
4
FED corresponding to Site J

i.

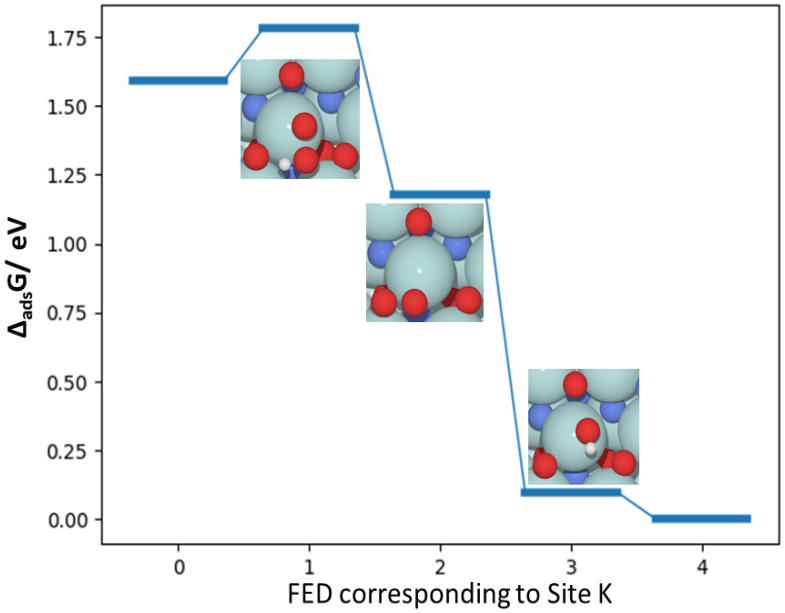
1.75
1.50
1.25
1.00
0.75
0.50
0.25
0.00
$\Delta_{ads}G$/ eV
0
1
2
3
4
FED corresponding to Site K

j.

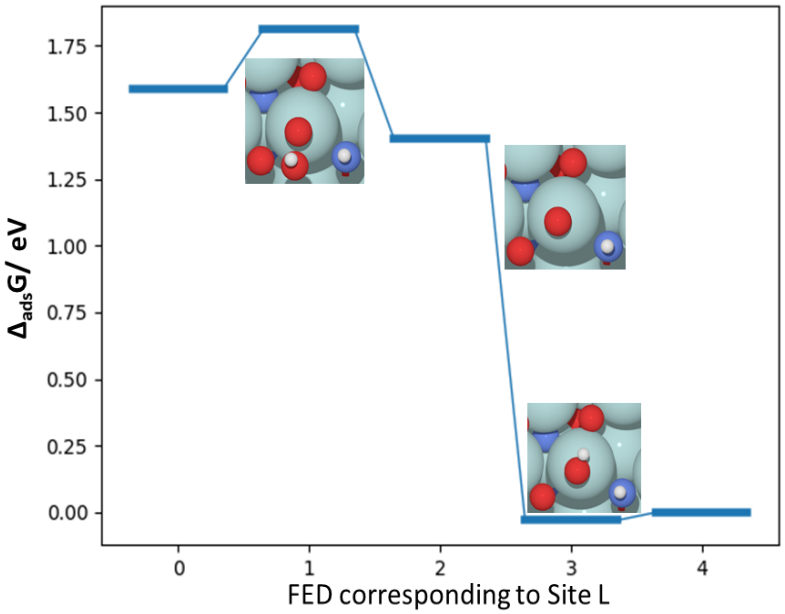
1.75
1.50
1.25
1.00
0.75
0.50
0.25
0.00
$\Delta_{ads}G$/ eV
0
1
2
3
4
FED corresponding to Site L

l.

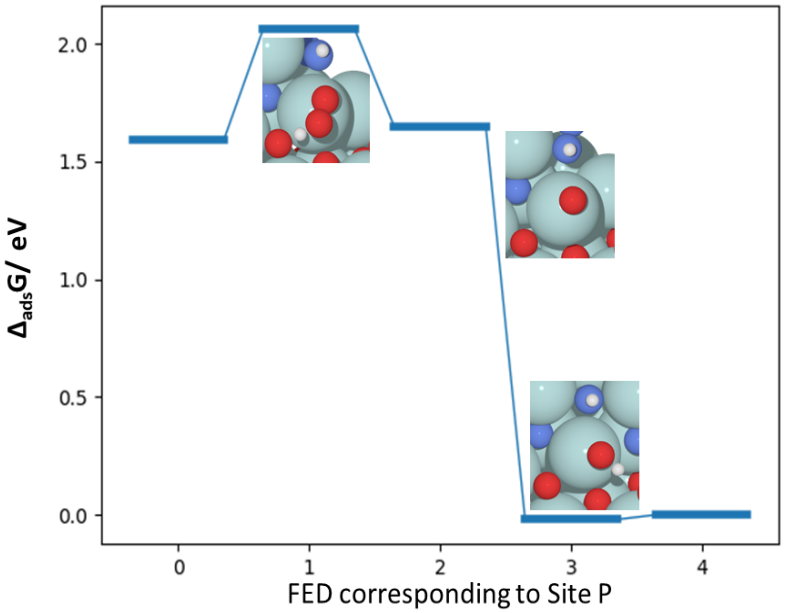
2.0
1.5
1.0
0.5
0.0
$\Delta_{ads}G$/ eV
0
1
2
3
4
FED corresponding to Site P

Free Energy Diagram at equilibrium potential

Free Energy Diagram drawn at equilibrium potential corresponding to the site B.

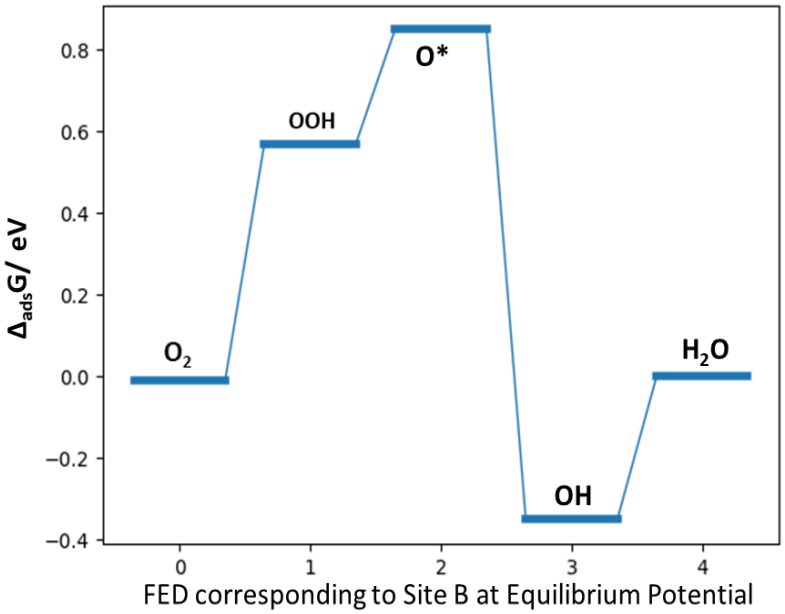

Volcano plot with OH adsorption energy as descriptor

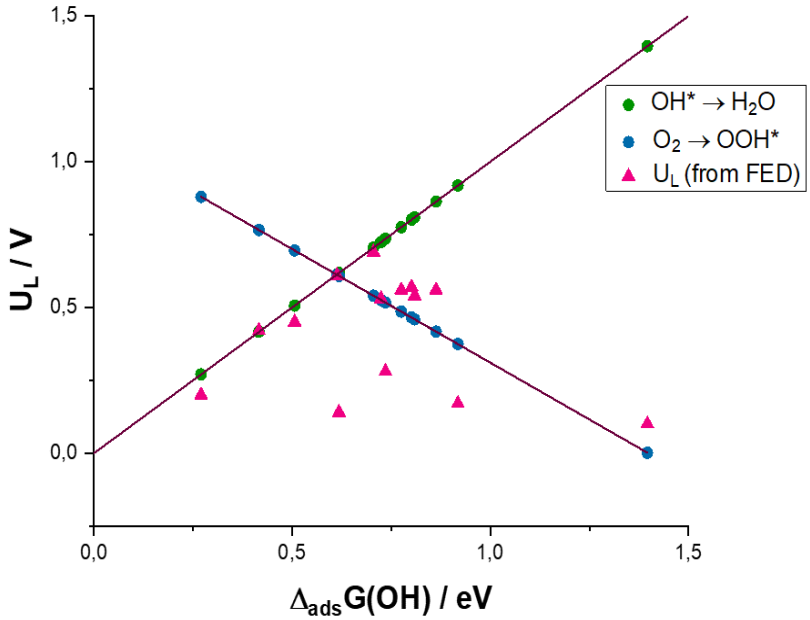

Table 1: Limiting potential and corresponding theoretical overpotential for each ontop Zr adsorption site for Zr_2ON_2 Oxygen Reduction Reaction (ORR) catalyst

Ontop Zr site	Limiting Potential, U_L (eV)	Theoretical Overpotential, η (eV)
Site A	N/A	N/A
Site B	0.57	0.58
Site C	N/A	N/A
Site D	0.27	0.88
Site E	0.14	1.01
Site F	0.46	0.69
Site G	0.1	1.05
Site H	0.45	0.70
Site I	0.54	0.61
Site J	0.17	0.98
Site K	0.56	0.59
Site L	0.53	0.62
Site M	0.56	0.59
Site N	0.42	0.73
Site O	0.69	0.42
Site P	0.28	0.68

Table 2: Limiting potential and corresponding theoretical overpotential for each ontop Zr adsorption site for Zr_2ON_2 Oxygen Evolution Reaction (OER) catalyst

Since the reaction intermediates and reaction steps are identical for ORR (Oxygen Reduction Reaction) and OER (Oxygen Evolution Reaction), the scaling relations between the adsorption energies of intermediates for ORR and OER tend to be same [**?**]. Hence, we can presume that the break in G_{O*}-G_{OOH} scaling relation for ORR should similarly translate for OER. Our preliminary calculations indicate that the OER overpotential for most of the sites on the Zr_2ON_2 surface is quite high. Hence it is unlikely that Zr_2ON_2 would be a suitable OER catalyst. It is important, though, to note that experimentally Zr_2ON_2 is yet to be explored as an OER catalyst.

Ontop Zr site	Limiting Potential, U_L (eV)	Theoretical Overpotential, η (eV)
Site A	2.92	1.69
Site B	02.35	1.12
Site C	3.05	1.82
Site D	2.23	1.00
Site E	2.02	0.79
Site F	2.40	1.17
Site G	2.90	1.67
Site H	1.85	0.62
Site I	1.94	0.71
Site J	2.23	1.00
Site K	1.82	0.59
Site L	2.18	0.95
Site M	2.21	0.98
Site N	2.28	1.05
Site O	2.34	1.11
Site P	2.42	1.19

Vacancy Formation Energies

The figure below helps visualize the vacancy sites. Twelve different calculations were carried out with different vacancies corresponding to a surface anion.

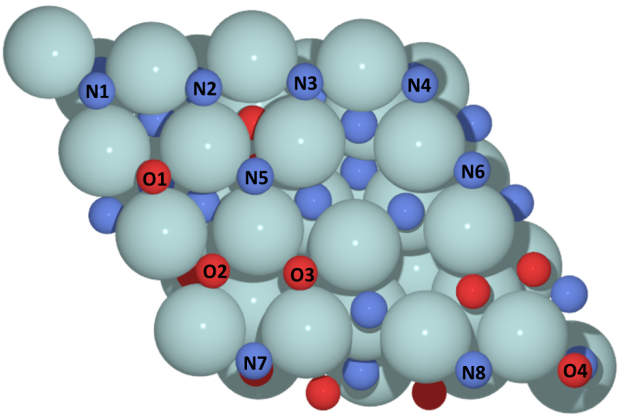

Table 2: N and O vacancy formation energies for Zr_2ON_2 surface

Vacancy site	Vacancy formation energy (eV)
Vacancy site N1	2.10
Vacancy site N2	2.17
Vacancy site N3	2.33
Vacancy site N4	2.43
Vacancy site N5	2.09
Vacancy site N6	2.09
Vacancy site N7	2.40
Vacancy site N8	2.46
Vacancy site O1	3.40
Vacancy site O2	3.45
Vacancy site O3	3.73
Vacancy site O4	3.65

Charge Density Difference Plots

In charge density difference maps, we can see two different kinds of spatial distribution of electronic charge density denoted by different colours. The yellow regions of the charge cloud signify increase in electronic charge density and blue region signify decrease in electronic charge density in those regions.

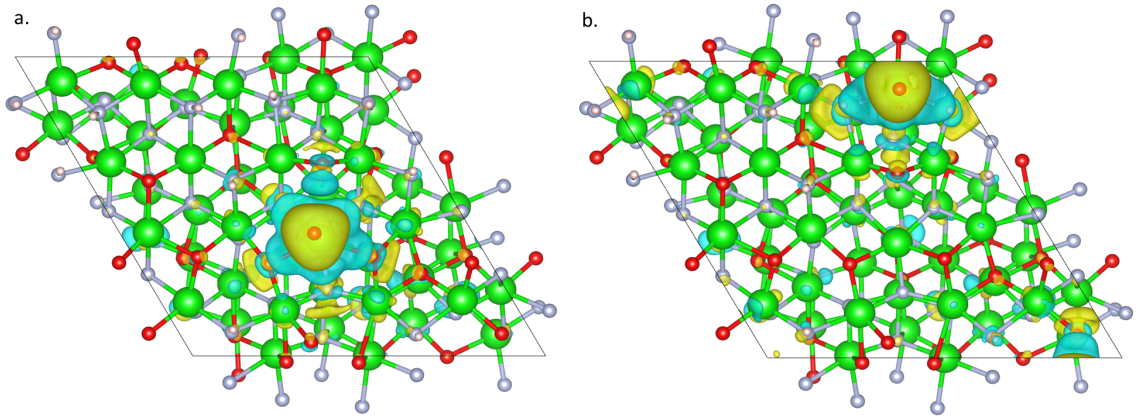

Figure 7: Charge Density Difference Diagrams corresponding to a) site D and b) site H (The lime green atom is Zr, red is O, steel grey is N and pink is H)

Appendix B

Supplementary material for ’Electronic and Structural Effects of ORR catalyst on Intermediate Binding’

This appendix is the supplemantary material of Chapter 4, which is based on the supporting information of Paper II.

Supporting Information

Bond length and ICOHP

The following figure gives us an overview of the relation between bond lengths between different pairs of atoms for OH adsorption over nitrogen and carbon substituted zirconia slabs (unconstrained and constrained).

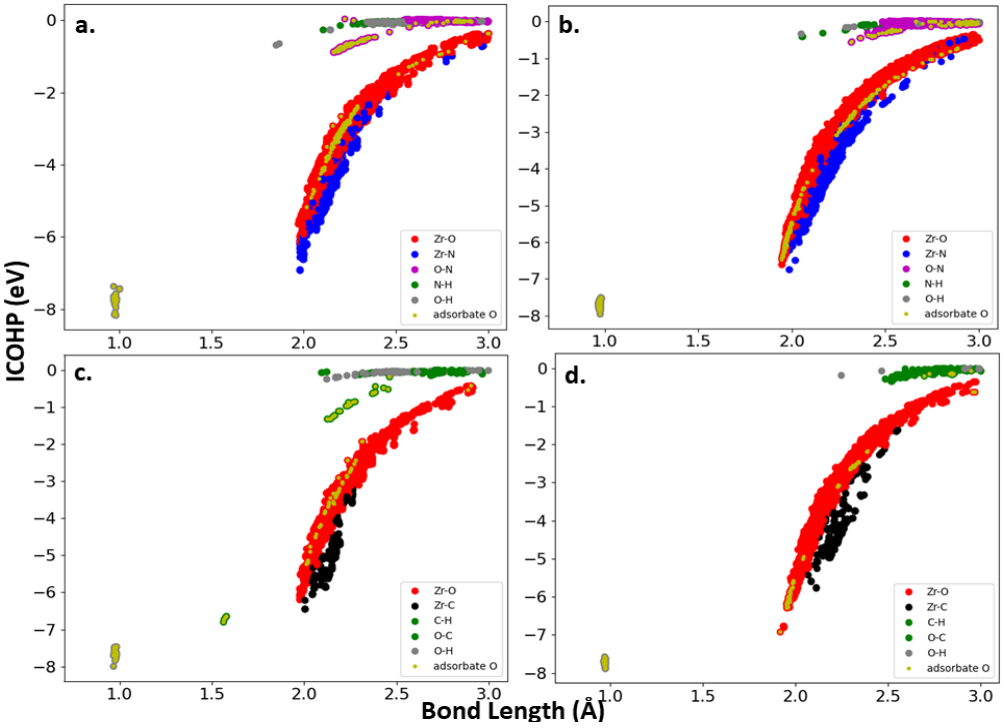

Figure 1: ICOHP vs bond length plots a) Constrained Nitrogen substituted zirconia slab b) Nitrogen substituted zirconia slab c) Constrained Carbon substituted zirconia slab d) Carbon substituted zirconia slab

Scaling Relations

The G_{O*}-G_{OH} and G_{OOH}-G_{OH} scaling relations for nitrogen substituted zirconia slab is given below.

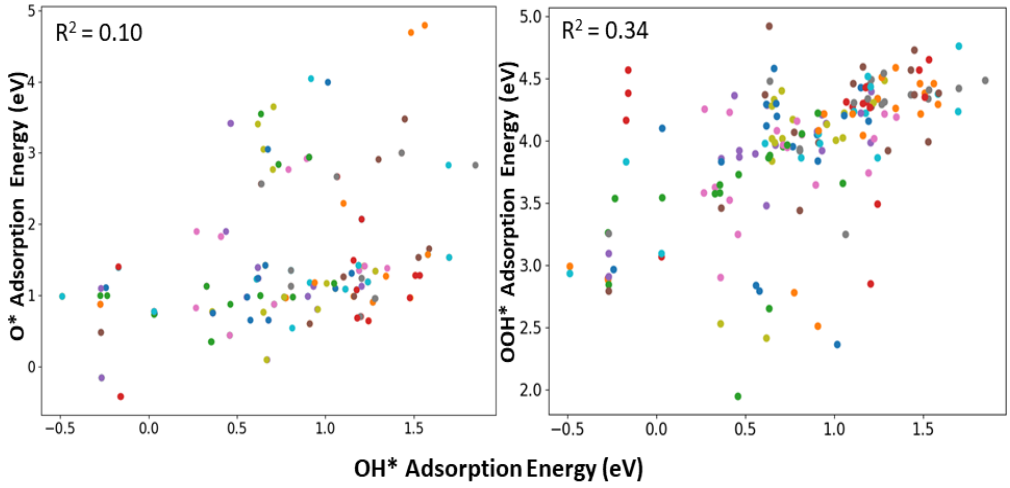

Figure 2: Scaling relations on nitrogen substituted surface corresponding to a) G_{O*}-G_{OH} scaling and b) G_{OOH}-G_{OH} scaling

The G_{O*}-G_{OH} and G_{OOH}-G_{OH} scaling relations for carbon substituted zirconia slab is given below.

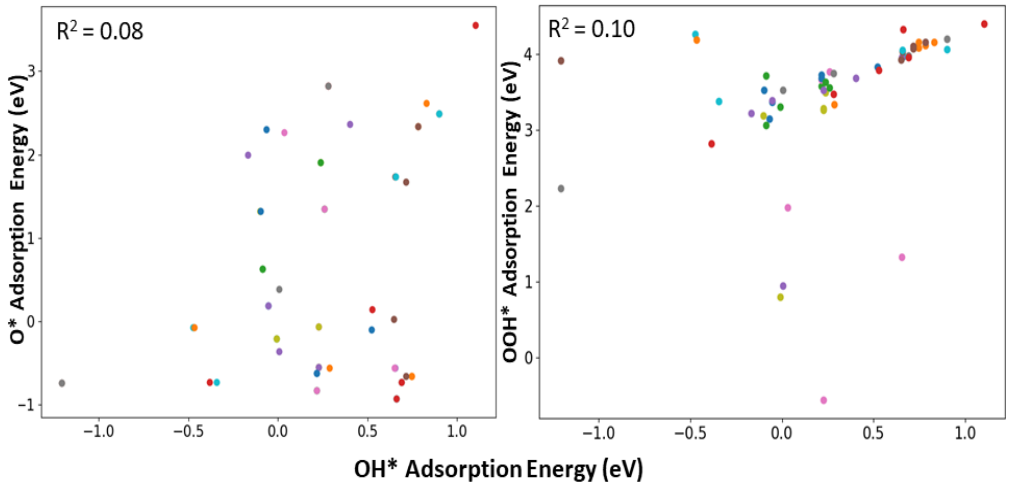

Figure 3: Scaling relations on carbon substituted surface corresponding to a) G_{O*}-G_{OH} scaling and b) G_{OOH}-G_{OH} scaling

Limiting Potential and Relative Slab Stability

The scatter plot comparing the limiting potentials with the relative stability of the slabs, in terms of DFT energy of the slab, is given below. The relative stability of the slab is computed by subtracting the DFT energy of the most stable slab from the rest. The slab with the lowest DFT energy is considered to be the most stable slab.

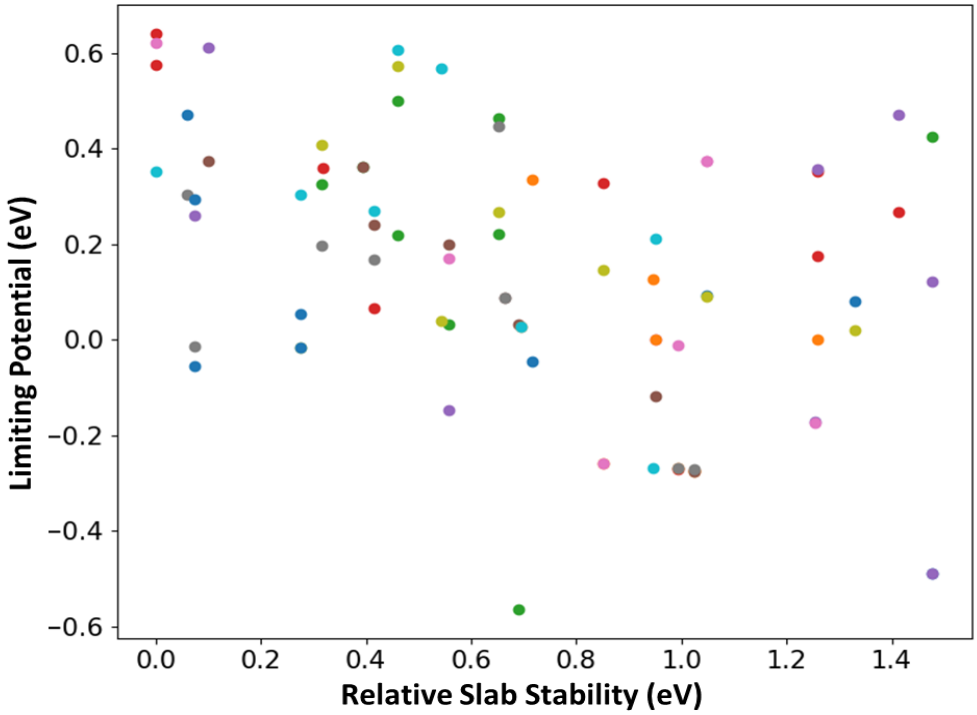

Figure 4: Limiting potential vs relative slab stability plot

Contribution to Adsorption Energy by Structural Effects

The adsorption energies obtained from optimization of constrained slabs are affected by electronic changes in the slab upon adsorption, while the ones obtained from unconstrained slabs are affected by both electronic and structural changes in the slab upon adsorption. To quantify only the structural changes in the slab we have computed the differences in the adsorption energies of the constrained and unconstrained slabs and have presented them in form of a histogram. From the histogram we can understand adsorption of O* intermediate induces structural changes in the slab to a greater degree than the other two intermediates i.e. OH and OOH intermediates.

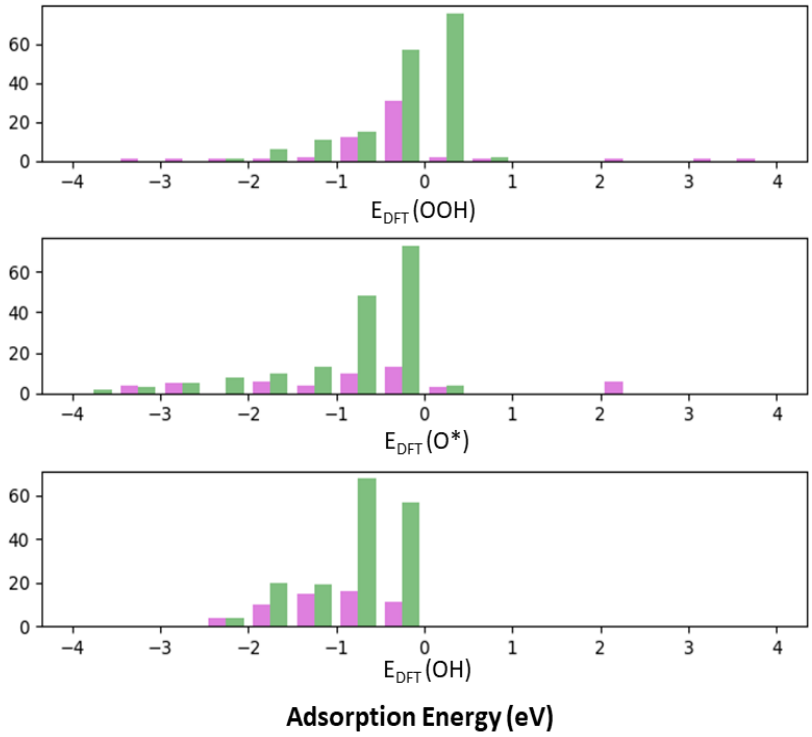

Figure 5: Histogram of structural change contribution to adsorption energies

Included Publications

Paper I

Bending the ORR Scaling Relations on Zirconium Oxynitride for Enhanced Oxygen Electrocatalysis
Sukanya Sinha, Tejs Vegge and Heine Anton Hansen
ChemCatChem, **2023**, e202300349

ChemCatChem

Research Article
doi.org/10.1002/cctc.202300349

Chemistry Europe
European Chemical Societies Publishing

www.chemcatchem.org

Bending the ORR Scaling Relations on Zirconium Oxynitride for Enhanced Oxygen Electrocatalysis

Sukanya Sinha,[a] Tejs Vegge,[a] and Heine Anton Hansen*[a]

Technologies like polymer electrolyte membrane fuel cells play an important role in environmentally friendly energy conversion. Essential for their commercialization is the development of cheap and efficient electrocatalyst for the oxygen reduction reaction (ORR). Non-platinum group metal (PGM) based catalysts has exhibited favourable activity in acidic electrolytes. In this study, we computationally explore the catalytic sites on the (111) surface of hydrated zirconium oxynitride using periodic DFT calculations. The thermodynamically limiting step is determined to be the O_2 activation step, ($O_2 \rightarrow$OOH*) for the majority of the sites, hence strengthening the OOH* intermediate binding will improve ORR activity. The calculations also reveal that the determined scaling relation for G_{OH}-G_{OOH} ($\Delta G_{OOH} = 0.78\Delta G_{OH} + 3.52$ eV) is comparable to the standard ORR scaling relation ($\Delta G_{OOH} = \Delta G_{OH} + 3.2$ eV) however G_{O*}-G_{OH} scaling ($\Delta G_{O*} = 1.04\Delta G_{OH} + 2.16$ eV) deviates dramatically from the typical ORR scaling relation ($\Delta G_{O*} = 2\Delta G_{OH}$).

Introduction

The increasing fossil fuel consumption has led to increased levels of atmospheric carbon dioxide. The combustion of fossil fuels has been linked to anthropogenic global warming, which might result in a 4 °C increase in the global mean temperature during the 21st century under certain "business as usual" fossil-rich scenarios.[1,2] Apart from carbon dioxide emission, fossil fuel combustion is also responsible for the emission of many other toxic air pollutants. The synergistic effect between climate change and air pollution can magnify health hazards.[3] Thus technologies for more environmentally friendly energy conversion are actively being pursued. One such technology is the polymer electrolyte membrane fuel cell (PEMFC).

In PEMFCs, a fuel such as methanol or hydrogen is oxidized at the anode and oxygen is reduced to water at the cathode.[4] Possible applications of PEMFC ranges from stationary to mobile and portable applications, in e.g. auxiliary power units (APU) and fuel cell electric vehicles (FCEV).[5] However the widespread use of hydrogen fuel cells continue to face several challenges the most significant of which is the high cost of the platinum-based catalyst used in the electrodes, which contributes to almost 55% of the total cost.[6] Ideally to decrease the overall cost of PEMFCs, catalysts for both the electrodes should be replaced but the slow oxygen reduction reaction (ORR) at the cathode requires much more platinum than the much faster hydrogen oxidation reaction at anode. The sluggish kinetics of the ORR at the PEMFC cathode can lead to nearly 30% efficiency decrease of the PEMFCs.[7] Thus, the development of non-precious metal catalyst for the oxygen reduction reaction, that would be cheap and effective, has received much attention.[8–11]

Some of the possible alternatives can be catalysts based on transition metal in nitrogen doped graphitic cathodes,[11] oxides and oxynitrides of transition metals e.g. tantalum,[12,13] zirconium oxide based catalysts with multiwalled carbon nanotube (MWCNTs) support[14] and niobium-titanium complex oxides,[15] among others. Exploring the ORR mechanisms on various catalyst surface, and consequently the active sites, using Density Functional Theory (DFT), helps us gain fundamental understanding regarding the same. This knowledge can be used in developing rational design strategies for improved ORR catalysts.[16–20]

Ideal electrocatalysts for hydrogen fuel cells should allow reversible reaction. For ORR to be reversible the adsorption Gibbs energy (ΔG_{ads}) profile plotted along the reduction steps should be flat.[21,22] None of the currently identified catalysts, however, satisfy the ideal ORR condition. Even on a platinum surface, the ORR intermediates HOO* is adsorbed too weakly and HO* too strongly.

Nevertheless, finding a material with larger (ΔG_{OOH}) and smaller (ΔG_{OH}) is restricted by the linear scaling existing within the (ΔG_{ads}) of the reaction intermediates which is observed almost universally for many materials.[22,23] Scaling relations refer to the correlation between binding energies of different reaction intermediates. One can explain universal scaling of ORR as strong adsorption of HOO* on a metal surface being associated with similarly strong adsorption of HO* on the same when both adsorbates have similar bonding configuration with the surface. However, this might not hold true for complex oxides and oxynitrides of transition metals since they allow various bonding configurations. These oxides and oxynitrides can provide different adsorption sites like the lattice oxygen, metal sites, oxygen vacancy or impurity sites.[24] Computational

[a] S. Sinha, Prof. T. Vegge, Prof. H. A. Hansen
Department of Energy Storage and Conversion,
Technical University of Denmark,
2800 Kongens Lyngby (Denmark)
E-mail: heih@dtu.dk

Supporting information for this article is available on the WWW under https://doi.org/10.1002/cctc.202300349

investigations of ORR on defective titanium oxide surfaces indicate possible deviations from the standard scaling relations.[24] Experimental investigations also reveal that several transition metal complex oxides and oxynitrides, like that of zirconium, titanium and tantalum, show promising activity as ORR catalysts in terms of lower overpotential than platinum ORR catalysts.[14,24,25] Hence, we would like to explore the possibility of oxynitride of another transition metal, i.e. zirconium, exhibiting deviations from standard scaling relations while showing lower overpotential than the standard platinum catalysts.

Results and Discussion

Structure of Zirconium Oxynitride

Zirconium Oxynitride are compounds with structure similar to fluorite type crystal in which part of oxygen of zirconia is replaced by nitrogen and anion vacancies. Zr_2ON_2 crystal belongs to space group Ia-3 (206) or according to the Pearson notation has the Pearson symbol of cI80.[26,27] The Pauling electronegativity difference between for oxygen (3.50) and nitrogen (3.07) gives the oxynitride covalent characteristics, which different from oxides with ionic characteristics.[28] Bulk optimisation of the representative structure of Zr_2ON_2 gives us a cubic lattice crystal structure with lattice constant of 1.01 nm which agrees very well with the experimental value of 1.0135 nm.[26] In our study we are exploring ORR on the (111) surface of Zr_2ON_2 slab.[29–31] It has a hexagonal lattice structure with lattice parameter a = 1.42 nm and a total vacuum of 1.6 nm (with 0.8 nm on both side of the slab). Water, being one of the products of the ORR, is expected to be present in the fuel cell, hence we investigate the possibility of water molecule(s) interacting with and dissociating on the catalyst surface. From Pourbaix stability analysis,[32] we conclude that water molecules interacts with the catalyst surface, dissociates over it and gets adsorbed on the surface. Various dissociation and the subsequent adsorption mechanism is studied as illustrated in Figure 1c. We presumed the water molecule could, potentially, split in different ways, either into an O atom and an OH ion or an O atom and two H atoms. These species, so formed, could further be adsorbed on the surface in many different ways. For example, the OH ion could be adsorbed into an intrinsic vacancy site and H on a surface N. Further, we have also tested low coverage (1 site) and high coverage (4 sites) configuration. The entries in the legend of Figure 1c represent the different configurations tested. The subscript V denotes an interstitial vacancy site, and the subscript L denotes a lattice site; for example, N_L and O_L represents nitrogen and oxygen lattice adsorption site. O_V in the label stands for an oxygen atom getting adsorbed in an intrinsic vacancy site. In contrast, an N_L and O_L associated with H is a hydrogen atom getting adsorbed over an oxygen or nitrogen atom lattice. For example, the $(O_V + N_LH + N_LH_2)$ would stand for the configuration where, after the water split, the O atom has adsorbed into an intrinsic vacancy site. In contrast, one H atom has adsorbed onto a surface N while two have adsorbed onto another N. According to the stability plot for water splitting over Zr_2ON_2 slab, the energetically most favorable configuration is water dissociating into an O atom and two H atoms with the O getting adsorbed in the intrinsic anion vacancy sites and the H on surface N, the configuration of the same is illustrated in Figure 1b. The structural illustration for the rest of the configurations of water splitting has been provided in the Supporting Information. The catalytic activity of the hydrated Zr_2ON_2 towards ORR is evaluated systematically by studying all the Zr-ontop site for their ORR activity.

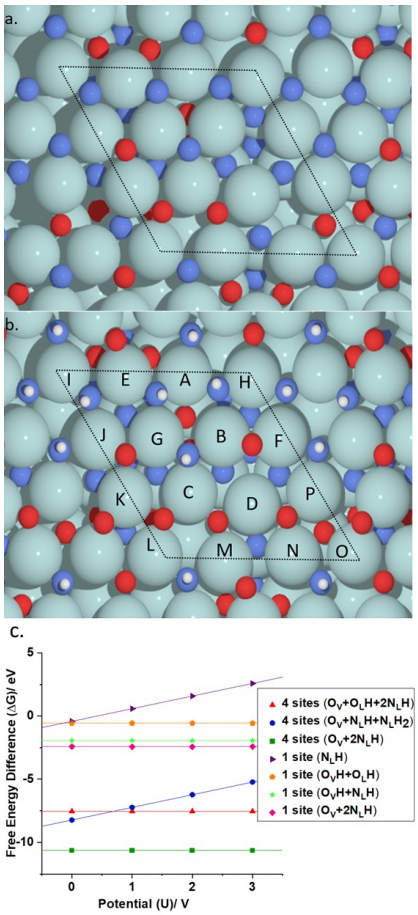

Figure 1. Geometries of Zirconium OxyNitride. (The light cyan atom is Zr, red is O, blue is N and white is H.) a) Stoichiometric slab; b) Hydrated slab: Stoichiometric slab with dissociated water adsorbed on the surface. The letters on the zirconium atoms indicate the nomenclature of the ontop-Zr sites. c) Stability plot for water splitting over Zr_2ON_2 slab.

Free Energy Diagram

It is assumed the ORR catalysed by Zr_2ON_2 proceeds through an associative mechanism, which involves hydrogenation of adsorbed molecular oxygen on the catalytic surface[33] which is evidenced from the free energy diagrams (FED) in Figure 2. The possibility of ORR on stoichiometric Zr_2ON_2 surface taking place through dissociative mechanism was also investigated. Since

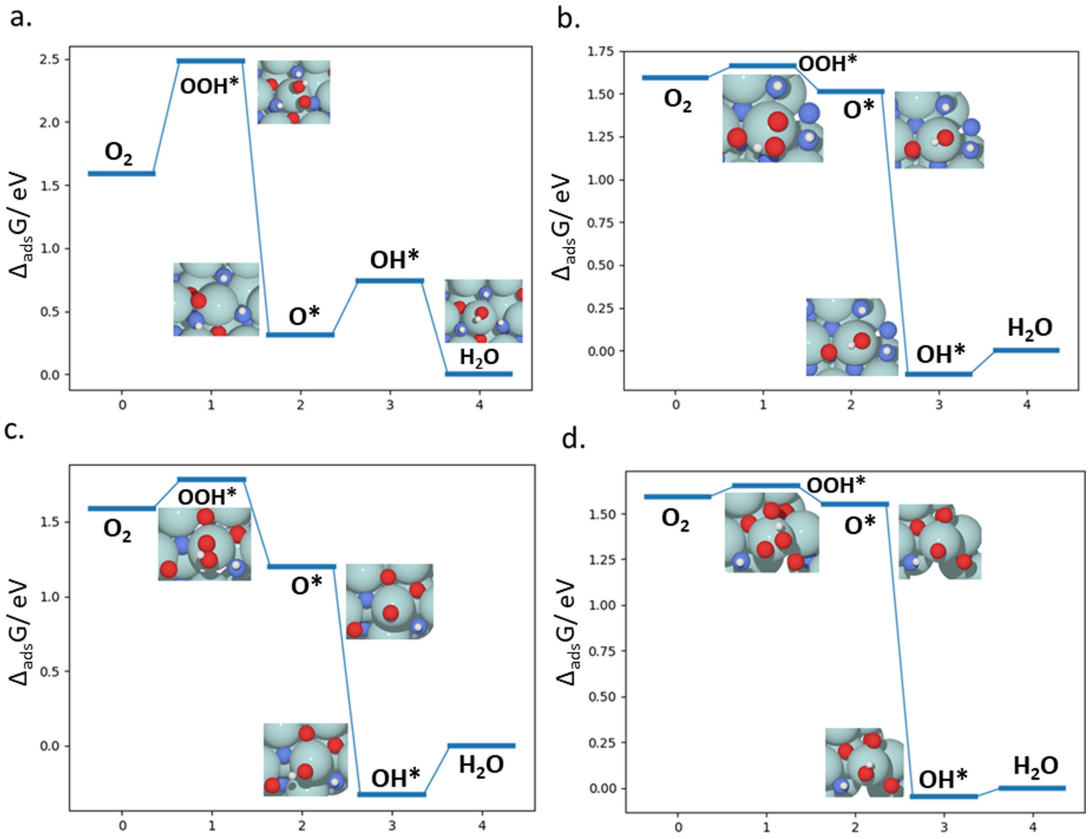

Figure 2. Free energy diagrams for the ORR taking place over selected catalytic sites. (The light cyan atom is Zr, red is O, blue is N and white is H.) A) Site A where NHO* complex formation takes place. B) Site F where O–O peroxide like complex formation takes place. C) Site N with no complex formation. D) Site O with no complex formation.

the dissociative mechanism involves direct dissociation of O_2 without the formation of the OOH* intermediate, the energy barrier of O_2 dissociation is relevant in this scenario. Our test calculations found a high O_2 dissociation barrier in the range of 1.2 to 1.55 eV. A barrier of more than 0.8 eV is generally considered unfavorable for the dissociative mechanism at low temperature; therefore, we concluded that the Zr_2ON_2 surface favours the associative mechanism for ORR.

We calculated the Gibb's free energy of adsorption for the three ORR intermediates i.e. hydroxyl (OH*), hydroperoxyl (OOH*) and oxide (O*) using the computational hydrogen electrode (CHE) approach and have investigated all the Zr-ontop sites as potential catalytic sites and the free energy diagrams (FED) show that majority of them provide stable binding sites for these ORR intermediates. We had also sampled various orientations of the adsorbates over the Zr_2ON_2 slab and the reported adsorption energies correspond to the geometric configurations that give us the lowest adsorption energy. With respect to adsorption of different intermediates on the catalytic sites of the hydrated Zr_2ON_2(111) slab, we can make certain observations. During adsorption of OH and OOH intermediates; they adsorb directly on all of the ontop Zr sites. Although for most of the ontop-Zr catalytic sites, direct adsorption of the O* intermediate also takes place, for certain sites they form NHO* or O–O* peroxide-like intermediates upon adsorption. Even in the cases where there is no complex formation, we can see some of the O* adsorbs on the Zr-ontop sites while others move towards a bridge site.

The FEDs for each adsorption sites are initially constructed at the equilibrium potential. (All the FEDs are provided in the Supporting Information). The favourable ORR catalytic sites are the ones for which the constructed FEDs have reaction steps have potential energy that are downhill at the highest possible potential. Within the CHE model the highest potential at which all the reaction steps are downhill in free energy is called the thermodynamic limiting potential, (U_L). The theoretical over-potential (η) is defined as the difference between the equilibrium potential and the values of U_L. The η as well as the U_L gives us the measure of the activity of a catalyst. Higher the U_L and correspondingly lower the η implies higher catalytic activity.

In Figure 2, the FEDs have been drawn at an overpotential of 0.4 V. A FED constructed at equilibrium potential is provided in the Supporting Information for reference. In Figure 2, we have different subfigures corresponding to different adsorption configuration of the O* intermediates. Since adsorption of OH* and OOH* intermediates are similar, directly on the ontop-Zr sites, we have chosen adsorption of O* intermediate as the differentiating factor to group different FEDs. Hence we have a subfigures which are FEDs corresponding to situations where

formation of NHO* complex, O–O peroxide like complex or no complex forms upon adsorption of O*.

When we observe all the FEDs together, we can observe that there are different values of U_L corresponding to every Zr-ontop sites. The values for the U_L and η corresponding to every Zr-ontop sites is given in Table S1 of the Supporting Information. This brings us to the conclusion that different catalytic sites possess different catalytic activity, where the sites with higher U_L are more active. We observe the presence of two catalytic sites where the U_L is negative; this means those two sites are unfavorable for the ORR in an H_2 fuel cell. These two sites, site A and C, along with another site, G, with very low limiting potential ($U_L = 0.1$), are the ones where formation of a NHO* complex takes place upon O* adsorption. The FED corresponding to site A is illustrated in Figure 2a. Hence this leads us to believe that the formation of this NHO* complex leads to deactivation or very low activity of the catalytic sites. We also notice the formation of a peroxide-like complex upon O* adsorption on certain sites. For sites B, F, and K the value of U_L is high (< 0.5 V) while for other site E it is low (> 0.15 V). Hence it can be concluded that the O–O peroxide-like complex formation does not seem to have any effect on the catalytic activity of those sites. For most of the sites, however, the adsorption of O* does not give rise to formation of any complex.

We have also, very briefly, explored the possibility of Zr_2ON_2 surface as a catalyst for oxygen evolution reaction (OER). The reader can refer to the Supporting Information regarding the same.

We had, also, investigated the possibility of the Zr_2ON_2 surface undergoing a Mars van-Krevelen mechanism[34] involving N or O vacancies and computed the O and N vacancy formation energies for the same. However the O and N vacancy formation energies were quite high, in the range of more than 2 eV for N-vacancy formation and around 3.5 eV for O-vacancy formation. These values lead us to conclude that such a mechanism was unlikely to take place on the Zr_2ON_2 surface. A detailed table with all the vacancy formation energies is given in the Supporting Information. Additionally, vacancy formation energy values indicate the stability of the Zr_2ON_2 surface. This conclusion is also corroborated by various experimental studies.[35,36]

Scaling Relations and Volcano Plots

Observing Figure 3a and 3b, we can conclude that scaling relations exist between the ORR intermediates on Zr_2ON_2 catalyst. The OOH* or O* vs OH* scaling relations imply that there exists a single independent variable that can be used to describe the binding energies of all the ORR intermediates on the catalyst surface. We have used OH adsorption free energy as the descriptor for our scaling relations. (Note: The O* adsorption energies corresponding sites where NHO* complex formation takes place are not included in the G_{O*}-G_{OH} scaling relation since they form outliers.) Since the theoretical overpotential is a function of free energy and correspondingly that

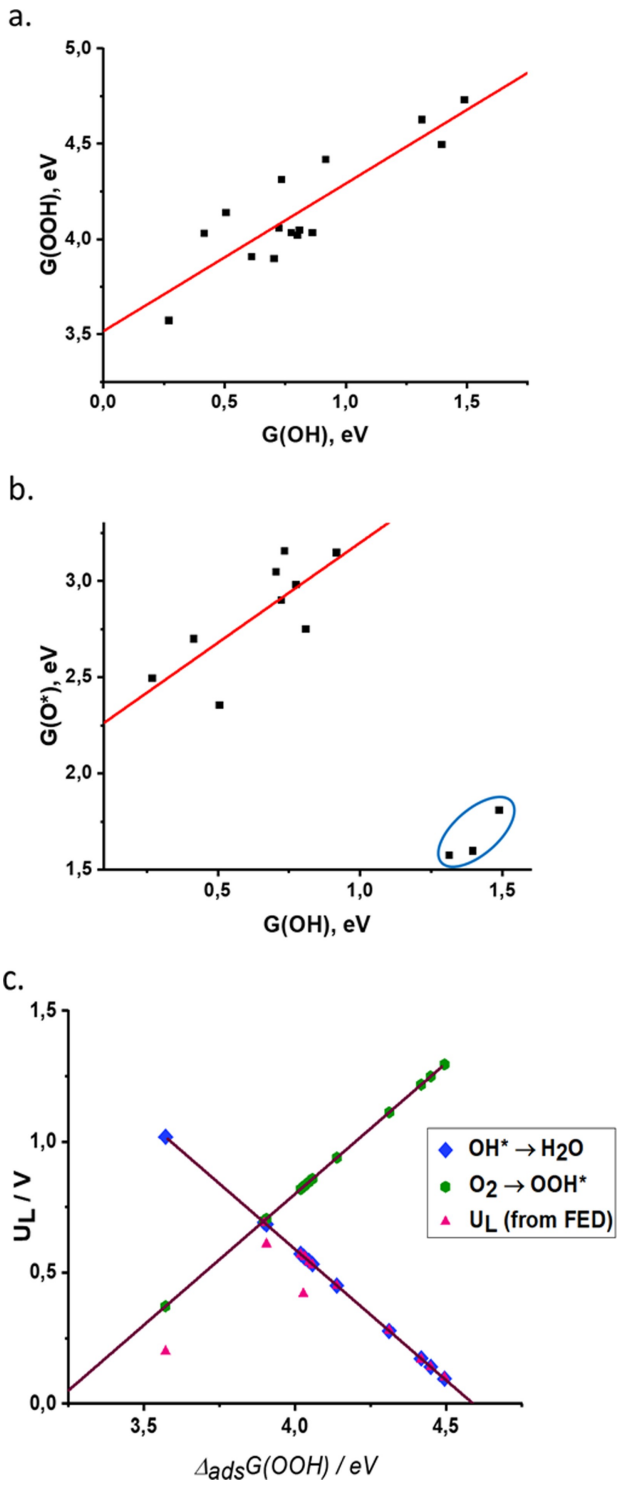

Figure 3. Scaling relations for adsorption energies of ORR intermediates at ontop Zr sites. A) Scaling relation between OH and OOH intermediates. B) Scaling relation between OH and O* intermediates. (The outliers circled in blue correspond to the O* adsorption where formation of NHO* complex takes place.) C) Volcano plot with OOH adsorption free energy as the descriptor.

of binding energy, scaling relations are also used to determine the limiting potential. From the scaling relation plots in Figure 3, it can be seen that there exists a linear correlation

between the the adsorption energies of OOH* and O* vs OH*. The scaling relations that are determined for the Zr_2ON_2 catalyst from the adsorption energies of the intermediates are as follows:

$$\Delta G_{OOH} = 0.78\Delta G_{OH} + 3.52\ \text{eV} \quad (1)$$

$$\Delta G_{O*} = 1.04\Delta G_{OH} + 2.16\ \text{eV} \quad (2)$$

The determined scaling relation for G_{OH}-G_{OOH} is comparable to that of the standard ORR scaling relation:

$$\Delta G_{OOH} = \Delta G_{OH} + 3.2\ \text{eV} \quad (3)$$

however the one for G_{O*}-G_{OOH} deviates dramatically from the typical ORR scaling relation:

$$\Delta G_{O*} = 2\Delta G_{OH} \quad (4)$$

The standard scaling relation is typically observed for a wide range of materials like porphyrins,[37] boron nitride,[38] MoS_2,[38] ultrathin metal oxide sheets,[38] MN_4 motifs in graphene,[38] carbons and HAB-based coordination polymers.[22,39] A previous study[40] reports scaling relations for platinum slab with explicit solvation with no significant deviation from the standard scaling relation. This leads makes us believe hydration is not the reason for the dramatic deviation of the G_{O*}-G_{OH} scaling that we observe here.

As we have discussed earlier, the OH and OOH intermediates adsorb directly on all of the ontop Zr sites without exception. However this is not true for the O* intermediate. On few sites it forms complexes like the NHO* complex or O–O* peroxide-like complex. Even in absence of complex formation, adsorption on bridge sites is observed for some sites while for others absorption on ontop sites is observed. We refer to this phenomena as the atypical adsorption of O* intermediate on the Zr_2ON_2 surface and believe this is the cause for deviation in OOH vs O* scaling relation. This is evident from Figure 3b where we can see the outliers circled in blue corresponding to sites where NHO* formation takes place. Hence we believe the atypical adsorption of O* intermediate also causes the deviation in $\Delta G_{O*} = 2\Delta G_{OH}$ scaling relation.

While discussing the binding energies of the ORR intermediates to the catalytic sites on the Zr_2ON_2 surface it is worth mentioning that most sites bind the ORR intermediates too weakly. Hence, contrary to many transition metal ORR catalysts where $*OH \rightarrow H_2O$ is the potential limiting step,[32,41] in case of Zr_2ON_2 catalyst O_2 activation, $O_2 \rightarrow *OOH$, is the potential limiting step for majority of the catalytic sites. To maximise the descriptive power of the volcano plot, we therefore use *OOH adsorption free energy as the descriptor instead of using *OH adsorption free energy. The volcano plot with the commonly used *OH descriptor is shown in Supporting Information. The volcano indicates that the minimum theoretical overpotential of the Zr_2ON_2 catalyst is around 0.45 eV. This value of overpotential is in agreement with the experimentally determined values for ZrO_xN_y-MWCNT catalyst at a current density of 0.1 A cm^{-2}.[14] Similar values have been reported by other experimental studies as well.[42–44] The weak binding of ORR intermediates further agrees with the experimentally observed O_2 reduction.[17] The weak binding of reaction intermediates also indicates that several sites are also selective for the 2 electron pathway of ORR.[17]

The scope of our study is limited to the thermodynamics of reaction intermediates, which have been found to well describe trends in ORR activity on the terraces of metal surfaces well. Incorporating surface kinetics is expected to provide similar trends as the thermodynamic analysis while suppressing the activity around the apex of the volcano.[16]

Density of States

The total and partial density of states (TDOS and pDOS) are plotted to clarify the bond formation. As SCAN functional is better suited for computing band gaps, we use it for our density of states calculations.[45] In our DOS plot the Fermi level (E_f) is at 0 eV. Figure 4 shows the total and partial density of states of stoichiometric Zr_2ON_2 slab, hydrated Zr_2ON_2 slab and a hydrated Zr_2ON_2 slab with an O* adsorbate. From the Figures 4a and 4b, we can see that the there is a reduction of band gap upon hydration of the Zr_2ON_2 slab. The stoichiometric slab has a band gap of 0.8 eV which reduces to 0.4 eV when the slab is hydrated. This implies that the hydration of the slab makes it a better conductor. The fermi level is within the band gap, and the top of the valence band is formed mainly by N 2p states and to a lesser extend O 2p and Zr states. The conduction band has mainly Zr 3d character. As we can see from Figures 4b and 4c, there is a increase in DOS and N pDOS intensity around the E_f upon adsorption of O* on the hydrated Zr_2ON_2 slab. Upon adsorption of O*, the fermi level moves below the top of the valence band indicating that N, O, and Zr contributes with charge to bind the O* adsorbate. The magnitude of DOS at E_f can serve as indicator for the ability to form bonds with adsorbed species.[46] Along with the DOS and pDOS plots, we have also studied several electronic properties like band centre, band-width and fractional band filling.[47–49] We have also tried to find out if relationships between electronic properties and binding energies exist. However none of the analysis carried out could capture the complexity of the Zr_2ON_2 catalyst.

In charge density difference maps (present in the Supporting Information) we can see two different kinds of spatial distribution of electronic charge density denoted by different colours. The yellow regions signify increase in electronic charge density and blue region signify decrease in electronic charge density in those regions. This helps us to draw the conclusion that the charge transfer occurs at the adsorption site. Most significant charge transfer is near the surface with the charge being transferred from the zirconium atom to the O* adsorbate. Some charge transfer is also observed for the neighbouring nitrogen and oxygen atoms near the ontop-Zr sites.

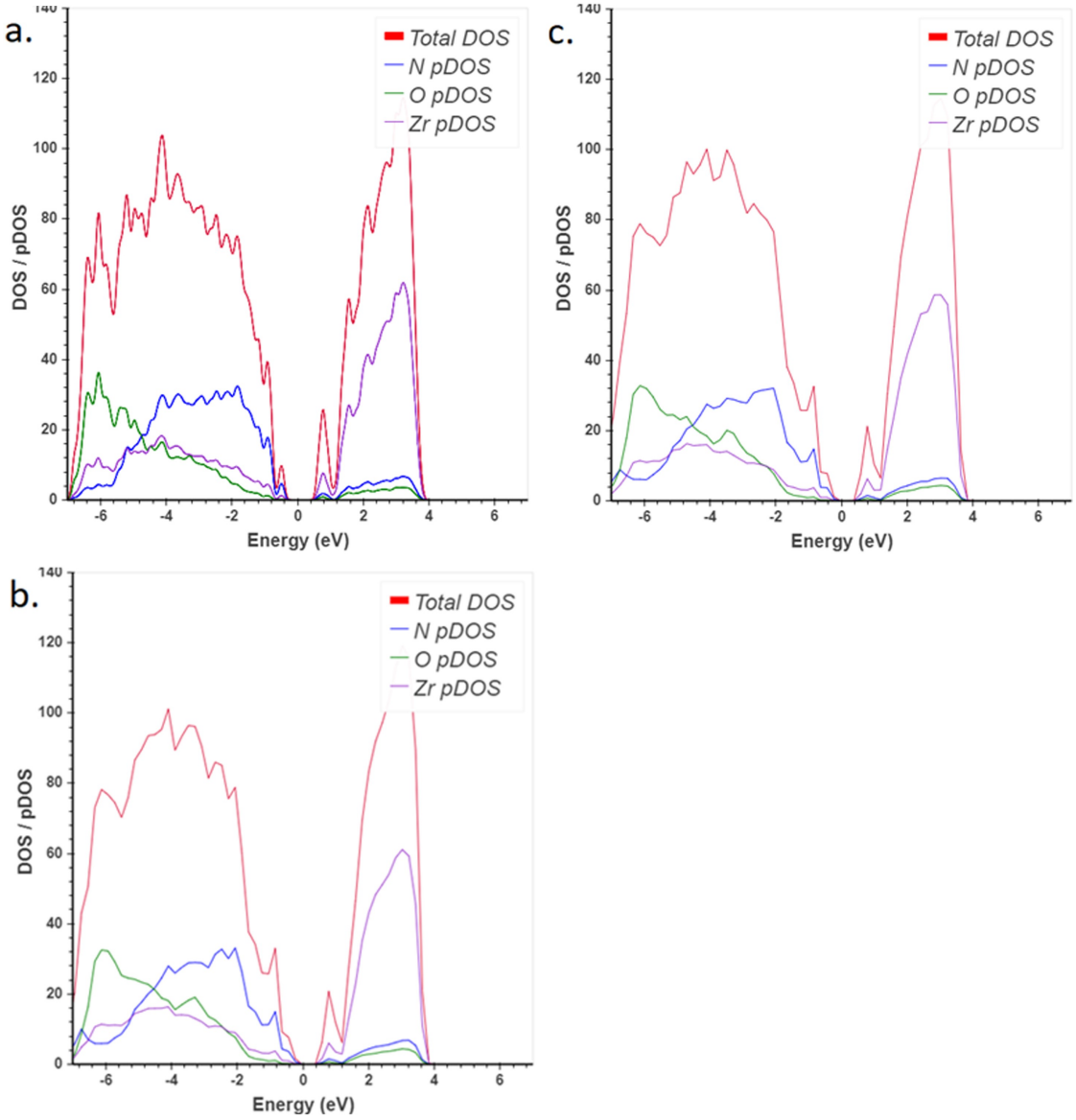

Figure 4. Calculated total and projected density of states for Zirconium Oxynitride. A) Stoichiometric slab; B) Hydrated slab: Stoichiometric slab with dissociated water adsorbed on the surface. C) Hydrated slab with O* adsorbate on ontop Zr site O.

Conclusions

Our DFT calculations show that Zr_2ON_2 is a viable candidate as an ORR catalyst with Zr-ontop sites acting as the active catalytic sites. However, the sites that shows NHO* complex formation during O* adsorption are either inactive or very mildly active sites. Ideal electrocatalysts for ORR must allow it to occur reversibly and complex oxides of transition metals are viable candidates for the same.[50] Our calculations also revealed that the universal scaling line between O* and OH* adsorption free energy can be broken by using a complex oxide surface of a transition metal oxynitride. This does, however, not lead to improved ORR activity. On the basis of scaling relations, we also plot the activity volcano which helps us draw the conclusion that the maximum limiting potential for the Zr_2ON_2 catalyst is approximately 0.70 V which agrees with the experimentally determined onset potential.[14,42,43] From the ORR kinetics and FEDs of individual catalytic sites we also understand that all sites are not equally active.

Computational Details

All density functional theory (DFT) calculations are done using the Vienna Ab Initio Simulation Package (VASP) and the core electrons are described with the projector augmented wave (PAW) method.[51,52] The Perdew-Burke-Ernzerhof functional (PBE) is used to describe the exchange and correlation energy.[53] The Atomic Simulation Environment (ASE) is used to set up and analyse the structures, which are optimised with a plane wave cutoff of 500 eV and Brillouin-zone integration is performed with a Monkhorst-Pack

k-point mesh of 2×2×1.[54,55] The self-consistent electron density loop is converged to 10^{-6} eV and the structures are relaxed until all forces are below 0.02 eV Å^{-1}.

We have studied the (111) surface of zirconium oxynitride (Zr_2ON_2) which is modeled by a periodic non-polar slab. The model includes 3 cationic layers with the bottom layer fixed in its position and the upper two layers allowed to relax. The associative mechanism for ORR, given below, is well established, where the reaction proceeds through four electron-proton transfer steps.[40]

$$^* + O_2 + H^+ + e^- \rightarrow ^* OOH \quad (5)$$

$$^*OOH + H^+ + e^- \rightarrow ^* O + H_2O \quad (6)$$

$$^*O + H^+ + e^- \rightarrow ^* OH \quad (7)$$

$$^*OH + H^+ + e^- \rightarrow ^* + H_2O \quad (8)$$

where * denotes the active sites on the catalyst surface.

Adsorption Free Energy

The standard computational hydrogen electrode (CHE) approach is used to calculate the reaction free energies of electrochemical reaction steps.[21] Using the CHE, the reaction free energy, ΔG_i, of a reduction step can be written as:

$$\Delta G_i = \Delta G_i^0 + eU \quad (9)$$

where ΔG_i^0 is the reaction free energy at 0 V versus the reversible hydrogen electrode (RHE) and U_L is the potential measured against the reversible hydrogen electrode. The DFT reaction energy corresponding to the following reactions are defined here as the adsorption energies.

$$^* + H_2O \rightarrow ^* O + H_2, \quad \Delta_{ads}E(O^*) \quad (10)$$

$$^* + H_2O \rightarrow ^* OH + 0.5H_2, \quad \Delta_{ads}E(OH) \quad (11)$$

$$^* + 2H_2O \rightarrow ^* OOH + 1.5H_2, \quad \Delta_{ads}E(OOH) \quad (12)$$

For the adsorbed species, the Gibb's free energies are calculated using the ASE package with the assumption that adsorbate degrees of freedom can be approximated by independent quantum mechanical harmonic oscillators and the vibrational frequencies of only the adsorbates are calculated. The free energy calculations for gas molecules are carried out with the ideal gas approximation[56] and those for adsorbates are carried out with harmonic approximation[57–59] where finite differences with 2 displacements of 0.01 Å are used to calculate force constants. The Gibb's free energy includes the zero point energy and entropy. For the gas phase molecules, Gibb's free energies are calculated assuming them to be ideal gas molecules.

$$\Delta G(U=0) = \Delta E_{DFT} + \Delta E_{ZPE} + \Delta U_{vib}(T) - T\Delta S_{vib}(T) \quad (13)$$

Here, the ΔG is calculated from DFT and it includes changes in electronic energy (ΔE_{DFT}) along with contributions from zero-point energy (ΔE_{ZPE}), vibration energy ($\Delta U_{vib}(T)$) and entropy ($\Delta S_{vib}(T)$) at T = 298.15 K.

We use the equilibrium potential derived from DFT calculations in this study which is determined to be 1.15 V, slightly lower than the experimentally determined one of 1.23 V. The experimentally determined equilibrium potential corresponds to the value of reaction free energy of the overall reaction ($O_2 + 2H_2 \rightarrow 2H_2O$) that is 4.92 eV. However, the calculated value of equilibrium potential of 1.15 V is determined for our calculations of the H_2O formation free energy of 2.3 eV with the PBE functional. A simple one-to-one correspondence between equilibrium potential and adsorption free energy helps us determine the theoretical equilibrium potential of 1.15 V. Difference is due to DFT error on the reaction energy.

Acknowledgements

This work was supported by the Villum Foundation through the research center V-Sustain (grant number 9455).

Conflict of Interests

The authors declare no conflict of interest.

Data Availability Statement

The data that support the findings of this study are available in the supplementary material of this article.

Keywords: Oxygen Reduction Reaction · Density Functional Theory · zirconium oxynitride · scaling relations · non-PGM electrocatalyst

[1] P. Friedlingstein, M. O'sullivan, M. W. Jones, R. M. Andrew, J. Hauck, A. Olsen, G. P. Peters, W. Peters, J. Pongratz, S. Sitch, et al., Global carbon budget 2020 **2020**.
[2] M. Collins, R. Knutti, J. Arblaster, J. Dufresne, T. Fichefet, P. Friedlingstein, X. Gao, Gutowski, 10 WJ **2013**.
[3] F. Perera, *Int. J. Environ. Res. Public Health* **2018**, *15*, 16.
[4] S. Litster, G. McLean, *J. Power Sources* **2004**, *130*, 61.
[5] F. C. Handbook, Inc., Albuquerque, NM, DOE/NETL-2004/1206 **2004**, pages 1–10.
[6] Y. Bing, H. Liu, L. Zhang, D. Ghosh, J. Zhang, *Chem. Soc. Rev.* **2010**, *39*, 2184.
[7] M. J. Janik, C. D. Taylor, M. Neurock, *J. Electrochem. Soc.* **2008**, *156*, B126.
[8] A. Muthukrishnan, Y. Nabae, T. Hayakawa, T. Okajima, T. Ohsaka, *Catal. Sci. Technol.* **2015**, *5*, 475.
[9] M. Lefèvre, E. Proietti, F. Jaouen, J.-P. Dodelet, *Science* **2009**, *324*, 71.
[10] J. Shui, M. Wang, F. Du, L. Dai, *Sci. Adv.* **2015**, *1*, e1400129.
[11] G. Wu, K. L. More, C. M. Johnston, P. Zelenay, *Science* **2011**, *332*, 443.
[12] A. Ishihara, S. Doi, S. Mitsushima, K.-I. Ota, *Electrochim. Acta* **2008**, *53*, 5442.
[13] N. Uehara, A. Ishihara, T. Nagai, M. Matsumoto, H. Imai, Y. Kohno, K. Matsuzawa, S. Mitsushima, K. Ota, *Electrochim. Acta* **2015**, *182*, 789.
[14] M. Chisaka, A. Ishihara, H. Morioka, T. Nagai, S. Yin, Y. Ohgi, K. Matsuzawa, S. Mitsushima, K.-I. Ota, *ACS Omega* **2017**, *2*, 678.
[15] M. Hamazaki, A. Ishihara, Y. Kohno, K. Matsuzawa, S. Mitsushima, K.-I. Ota, *Electrochemistry* **2015**, *83*, 817.
[16] V. Viswanathan, H. A. Hansen, J. Rossmeisl, J. K. Nørskov, *ACS Catal.* **2012**, *2*, 1654.
[17] V. Viswanathan, H. A. Hansen, J. Rossmeisl, J. K. Nørskov, *J. Phys. Chem. Lett.* **2012**, *3*, 2948.
[18] V. Tripković, E. Skúlason, S. Siahrostami, J. K. Nørskov, J. Rossmeisl, *Electrochim. Acta* **2010**, *55*, 7975.
[19] W. Liang, J. Chen, Y. Liu, S. Chen, *ACS Catal.* **2014**, *4*, 4170.

[20] J. Greeley, I. Stephens, A. Bondarenko, T. P. Johansson, H. A. Hansen, T. Jaramillo, J. Rossmeisl, I. Chorkendorff, J. K. Nørskov, *Nat. Chem.* **2009**, *1*, 552.
[21] J. K. Nørskov, J. Rossmeisl, A. Logadottir, L. Lindqvist, J. R. Kitchin, T. Bligaard, H. Jonsson, *J. Phys. Chem. B* **2004**, *108*, 17886.
[22] A. Kulkarni, S. Siahrostami, A. Patel, J. K. Nørskov, *Chem. Rev.* **2018**, *118*, 2302.
[23] Y. Okamoto, O. Sugino, *J. Phys. Chem. C* **2010**, *114*, 4473.
[24] Y. Yamamoto, S. Kasamatsu, O. Sugino, *J. Phys. Chem. C* **2019**, *123*, 19486.
[25] A. Ishihara, K. Lee, S. Doi, S. Mitsushima, N. Kamiya, M. Hara, K. Domen, K. Fukuda, K.-I. Ota, *Electrochem. Solid-State Lett.* **2005**, *8*, A201.
[26] Zr2ON2 (Zr2 N2O cub) Crystal Structure: Datasheet from "PAULING FILE Multinaries Edition – 2012" in SpringerMaterials.
[27] https://materials.springer.com/isp/crystallographic/docs/sd_0382 copyright 2016 Springer-Verlag Berlin Heidelberg & Material Phases Data System (MPDS), Switzerland & National Institute for Materials Science (NIMS), Japan.
[28] S. Clarke, C. Michie, M. Rosseinsky, *J. Solid State Chem.* **1999**, *146*, 399.
[29] I. Bertóti, *Catal. Today* **2012**, *181*, 95.
[30] G. Cubillos, J. Olaya, D. Clavijo, J. Alfonso, C. Cardozo, *Thin Solid Films* **2013**, *529*, 342.
[31] G. Cubillos, M. Mendoza, J. Alfonso, G. Blanco, M. Bethencourt, *Mater. Charact.* **2017**, *131*, 450.
[32] J. Probst, U. Gbureck, R. Thull, *Surf. Coat. Technol.* **2001**, *148*, 226.
[33] H. A. Hansen, J. Rossmeisl, J. K. Nørskov, *Phys. Chem. Chem. Phys.* **2008**, *10*, 3722.
[34] H. He, Y. Lei, C. Xiao, D. Chu, R. Chen, G. Wang, *J. Phys. Chem. C* **2012**, *116*, 16038.
[35] C. Doornkamp, V. Ponec, *J. Mol. Catal. A* **2000**, *162*, 19.
[36] S. Doi, Y. Liu, A. Ishihara, S. Mitsushima, N. Kamiya, K.-I. Ota, *ECS Trans.* **2006**, *1*, 17.
[37] S. Doi, A. Ishihara, S. Mitsushima, N. Kamiya, K.-I. Ota, *J. Electrochem. Soc.* **2007**, *154*, B362.
[38] F. Calle-Vallejo, A. Krabbe, J. M. García-Lastra, *Chem. Sci.* **2017**, *8*, 124.
[39] S. Siahrostami, C. Tsai, M. Karamad, R. Koitz, M. García-Melchor, M. Bajdich, A. Vojvodic, F. Abild-Pedersen, J. K. Nørskov, F. Studt, *Catal. Lett.* **2016**, *146*, 1917.
[40] G. Gao, E. R. Waclawik, A. Du, *J. Catal.* **2017**, *352*, 579.
[41] H. A. Hansen, V. Viswanathan, J. K. Nørskov, *J. Phys. Chem. C* **2014**, *118*, 6706.
[42] S. Kattel, P. Atanassov, B. Kiefer, *Phys. Chem. Chem. Phys.* **2014**, *16*, 13800.
[43] G. Liu, H. M. Zhang, M. R. Wang, H. X. Zhong, J. Chen, *J. Power Sources* **2007**, *172*, 503.
[44] Y. Maekawa, A. Ishihara, J.-H. Kim, S. Mitsushima, K.-I. Ota, *Electrochem. Solid-State Lett.* **2008**, *11*, B109.
[45] G. Wang, F. Huang, X. Chen, Y. Yu, C. Gong, H. Liu, S. Wen, G. Zheng, M. Pan, *Solid State Ionics* **2018**, *317*, 15.
[46] J. Sun, R. C. Remsing, Y. Zhang, Z. Sun, A. Ruzsinszky, H. Peng, Z. Yang, A. Paul, U. Waghmare, X. Wu, et al., *Nat. Chem.* **2016**, *8*, 831.
[47] D. Fuks, D. Vingurt, M. V. Landau, M. Herskowitz, *J. Phys. Chem. C* **2010**, *114*, 13313.
[48] A. Seifitokaldani, O. Savadogo, M. Perrier, *Electrochim. Acta* **2014**, *141*, 25.
[49] S. Nigam, C. Majumder, *Phys. Chem. Chem. Phys.* **2017**, *19*, 19308.
[50] F. Liu, G. Zhu, D. Yang, D. Jia, F. Jin, W. Wang, *RSC Adv.* **2019**, *9*, 22656.
[51] A. Ishihara, S. Tominaka, S. Mitsushima, H. Imai, O. Sugino, K.-I. Ota, *Curr. Opin. Electrochem.* **2020**, *21*, 234.
[52] G. Kresse, J. Hafner, *Phys. Rev. B* **1993**, *47*, 558.
[53] P. E. Blöchl, *Phys. Rev. B* **1994**, *50*, 17953.
[54] J. P. Perdew, K. Burke, M. Ernzerhof, *Phys. Rev. Lett.* **1996**, *77*, 3865.
[55] A. H. Larsen, J. J. Mortensen, J. Blomqvist, I. E. Castelli, R. Christensen, M. Dułak, J. Friis, M. N. Groves, B. Hammer, C. Hargus, et al., *J. Phys. Condens. Matter* **2017**, *29*, 273002.
[56] H. J. Monkhorst, J. D. Pack, *Phys. Rev. B* **1976**, *13*, 5188.
[57] C. J. Cramer, F. Bickelhaupt, *Angew. Chem., Int. Ed. Engl.* **2003**, *42*, 381.
[58] C. T. Campbell, L. H. Sprowl, L. Árnadóttir, *J. Phys. Chem. C* **2016**, *120*, 10283.
[59] L. H. Sprowl, C. T. Campbell, L. Arnadottir, *J. Phys. Chem. C* **2016**, *120*, 9719.
[60] L. H. Sprowl, C. T. Campbell, L. Arnadottir, *J. Phys. Chem. C* **2017**, *121*, 9655.

Manuscript received: February 28, 2023
Revised manuscript received: June 1, 2023
Accepted manuscript online: June 1, 2023
Version of record online: ■■, ■■

RESEARCH ARTICLE

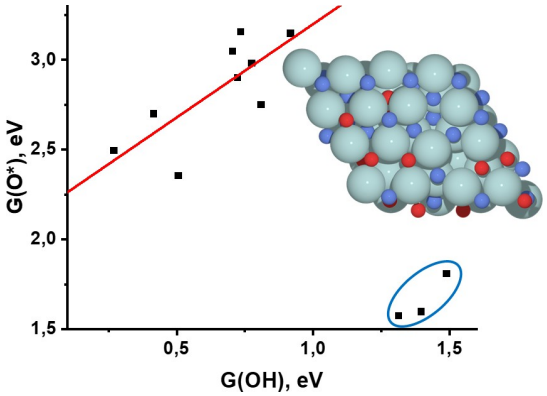

*S. Sinha, Prof. T. Vegge, Prof. H. A. Hansen**

Non-PGM transition metal based catalysts like zirconium oxynitride (Zr_2ON_2) has been recognized as electrocatalysts exhibiting encouraging ORR activity in acidic electrolytes. Apart from identifying the thermodynamic limiting step for ORR for Zr_2ON_2, in our study we also observe the dramatic deviations in G_{O^*}-G_{OH} scaling relations for the system from standard scaling. (In the rendering of the Zr_2ON_2 structure, the light cyan atom is Zr, red is O, blue is N and white is H.)

Paper II

Understanding the electronic and structural effects in ORR intermediate binding on anion-substituted zirconia surfaces

Sukanya Sinha, Tejs Vegge, Kirsten T. Winther and Heine Anton Hansen

To be submitted

Understanding the electronic and structural effects in ORR intermediate binding on anion-substituted zirconia surfaces

Sukanya Sinha,[†] Tejs Vegge,[†] Kirsten T. Winther,[*,‡] and Heine Anton Hansen[*,†]

†*Department of Energy Storage and Conversion,Technical University of Denmark, 2800 Kongens Lyngby, Denmark*

‡*SUNCAT Center for Interface Science and Catalysis, SLAC National Accelerator Laboratory, Menlo Park, California 94025, United States*

E-mail: winther@slac.stanford.edu; heih@dtu.dk

Abstract

For oxygen reduction reaction (ORR), the surface adsorption energies of O* and OH* intermediates are key descriptors for catalytic activity. In this work, we investigate anion-substituted zirconia catalyst surfaces and come to understand that adsorption energies of O* and OH* intermediates is influenced by both structural and electronic effects. When the adsorption energies are not influenced by the structural effects of the catalyst surface, they exhibit a linear correlation with integrated crystal orbital Hamiltonian population (ICOHP) of the adsorbate-surface bond. The influence of structural effects, due to re-optimisation slab geometry after adsorption of intermediate species, leads to stronger adsorption of intermediates. Our calculations show that there is a change in the bond order to accommodate the incoming adsorbate species which leads to stronger adsorption when both structural and electronic effects influence the

adsorption phenomena. The insights into the catalyst-adsorbate interactions can guide the design of future ORR catalysts.

1 Introduction

Among various alternatives for environmentally friendly energy conversion technologies, fuel cells offer a great deal of promise as a highly efficient device for the same. Polymer electrolyte membrane fuels cells (PEMFCs) are fuel cells where a fuel like hydrogen or methanol is oxidized at the anode and oxygen is reduced at the cathode to produce energy.[1] The interest in PEMFCs arise due to their varied applications, ranging from transportation in form of fuel cell electric vehicles (FCEV)[2] to potable and stationary power systems in form of auxiliary power units (APU).[3] There are several challenges associated with PEMFCs like lifetime,[4] component durability[5] and most importantly the cost of the conventional platinum-based catalyst which constitute almost 55% of the total cost.[6] The cathodic oxygen reduction reaction (ORR) has sluggish kinetics and consequently high overpotential as compared to the swift kinetics of anodic hydrogen oxidation reaction (HER), hence the cathode requires higher catalyst loading than the anode. In order to accelerate PEMFC technology development, it is crucial to explore non-platinum ORR catalysts that are highly efficient as well is affordable. In the course of development of non-platinum based ORR catalysts, numerous candidates have been studied like polymer based catalysts, transition metal oxides, nitrides, oxynitrides, carbides, carbonitrides.[7–13]

In the PEMFCs, oxygen reduction reaction can take place through two different pathways at the fuel cell cathode, the two-electron pathway and the four-electron pathway.[14] However, for the PEMFC cathodic catalyst, the two-electron pathway is not desirable; it is the four-electron pathway which is preferred for the long-term operation of PEMFC. Previous studies have demonstrated that the four-electron pathway can involve two different mechanisms.[15]

One is the 'associative mechanism' which can be described as follows:

$$* + O_2 + H^+ + e^- \longrightarrow *OOH \tag{1}$$

$$*OOH + H^+ + e^- \longrightarrow *O + H_2O \tag{2}$$

$$*O + H^+ + e^- \longrightarrow *OH \tag{3}$$

$$*OH + H^+ + e^- \longrightarrow * + H_2O \tag{4}$$

The other mechanism is called the 'dissociative mechanism' where the initial step is oxygen dissociation.

$$* + O_2 \longrightarrow *O \tag{5}$$

$$*O + H^+ + e^- \longrightarrow *OH \tag{6}$$

$$*OH + H^+ + e^- \longrightarrow * + H_2O \tag{7}$$

where * denotes the active sites on the catalyst surface.[16]

Previous studies have demonstrated O* and OH intermediates are the key descriptors that can help in predicting the ORR activity of catalysts.[15,17,18] While there are a number of studies which has studied the relative binding energies of these two species in terms of scaling relations,[19,20] their underlying descriptors are not very well-understood.[18,21] Fung et al showed that the integrated crystal orbital Hamiltonian population (ICOHP)[22] of the bond between lattice metal and oxygen is a good descriptor for the adsorption energy of hydrogen on lattice oxygen in perovskites,[23] and recently Winther et al demonstrated that the O and OH adsorption energies on transition metal MO_2 surfaces is well captured by the metal-oxygen ICOHP of the bulk oxide.[24] In this work, we are studying the trends in the adsorption energy of O* and OH adsorbates on the surface of anion-substituted zirconia. We find that in the absence of structural reorganization in the zirconia slabs the adsorption

energies are captured by the integrated COHP with a high accuracy.

While a number of studies has previously reported zirconium oxynitride (Zr_2ON_2) as an promising alternative to platinum based ORR catalysts,[25,26] the reason behind the favourable ORR activity of the same is not well understood. A number of transition metal-based ORR catalysts which show promising ORR activity[25,27,28] also exhibits deviations from standard scaling relations.[29] It is generally accepted that deviation from these scaling relations is the key to enhanced ORR electrocatalysis.[30] In our previous work we have explored the possibility of enhanced ORR activity due to bending of ORR scaling relations.[31] We concluded that the G_{O*}-G_{OH} scaling relation for ORR on Zr_2ON_2 catalyst indeed shows deviation from the standard scaling relation, however, there was no indication that it necessarily results in enhanced electrocatalysis. Several electronic descriptors failed to capture the complexity of the Zr_2ON_2 catalyst surface that arises from presence of two different anions i.e. oxygen and nitrogen in the anionic layers. Hence, in order to simplify the system, we have created model systems where we substitute one or two lattice oxygen for a carbon or two nitrogen atoms for this study. Further, we use ICOHP as an electronic descriptor for describing trends in the adsorption energies of the O* and OH adsorbates as well as to gain insights into bonding configurations of the same.

2 Methods

All the DFT calculations have been performed using the Vienna Ab Initio Simulation Package (VASP)[32] and the core electrons are described with the projector augmented wave (PAW) method.[33] To describe the correlation and exchange energy the Perdew-Burke-Ernzerhof functional (PBE)[34] is used. The Atomic Simulation Environment (ASE)[35] is used to set up and analyse the structures, which are optimised with a plane wave cutoff of 500 eV and Brillouin-zone integration is performed with a Monkhorst-Pack k-point mesh[36] of 2x2x1. All the calculations were done with spin polarization. The self-consistent electron density loop

is converged to 10^{-6} eV and the structures are relaxed until all forces are below 0.02 eV $\mathring{A}^{-1}$. We have studied nitrogen and carbon substituted zirconia slabs. The model includes three cationic layers with the bottom layer fixed in its bulk position and the upper two layers are allowed to relax. A high throughput workflow was used to create the nitrogen and carbon substituted zirconia slabs. Another similar high throughput workflow was used to optimize the slabs and carry out the adsorption calculations for the different ORR intermediates. The workflow was interfaced with the Atomic Simulation Environment (ASE) and was managed with the workflow management software, MyQueue.[35,37]

The Lobster package[38] was used to perform COHP calculations. The calculations were started from re-converging electronic structure with symmetry being disabled. ICOHP between all pairs of atoms were included in the Lobster calculation up to a radial cutoff of 3 $\mathring{A}$ were investigated. More specifically we focus on the bond between the adsorbed oxygen, and the surface Zr, C and N atomic species.

3 Results and discussion

Nitrogen and Carbon substituted Zirconia

Zirconia is a crystalline compound with polymorphic crystal structure and exhibits three different crystalline forms: monoclinic, tetragonal and cubic form.[39,40] Previous studies have demonstrated the tetragonal phase shows the highest ORR activity among all three, hence that is the phase we have selected for our study.[41] Our selected ZrO_2 crystal belongs to space group $P4_2/nmc$ (137) or according to the Fedorov notation has the Fedorov symbol of 67a.[42] In our study we are exploring adsorption of ORR intermediates on the (011) surface of a ZrO_2 slab. It has a hexagonal lattice structure with a total vacuum of 1.6 nm (with 0.8 nm on both sides of the slab). The model structures that has been studied in this work are two different types of anion-substituted zirconia; nitrogen substituted zirconia and carbon substituted zirconia slabs. In order to prepare the model structure for nitrogen

substituted zirconia, two lattice oxygen atoms were substituted with two nitrogen atoms. The nitrogen atom has a formal oxidation state of -3 while oxygen has a oxidation state of -2. Therefore, to preserve the charge neutrality of the system an oxygen vacancy is introduced. For preparing the model structure of carbon substituted zirconia, a similar strategy is used, one lattice oxygen atom was substituted with a carbon atom. In order to maintain charge neutrality of the model system, since carbon has a formal oxidation state of -4 while oxygen has an oxidation state of -2, we introduced an oxygen vacancy. The anionic substitutions were carried out on the surface and/or the sub-surface anion layers. However, the oxygen vacancy was introduced only in the sub-surface anion layer. This was done since our test calculations show surface vacancies are unstable. Hence, we have 8 lattice oxygen atoms in the surface and sub-surface anion layer, where potential anionic substitutions could be carried out and 4 lattice oxygen atoms, in sub-surface anion layer, where potential oxygen vacancies can be introduced. Different combinations of anionic substitutions and introduction of oxygen vacancy to the zirconia slab leads to creation of 84 different nitrogen-substituted slabs and 28 different carbon-substituted slabs. 1 illustrates two such anion-substituted zirconia structures, a nitrogen substituted zirconia and a carbon substituted zirconia slab. High throughput workflows were used to create and optimize the anion substituted zirconia slabs in addition to carrying out the adsorption calculations for the adsorption of the ORR intermediates. The structural and electronic trends for the adsorption of the O*, *OH and *OOH intermediates on the anion substituted ZrO_2 slab is evaluated systematically by studying the adsorption over all the Zr-ontop sites. The adsorption energies of the ORR adsorbates are calculated relative to the gas phase water and hydrogen in molecular form.

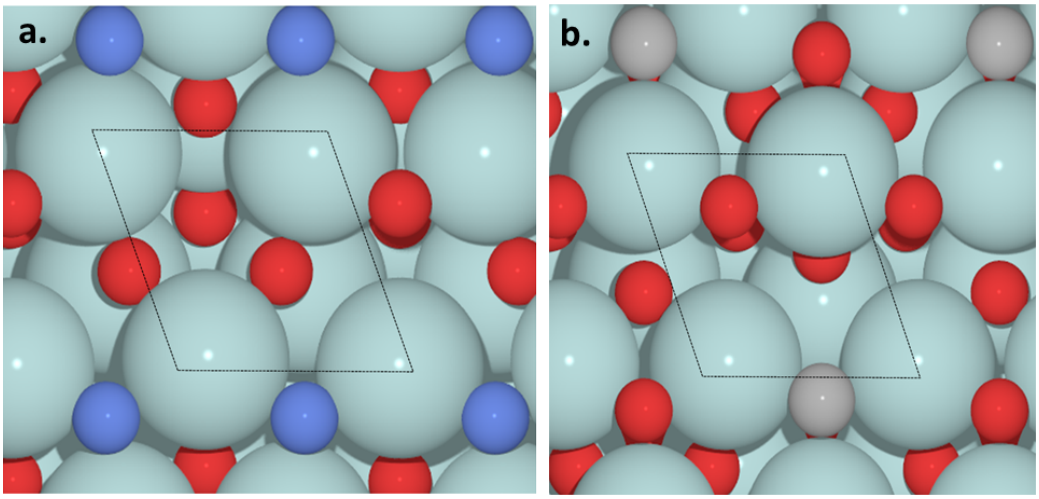

Figure 1: Geometries of anion substituted zirconia slab. a) Nitrogen substituted zirconia slab b) Carbon substituted zirconia slab

Adsorption Energy and Limiting Potential Distribution

The range of distribution of adsorption energies can help us understand the adsorption configurations of ORR adsorbates (O*, OH or OOH) on nitrogen or carbon substituted zirconia surface. From the histogram of O*, OH and OOH adsorption energies, shown in Figure 2, one can observe the OOH adsorption energies for both nitrogen and carbon substituted slabs are spread over a modest range of around 4 eV. The variation of OOH adsorption energy is largely due to variation in the alignment of the OOH adsorbate with the anion-substituted zirconia surface. The OH adsorption energy show a narrow range of 2 eV which is due to OH adsorption taking place mainly on the ontop zirconia site. However we noted the most surprising observation for O* adsorption energy. For both nitrogen and carbon substituted slabs, they are spread over a large range of around 5 eV. We attribute the reason for this large range of adsorption energy to the wide variety of configurations of O* adsorption. The O* adsorbate adsorbs on ontop zirconia sites, bridge sites and in some cases forms a complex with the substituent anion, nitrogen or carbon. There are different ranges of adsorption energy associated with each adsorption configuration; the adsorption on ontop zirconia sites being the weakest followed by adsorption on the bridge sites and the

strongest adsorption configuration being the anionic complex formation.

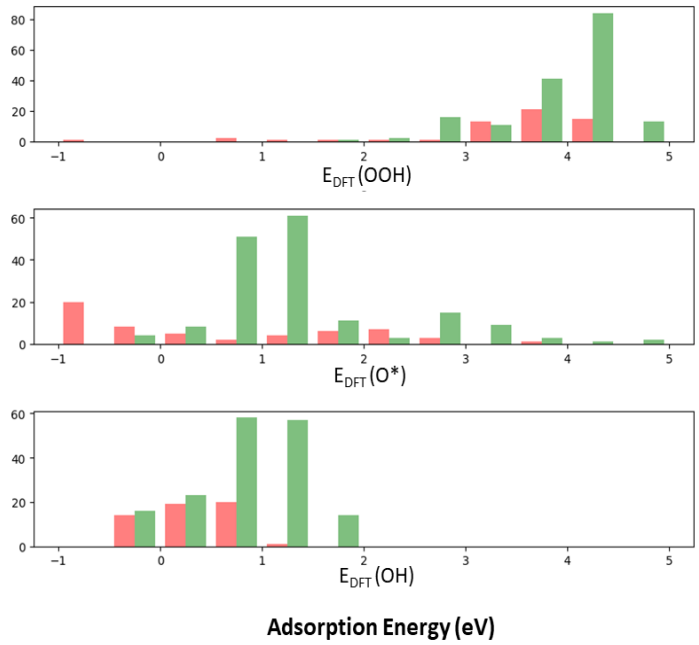

Figure 2: Histogram of adsorption energies of ORR intermediates i.e. OOH, O* and OH. The red bars represent adsorption energies for carbon substituted slabs while green represents adsorption energies for nitrogen substituted slabs.

For most of the materials the adsorption of ORR intermediates are restricted by a linear scaling.[18,30,43] Hence we wanted to explore whether such scaling relations exist for the systems explored in this study. The OOH-OH and O*-OH scaling relations are provided in the Supporting Information. From these plots of scaling relations, we can understand the adsorption energies do not scale well with each other for nitrogen and carbon substituted zirconia systems.

Within the CHE model the highest potential at which all the reaction steps are downhill in free energy is called the thermodynamic limiting potential, (U_L). The U_L gives us a measure of the activity of a catalyst. Higher U_L implies higher catalytic activity. A negative value of U_L implies catalytic inactivity. From the histogram of limiting potentials in 3, we can observe the U_L for most of the carbon substituted slabs is negative. On the other hand U_L for most of the nitrogen substituted slabs are positive and the peak is obtained at 0.25V with

some of the values reaching upto 0.65V. Hence we can conclude that anionic substitution with nitrogen on zirconia is more favorable to ORR activity than that with carbon.

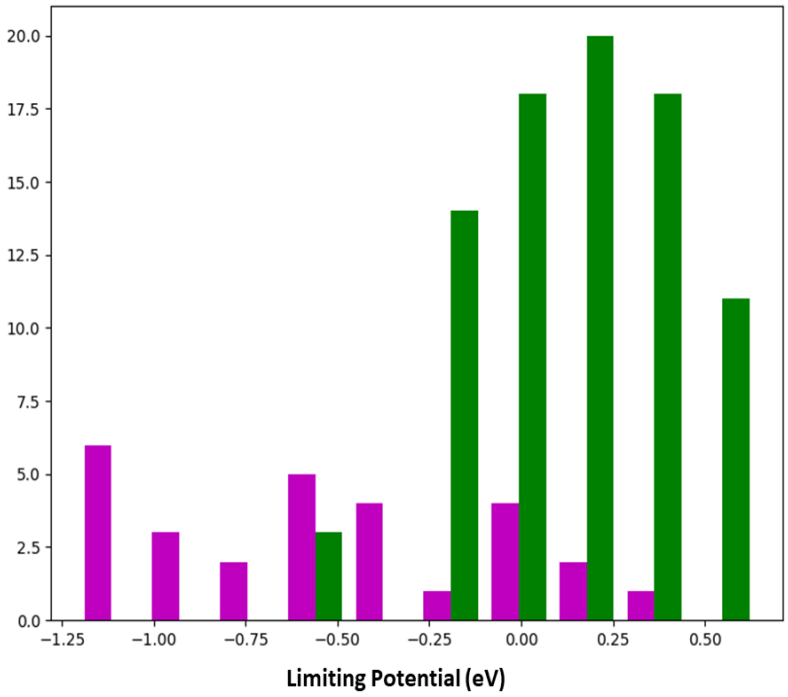

Figure 3: Histogram of limiting potentials for both carbon and nitrogen substituted zirconia slabs. The magenta bars represent limiting potentials for carbon substituted slabs while green represents limiting potentials for nitrogen substituted slabs.

We have also explored potential correlation between U_L and relative slab stability by plotting them in form of a scatter plot. It has been provided in the Supporting Information. From the plot, we can conclude that the U_L does not show any correlation with the relative slab stability of the anion substituted zirconia slabs.

ICOHP as a Electronic Descriptor for O* Adsorption

The bonding and anti-bonding interactions in a chemical system can be studied with a method known as crystal orbital Hamiltonian population (COHP).[44,45] In our study, we have found that the integrated crystal orbital Hamiltonian populations (ICOHP)[22] can provide valuable insights to the origin of adsorption energy variations. The calculation of ICOHP involves projection of plane wave basis sets solution, which is obtained from calculations

carried out using ground state DFT method, into LCAO basis functions. We can calculate the Hamiltonian between two projected orbitals from the basis functions, which would indicate whether the net interaction is bonding or anti-bonding at a particular band energy.[22,46] Hence, the ICOHP can be considered as energy contribution from overlap of two orbitals. Such an energy contribution can be negative (bonding) or positive (anti-bonding).

One of the aims of our study is to gain an understanding of the structural and electronic effects on the adsorption of ORR intermediates on anion-substituted zirconia slabs. In order to achieve this, we create two types of structural models, the unconstrained model and the constrained model. In the unconstrained model, the top two layers of the slab and the adsorbate is relaxed during the optimisation calculations (the bottom layer is constrained) while in the constrained model, the entire slab is constrained during the optimization calculation with only the adsorbates being free to move (where the two top layers of the slab are relaxed for the slab without adsorbates). The adsorption of O* species is carried out on the ontop-Zr sites on nitrogen and carbon-substituted slabs (both unconstrained and constrained). Our adsorption calculations over the unconstrained slab reveal that the incoming adsorbates introduce significant structural changes in the anion-substituted slabs which implies that there are both structural and electronic effects that influences the adsorption energy. In terms of structural change, the displacement of lattice anions i.e. oxygen , nitrogen and carbon is much more significant than that of the zirconium. Previous studies report similar influence of structural and electronic effects on different electrocatalysts.[47–49] Fig 4a and 4c shows the correlation between the total ICOHP of the O* adsorbate (considering bonds to all nearest Zr, N and C neighbours) and O* adsorption energy over constrained slabs. Since the constrained slab cannot move during O* adsorption, the adsorption energy in this case is affected by electronic effects only. Thus, in the constrained case the adsorption energy is expected to be proportional to the O-surface bond energy, captured by the ICOHP. As such we can observe quite a linear dependence of adsorption energy on ICOHP, except for in the weak binding limit ($\Delta E \approx 4.6$)eV. However in the unconstrained case shown in fig 4b and

4d, we see a strong deviation from the linear trend. We therefore conclude that, in addition to electronic effects, structural reorganization effects in the zirconia slab play a major role in adsorption of O* intermediate.

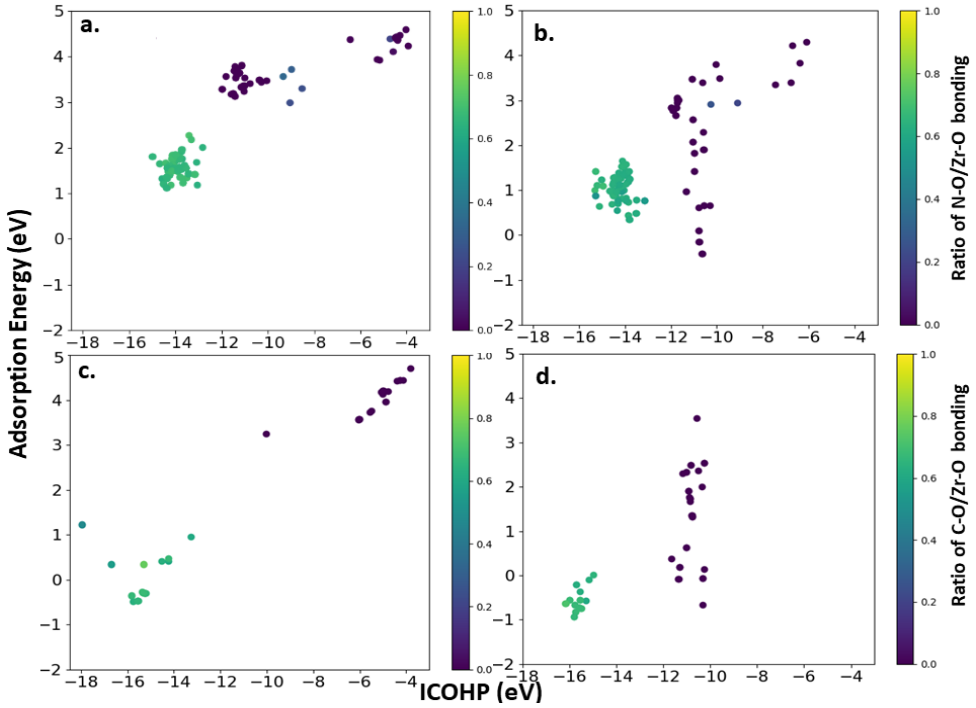

Figure 4: ICOHP vs Adsorption energy plots a) Constrained Nitrogen substituted zirconia slab b) Nitrogen substituted zirconia slab c) Constrained Carbon substituted zirconia slab d) Carbon substituted zirconia slab

ICOHP as a Electronic Descriptor for OH Adsorption

Similar adsorption calculations are carried out with OH adsorbate on ontop-Zr sites on the nitrogen and carbon substituted zirconia slabs (both unconstrained and constrained). Since adsorption of OH over the constrained slab is influenced only by the electronic effects, in the Fig 5a and Fig 5c we can observe a linear dependence of adsorption energy on ICOHP. Since ICOHP magnitude is an indicator of bond strength, higher ICOHP magnitude indicates a stronger bond. As higher adsorption energy also indicates stronger bond, ICOHP shows a strong correlation with adsorption energy in this case. However, when the slab is unconstrained, the adsorption energy is influenced not only by the electronic effects but also

the structural effects. The structural effects are caused, mainly, by the reorganisation of the anion-substituted zirconia lattice caused by the incoming adsorbate species. The synergistic effect of the structural and electronic changes cause a deviation from the linear trend between the adsorption energy and ICOHP which can be observed in Fig 5b and 5d. This is similar to the deviation from the linear dependence of O* adsorption energy on ICOHP we observe in figure 4b and 4d.

We have quantified the the effect of structural changes only on the adsorption energies by computing the differences in the adsorption energies of the constrained and unconstrained slabs and have presenting them in form of a histogram which is provided in the Supporting Information. From the histogram we can understand adsorption of O* intermediate induces structural changes in the slab to a greater degree than the OH intermediate.

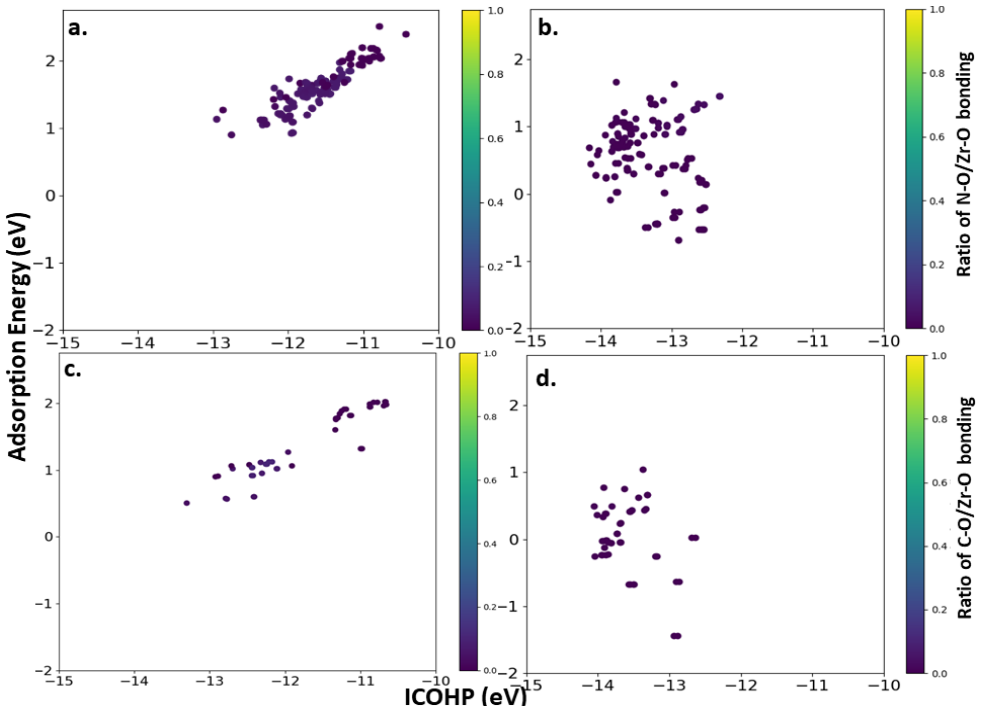

Figure 5: ICOHP vs Adsorption energy plots a) Constrained Nitrogen substituted zirconia slab b) Nitrogen substituted zirconia slab c) Constrained Carbon substituted zirconia slab d) Carbon substituted zirconia slab

Insights into Bond Configurations

As ICOHP is an indication of bond strength, there exists a correlation between bond length and ICOHP. Fig 6 gives us an overview of the relation between bond lengths between different pairs of atoms for O* adsorption over nitrogen and carbon substituted zirconia slabs (unconstrained and constrained). Similar plots have been made for OH adsorption have been provided in the Supporting Information. The yellow overlay indicates the bonds that are formed between an atom (zirconia, nitrogen or carbon) and the adsorbate oxygen. The trend that we observe across the unconstrained system versus the constrained system is that the adsorbate oxygen and zirconium tend to bond more strongly in the unconstrained system as opposed to the constrained system. In order for the O* adsorbate to adsorb over the unconstrained system, the lattice zirconium atoms have to rearrange themselves. This is so as to change the bond order to accommodate the incoming O* species. If such a structural rearrangement is not possible or it does not change the bond order enough, then it is more favorable for the O* adsorbate to adsorb over the lattice nitrogen or carbon. The change in bond order is also evident from the fact that for the unconstrained system, the ICHOP for the zirconium-adsorbate oxygen bond is distributed over a larger range than in the constrained system. From Fig 6 it is also clear that only ICOHP, as a descriptor, is not enough to capture the trend in the adsorption energies.

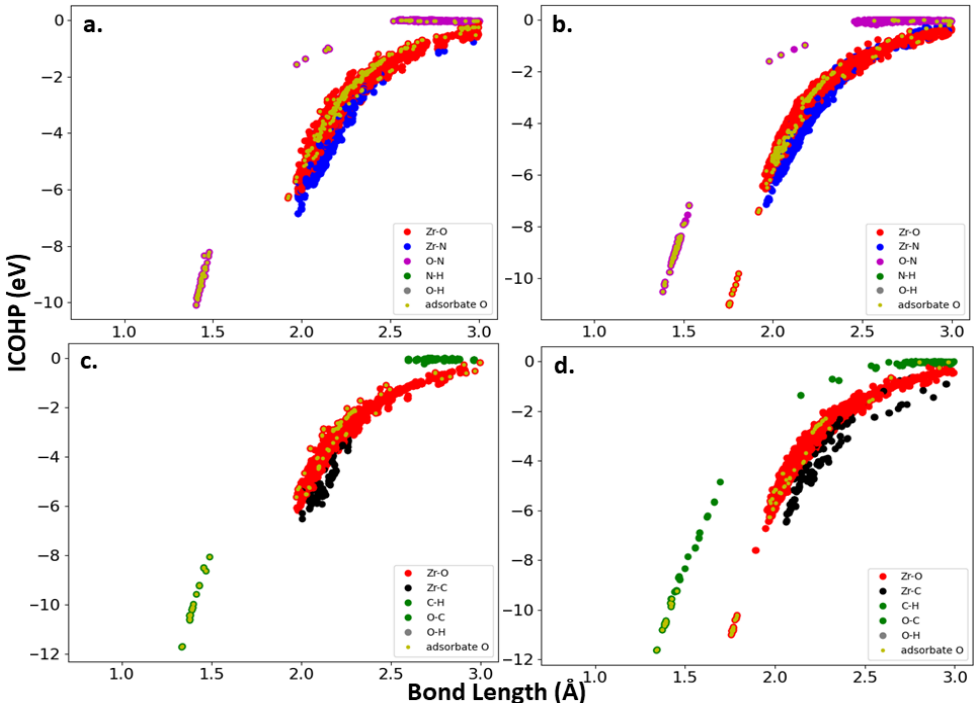

Figure 6: ICOHP vs bond length plots a) Constrained Nitrogen substituted zirconia slab b) Nitrogen substituted zirconia slab c) Constrained Carbon substituted zirconia slab d) Carbon substituted zirconia slab

4 Conclusion

ICOHP is a very useful electronic descriptor for prediction of O* and OH adsorption energies on zirconia-based catalytic systems. From our comparative study of constrained and unconstrained anion-substituted zirconia slabs, we understand both the structural as well electronic effects of the slabs play a role in the adsorption of the O* and OH intermediates. The incoming adsorbates introduces structural changes in the slab, the lattice Zr atoms gets displaced to change the bond order in order to accommodate the adsorbate species on the surface of the slab. The structural reorganisation of the nitrogen and carbon substituted zirconia slabs partially contributes to the bond strength between the active sites and the adsorbates.

Additionally, we can also state that anionic substitution on zirconia catalyst with nitrogen is

a better choice than that by carbon in terms of ORR activity. We draw this conclusion from the values of limiting potential calculated for the anion-substituted zirconia slabs illustrated in figure 3. The predominantly positive values of U_L with the peak at 0.25V and values reaching as high as 0.65V is indicative of the same. However, there was no correlation found between the stability of the slabs and their ORR activity.

Acknowledgement

S.S, T.V, and H.A.H. acknowledge support by the Villum Foundation through the research center V-Sustain (grant number 9455). K.T.W was supported by the U.S. Department of Energy, Office of Science, Office of Basic Energy Sciences, Chemical Sciences, Geosciences, and Biosciences Division, Catalysis Science Program to the SUNCAT Center for Interface Science and Catalysis.

Supporting Information Available

Bond lengths verses ICOHP plot for OH adsorption over anion-substituted zirconia surface, G_{O*}-G_{OH} and G_{OOH}-G_{OH} scaling relations for ORR on nitrogen and carbon substituted zirconia surface, limiting potential and relative slab stability plot and histogram for contribution to adsorption energy by structural effects.

References

(1) Litster, S.; McLean, G. PEM fuel cell electrodes. *Journal of power sources* **2004**, *130*, 61–76.

(2) Gittleman, C.; Jorgensen, S.; Waldecker, J.; Hirano, S.; Mehall, M.; others Automotive fuel cell R&D needs. DOE fuel cell pre-solicitation workshop. Department of Energy, Lakewood, Colorado. 2010.

(3) Wang, Y.; Chen, K. S.; Mishler, J.; Cho, S. C.; Adroher, X. C. A review of polymer electrolyte membrane fuel cells: Technology, applications, and needs on fundamental research. *Applied energy* **2011**, *88*, 981–1007.

(4) Cheng, N.; Mu, S.; Pan, M.; Edwards, P. P. Improved lifetime of PEM fuel cell catalysts through polymer stabilization. *Electrochemistry communications* **2009**, *11*, 1610–1614.

(5) Borup, R.; Meyers, J.; Pivovar, B.; Kim, Y. S.; Mukundan, R.; Garland, N.; Myers, D.; Wilson, M.; Garzon, F.; Wood, D.; others Scientific aspects of polymer electrolyte fuel cell durability and degradation. *Chemical reviews* **2007**, *107*, 3904–3951.

(6) Bing, Y.; Liu, H.; Zhang, L.; Ghosh, D.; Zhang, J. Nanostructured Pt-alloy electrocatalysts for PEM fuel cell oxygen reduction reaction. *Chemical Society Reviews* **2010**, *39*, 2184–2202.

(7) Antolini, E.; Gonzalez, E. R. Tungsten-based materials for fuel cell applications. *Applied Catalysis B: Environmental* **2010**, *96*, 245–266.

(8) Bezerra, C. W.; Zhang, L.; Lee, K.; Liu, H.; Marques, A. L.; Marques, E. P.; Wang, H.; Zhang, J. A review of Fe–N/C and Co–N/C catalysts for the oxygen reduction reaction. *Electrochimica Acta* **2008**, *53*, 4937–4951.

(9) Bezerra, C. W.; Zhang, L.; Liu, H.; Lee, K.; Marques, A. L.; Marques, E. P.; Wang, H.; Zhang, J. A review of heat-treatment effects on activity and stability of PEM fuel cell catalysts for oxygen reduction reaction. *Journal of Power Sources* **2007**, *173*, 891–908, X Polish Conference on Systems with Fast Ionic Transport.

(10) Feng, Y.; Alonso-Vante, N. Nonprecious metal catalysts for the molecular oxygen-reduction reaction. *physica status solidi (b)* **2008**, *245*, 1792–1806.

(11) Gewirth, A. A.; Thorum, M. S. Electroreduction of dioxygen for fuel-cell applications: materials and challenges. *Inorganic chemistry* **2010**, *49*, 3557–3566.

(12) Ishihara, A.; Ohgi, Y.; Matsuzawa, K.; Mitsushima, S.; ichiro Ota, K. Progress in non-precious metal oxide-based cathode for polymer electrolyte fuel cells. *Electrochimica Acta* **2010**, *55*, 8005–8012, EMERGING TRENDS AND CHALLENGES IN ELECTROCHEMISTRY.

(13) Zhang, L.; Zhang, J.; Wilkinson, D. P.; Wang, H. Progress in preparation of non-noble electrocatalysts for PEM fuel cell reactions. *Journal of Power Sources* **2006**, *156*, 171–182.

(14) Viswanathan, V.; Hansen, H. A.; Rossmeisl, J.; Nørskov, J. K. Unifying the 2e–and 4e–reduction of oxygen on metal surfaces. *The journal of physical chemistry letters* **2012**, *3*, 2948–2951.

(15) Nørskov, J. K.; Rossmeisl, J.; Logadottir, A.; Lindqvist, L.; Kitchin, J. R.; Bligaard, T.; Jonsson, H. Origin of the overpotential for oxygen reduction at a fuel-cell cathode. *The Journal of Physical Chemistry B* **2004**, *108*, 17886–17892.

(16) Hansen, H. A.; Viswanathan, V.; Nørskov, J. K. Unifying kinetic and thermodynamic analysis of 2 e–and 4 e–reduction of oxygen on metal surfaces. *J. Phys. Chem. C* **2014**, *118*, 6706–6718.

(17) Viswanathan, V.; Hansen, H. A.; Rossmeisl, J.; Nørskov, J. K. Universality in oxygen reduction electrocatalysis on metal surfaces. *Acs Catalysis* **2012**, *2*, 1654–1660.

(18) Kulkarni, A.; Siahrostami, S.; Patel, A.; Nørskov, J. K. Understanding catalytic activity trends in the oxygen reduction reaction. *Chemical Reviews* **2018**, *118*, 2302–2312.

(19) Christensen, R.; Hansen, H. A.; Dickens, C. F.; Nørskov, J. K.; Vegge, T. Functional independent scaling relation for ORR/OER catalysts. *The Journal of Physical Chemistry C* **2016**, *120*, 24910–24916.

(20) Sours, T.; Patel, A.; Nørskov, J.; Siahrostami, S.; Kulkarni, A. Circumventing scaling relations in oxygen electrochemistry using metal–organic frameworks. *The Journal of Physical Chemistry Letters* **2020**, *11*, 10029–10036.

(21) Dickens, C. F.; Montoya, J. H.; Kulkarni, A. R.; Bajdich, M.; Nørskov, J. K. An electronic structure descriptor for oxygen reactivity at metal and metal-oxide surfaces. *Surface Science* **2019**, *681*, 122–129.

(22) Dronskowski, R.; Blöchl, P. E. Crystal orbital Hamilton populations (COHP): energy-resolved visualization of chemical bonding in solids based on density-functional calculations. *The Journal of Physical Chemistry* **1993**, *97*, 8617–8624.

(23) Fung, V.; Wu, Z.; Jiang, D.-e. New bonding model of radical adsorbate on lattice oxygen of perovskites. *The Journal of Physical Chemistry Letters* **2018**, *9*, 6321–6325.

(24) Comer, B. M.; Li, J.; Abild-Pedersen, F.; Bajdich, M.; Winther, K. T. Unraveling electronic trends in O* and OH* surface adsorption in the MO2 transition-metal oxide series. *The Journal of Physical Chemistry C* **2022**, *126*, 7903–7909.

(25) Chisaka, M.; Ishihara, A.; Morioka, H.; Nagai, T.; Yin, S.; Ohgi, Y.; Matsuzawa, K.; Mitsushima, S.; Ota, K.-i. Zirconium oxynitride-catalyzed oxygen reduction reaction at polymer electrolyte fuel cell cathodes. *ACS omega* **2017**, *2*, 678–684.

(26) Maekawa, Y.; Ishihara, A.; Kim, J.-H.; Mitsushima, S.; Ota, K.-i. Catalytic activity of zirconium oxynitride prepared by reactive sputtering for ORR in sulfuric acid. *Electrochemical and Solid-State Letters* **2008**, *11*, B109.

(27) Ishihara, A.; Doi, S.; Mitsushima, S.; Ota, K.-i. Tantalum (oxy) nitrides prepared using reactive sputtering for new nonplatinum cathodes of polymer electrolyte fuel cell. *Electrochimica Acta* **2008**, *53*, 5442–5450.

(28) Uehara, N.; Ishihara, A.; Nagai, T.; Matsumoto, M.; Imai, H.; Kohno, Y.; Matsuzawa, K.; Mitsushima, S.; Ota, K. Kinetic study of oxygen reduction reaction on tantalum oxide-based electrocatalysts produced from oxy-tantalum phthalocyanines in acidic media. *Electrochimica Acta* **2015**, *182*, 789–794.

(29) Yamamoto, Y.; Kasamatsu, S.; Sugino, O. Scaling relation of oxygen reduction reaction intermediates at defective TiO2 surfaces. *The Journal of Physical Chemistry C* **2019**, *123*, 19486–19492.

(30) Man, I. C.; Su, H.-Y.; Calle-Vallejo, F.; Hansen, H. A.; Martínez, J. I.; Inoglu, N. G.; Kitchin, J.; Jaramillo, T. F.; Nørskov, J. K.; Rossmeisl, J. Universality in oxygen evolution electrocatalysis on oxide surfaces. *ChemCatChem* **2011**, *3*, 1159–1165.

(31) Sinha, S.; Vegge, T.; Hansen, H. A. Bending the ORR scaling relations on zirconium oxynitride for enhanced oxygen electrocatalysis. *ChemCatChem* **2023**, e202300349.

(32) Kresse, G.; Hafner, J. Ab initio molecular dynamics for liquid metals. *Physical review B* **1993**, *47*, 558.

(33) Blöchl, P. E. Projector augmented-wave method. *Physical review B* **1994**, *50*, 17953.

(34) Perdew, J. P.; Burke, K.; Ernzerhof, M. Generalized gradient approximation made simple. *Physical review letters* **1996**, *77*, 3865.

(35) Larsen, A. H.; Mortensen, J. J.; Blomqvist, J.; Castelli, I. E.; Christensen, R.; Dułak, M.; Friis, J.; Groves, M. N.; Hammer, B.; Hargus, C.; others The atomic simulation environment—a Python library for working with atoms. *Journal of Physics: Condensed Matter* **2017**, *29*, 273002.

(36) Monkhorst, H. J.; Pack, J. D. Special points for Brillouin-zone integrations. *Physical review B* **1976**, *13*, 5188.

(37) Mortensen, J. J.; Gjerding, M.; Thygesen, K. S. MyQueue: Task and workflow scheduling system. *Journal of Open Source Software* **2020**, *5*, 1844.

(38) Maintz, S.; Deringer, V. L.; Tchougréeff, A. L.; Dronskowski, R. LOBSTER: A tool to extract chemical bonding from plane-wave based DFT. 2016.

(39) Wang, D.; Guo, Y.; Liang, K.; Tao, K. Crystal structure of zirconia by Rietveld refinement. *Science in China Series A: Mathematics* **1999**, *42*, 80–86.

(40) Vagkopoulou, T.; Koutayas, S. O.; Koidis, P.; Strub, J. R. Zirconia in dentistry: Part 1. Discovering the nature of an upcoming bioceramic. *Eur. J. Esthet. Dent* **2009**, *4*.

(41) Wang, G.; Huang, F.; Chen, X.; Wen, S.; Gong, C.; Liu, H.; Cheng, F.; Zheng, X.; Zheng, G.; Pan, M. Density functional studies of zirconia with different crystal phases for oxygen reduction reaction. *RSC advances* **2015**, *5*, 85122–85127.

(42) Wu, H.; Duan, Y.; Liu, K.; Lv, D.; Qin, L.; Shi, L.; Tang, G. First-principles study of phase transition and band structure of ZrO2 under pressure. *Journal of Alloys and Compounds* **2015**, *645*, 352–357.

(43) Okamoto, Y.; Sugino, O. Hyper-volcano surface for oxygen reduction reactions over noble metals. *J. Phys. Chem. C* **2010**, *114*, 4473–4478.

(44) Hoffmann, R. *Solids and surfaces: a chemist's view of bonding in extended structures*; John Wiley & Sons, 1991.

(45) Van Santen, R. A.; Tranca, I.; Hensen, E. J. Theory of surface chemistry and reactivity of reducible oxides. *Catalysis Today* **2015**, *244*, 63–84.

(46) Deringer, V. L.; Tchougréeff, A. L.; Dronskowski, R. Crystal orbital Hamilton population (COHP) analysis as projected from plane-wave basis sets. *The journal of physical chemistry A* **2011**, *115*, 5461–5466.

(47) Bandarenka, A. S.; Koper, M. T. Structural and electronic effects in heterogeneous electrocatalysis: Toward a rational design of electrocatalysts. *Journal of Catalysis* **2013**, *308*, 11–24.

(48) Colmati, F.; Magalhaes, M. M.; Sousa Jr, R.; Ciapina, E. G.; Gonzalez, E. R. Direct Ethanol Fuel Cells: The influence of structural and electronic effects on Pt–Sn/C electrocatalysts. *International Journal of Hydrogen Energy* **2019**, *44*, 28812–28820.

(49) Chang, S.-H.; Su, W.-N.; Yeh, M.-H.; Pan, C.-J.; Yu, K.-L.; Liu, D.-G.; Lee, J.-F.; Hwang, B.-J. Structural and Electronic Effects of Carbon-Supported PtxPd1- x Nanoparticles on the Electrocatalytic Activity of the Oxygen-Reduction Reaction and on Methanol Tolerance. *Chemistry–A European Journal* **2010**, *16*, 11064–11071.

Technical
University of
Denmark

Anker Engelunds Vej
Building 301
Tlf. 4525 1700

www.energy.dtu.dk